

Investigation of cancer drug penetration in 2D and 3D tumor cell culture models

UNIVERSITY OF PITTSBURGH

SCHOOL OF PHARMACY

This thesis was presented

by

Feng Shan

It was defended on

07/25/2016

and approved by

Paul A. Johnston, PhD, Research Associate Professor

Barry Gold, PhD, Professor

Shilpa Sant, PhD, Assistant Professor

Thesis Advisor: Paul A. Johnston, PhD, Research Associate Professor

Investigation of cancer drug penetration in 2D and 3D tumor cell culture models.
Feng Shan, B.S.

University of Pittsburgh, 2016

Copyright © by Feng Shan

2016

Investigation of Cancer Drug Penetration in 2D and 3D Head and Neck Cancer Cell Culture Models.

Feng Shan, MS

University of Pittsburgh, 2016

Limited drug penetration into solid tumors may prevent cancer agents from achieving sufficient concentrations to exert their therapeutic effects. However, most pre-clinical *in vitro* drug discovery studies utilize two dimensional (2D) growth inhibition assays, which do not closely recapitulate either the three dimensional (3D) morphology or cellular microenvironments of solid tumors. In this study, we investigated the penetration of cancer drugs into 2D and 3D head and neck squamous cell carcinoma (HNSCC) cell culture models to determine whether differences in drug penetration might contribute to differences in growth inhibition in the two models. Ellipticine, idarubicin, daunorubicin and doxorubicin were selected as the test drugs because they are fluorescent and a linear relationship exists between fluorescent intensity and drug concentration. Cal33 and FaDu HNSCC cell lines were seeded into normal tissue culture microplates to generate 2D monolayers or Ultra Low Attachment microplates to generate spheroids. We used the Cell Titer Glo® reagent to measure cellular ATP levels as an indicator of cell viability and proliferation. The ImageXpress Micro automated high content platform was used to acquire fluorescent images of 2D and 3D cell cultures exposed to the four fluorescent drugs and the Hoechst DNA stain. We used the multi-wavelength cell scoring image analysis module to quantify the accumulation and distribution of fluorescent drugs in 2D and 3D cell cultures. Although 2D Cal33 cultures were

more sensitive than 3D cultures to growth inhibition by all four drugs, both models exhibited similar concentration and time dependent drug accumulation characteristics. In 2D, the distribution of compounds within cells was uniform and independent of the cell numbers seeded into the wells. In Cal33 spheroids however, the compounds exhibited an apparent distribution gradient from high in cells in the outer layers to low in cells in the interior. We speculate that the enhanced cell-cell and cell-ECM contacts in spheroids forms a barrier through which therapeutic agents must penetrate, and that the lower drug concentrations experienced by tumor cells in the interior of spheroids combines with their diminished proliferative capacity to confer the apparent resistance of 3D cultures to cancer drug induced growth inhibition and cell death.

TABLE OF CONTENTS

PREFACE.....	XVI
1.0 INTRODUCTION.....	1
1.1 DRUG DEVELOPMENT AND DRUG RESISTANCE	1
1.2 WHY MIGHT 3D TUMOR CELL CULTURES PROVIDE BETTER MODELS FOR CANCER DRUG DISCOVERY?	5
1.3 WAYS TO FORM 3D SPHEROIDS:	6
1.4 HEAD AND NECK SQUAMOUS CELL CARCINOMA:	8
1.5 DRUG PENETRATION IN 2D VS. 3D.....	8
2.0 MATERIALS AND METHODS	11
2.1 COMPOUNDS AND REAGENTS	11
2.2 CELL CULTURES.....	12
2.2.1 Generation of 3D tumor spheroids and 2D cell cultures.....	12
2.3 2D&3D HNSCC GROWTH INHIBITORY 50 CONCENTRATION (GI₅₀) ASSAY	13
2.4 DRUG PENETRATION CONCENTRATION-RESPONSE, TIME- COURSE AND SEEDING DENSITY ASSAYS.....	14
2.5 IMAGE ACQUISITION.....	15
2.6 MULTI-WAVELENGTH CELL SCORING (MWCS).....	16
2.7 DATA PROCESSING AND CURVE FITTING	19
3.0 RESULTS AND DISCUSSION	22

3.1	2D & 3D HNSCC GROWTH INHIBITORY 50 CONCENTRATION (GI₅₀)	
		22
3.2	ABSORPTION AND EMISSION SPECTRUM OF COMPOUNDS IN SOLUTION.....	30
3.3	COMPOUND PENETRATION IN 2D AND 3D CAL33 HNSCC CELL CULTURE MODELS	36
3.3.1	IMAGES AND CONCENTRATION DEPENDENT PENETRATION OF 2D AND 3D CULTURES.....	36
3.3.2	TIME DEPENDENT PENETRATION OF 2D AND 3D CULTURES .	53
3.3.3	Cal33 HNSCC 2D & 3D SEEDING DENSITY ASSAYS AND PSEUDOCOLOR IMAGES OF 2D&3D CULTURES	68
3.3.4	FADU HNSCC 3D CONCENTRATION DEPENDENT ASSAY.....	86
4.0	CONCLUSIONS	91
	APPENDIX A	94
	BIBLIOGRAPHY.....	96

LIST OF TABLES

Table 1 <i>GI50</i> values of ellipticine, idarubicin, daunorubicin and doxorubicin in 2D and 3D cell cultures.....	30
---	----

LIST OF FIGURES

Figure 1 *Chemical structures of (A) ellipticine, (B) idarubicin, (C) daunorubicin and (D) doxorubicin.* 10

Figure 2 *2D Cal33 Cultures: MWCS Nuclear & cellular Masks. Fluorescent images of Cal33 cells in 2D cell cultures \pm 12.5 μ M idarubicin in (A)Ch1 Hoechst; (B) Ch2 FITC and (C) Ch3 TRITC.* 18

Figure 3 *3D Cal33 Cultures: MWCS Spheroid Masks. Fluorescent images of Cal33 cells in 3D tumor spheroids + 12.5 μ M idarubicin in (A)Ch1 Hoechst; (B) Ch2 FITC and (C) Ch3 TRITC.* 21

Figure 4 *Generation of size-controlled 3D Cal33 HNSCC spheroids. (A) fluorescent images of Hoechst stained in Ch 1, calcein AM stained in Ch 2, ethidium homodimer-1 stained in Ch 3 and color composite of three fluorescent channels.*..... 24

Figure 5 *CellTiter-Glo (CTG) cell viability assay on 3D 384-well ULA microplate.* 26

Figure 6 *Signal to background ratios (S: B) and z'-factor of (A)2D cultures & (B) 3D ULA micro plates.* 27

Figure 7 *2D &3D Cal33 HNSCC GI50 assays. GI50 assay on 2D cell cultures and 3D tumor spheroids treated with (A) Ellipticine; (B) Idarubicin; (C) Daunorubicin; (D) Doxorubicin.* 29

Figure 8 *Idarubicin (A) Absorption spectrum of 20 μ M idarubicin in PBS; (B) Fluorescent emission spectrum of 20 μ M idarubicin in PBS Ex. 480 nm; (C) Fluorescent intensity of different concentrations of idarubicin in PBS, Ex 480 nm & Em. 570 nm.* 32

Figure 9 *Daunorubicin* (A) Absorption spectrum of 20 μ M daunorubicin in PBS; (B) Fluorescent emission spectrum of 20 μ M daunorubicin in PBS Ex. 480 nm; (C) Fluorescent intensity of different concentrations of daunorubicin in PBS, Ex 480 nm & Em. 590 nm. 33

Figure 10 *Doxorubicin* (A) Absorption spectrum of 20 μ M doxorubicin in PBS; (B) Fluorescent emission spectrum of 20 μ M doxorubicin in PBS Ex. 480 nm; (C) Fluorescent intensity of different concentrations of doxorubicin in PBS, Ex 480 nm & Em. 590 nm. 34

Figure 11 *Ellipticine* (A) Absorption spectrum of 20 μ M ellipticine in PBS; (B) Fluorescent emission spectrum of 20 μ M ellipticine in PBS Ex. 480 nm; (C) Fluorescent intensity of different concentrations of ellipticine in PBS, Ex 480 nm & Em. 570 nm. 35

Figure 12 *Grayscale and color composite images of 2D Cal33 HNSCC cells stained with Hoechst 33342. (A) Greyscale images of Hoechst 33342-stained nuclei (Ch 1), greyscale images of idarubicin-treated (Ch 2, Ch 3) and color composite images of Ch 1, Ch 2 and Ch 3 Cal33 HNSCC cells. 37*

Figure 13 *Grayscale and color composite images of 2D Cal33 HNSCC cells + idarubicin treatment. (A) Greyscale images of Hoechst 33342-stained nuclei (Ch 1), greyscale images of idarubicin-treated (Ch 2, Ch 3) and color composite images of Ch 1, Ch 2 and Ch 3 Cal33 HNSCC cells. 38*

Figure 14 *Grayscale and color composite images of 2D Cal33 HNSCC cells + daunorubicin treatment. (A) Greyscale images of Hoechst 33342-stained nuclei (Ch 1), greyscale images of daunorubicin-treated (Ch 2, Ch 3) and color composite images of Ch 1, Ch 2 and Ch 3 Cal33 HNSCC cells. 40*

Figure 15 *Grayscale and color composite images of 2D Cal33 HNSCC cells + doxorubicin treatment. (A) Greyscale images of Hoechst 33342-stained nuclei (Ch 1), greyscale images of*

<i>doxorubicin-treated (Ch 2, Ch 3) and color composite images of Ch 1, Ch 2 and Ch 3 Cal33 HNSCC cells.</i>	<i>41</i>
<i>Figure 16 Grayscale and color composite images of 2D Cal33 HNSCC cells + ellipticine treatment. (A) Greyscale images of Hoechst 33342-stained nuclei (Ch 1), greyscale images of ellipticine-treated (Ch 2) and color composite images of Ch 1 and Ch 2 Cal33 HNSCC cells. ..</i>	<i>43</i>
<i>Figure 17 Fluorescent intensity of 2D Cal33 cells seeded at 1000 cells/well and exposed to the indicated concentrations of the 4 compounds. Fluorescent intensity in 2D cell cultures from (A) Ch-1 Hoechst; (B) Ch-2 FITC; (C) Ch-3 TRITC.....</i>	<i>45</i>
<i>Figure 18 Grayscale and color composite images of 3D Cal33 HNSCC tumor spheroids + idarubicin treatment. (A) Greyscale images of Hoechst 33342-stained nuclei (Ch 1), greyscale images of idarubicin-treated (Ch 2 and Ch 3) and color composite images of Ch 1, Ch 2 and Ch 3 Cal33 HNSCC cells.....</i>	<i>47</i>
<i>Figure 19 Grayscale and color composite images of 3D Cal33 HNSCC tumor spheroids + daunorubicin treatment. (A) Greyscale images of Hoechst 33342-stained nuclei (Ch 1), greyscale images of daunorubicin-treated (Ch 2 and Ch 3) and color composite images of Ch 1, Ch 2 and Ch 3 Cal33 HNSCC cells.....</i>	<i>48</i>
<i>Figure 20 Grayscale and color composite images of 3D Cal33 HNSCC tumor spheroids + doxorubicin treatment. (A) Greyscale images of Hoechst 33342-stained nuclei (Ch 1), greyscale images of doxorubicin-treated (Ch 2 and Ch 3) and color composite images of Ch 1, Ch 2 and Ch 3 Cal33 HNSCC cells.....</i>	<i>49</i>
<i>Figure 21 Grayscale and color composite images of 3D Cal33 HNSCC tumor spheroids + ellipticine treatment. (A) Greyscale images of Hoechst 33342-stained nuclei (Ch 1), greyscale</i>	

<i>images of ellipticine-treated (Ch 2) and color composite images of Ch 1 and Ch 2 Cal33 HNSCC cells.</i>	<i>50</i>
<i>Figure 22 Fluorescent intensity of 3D Cal33 spheroids seeded 5000 cells/well and exposed to the indicated concentrations of the 4 compounds. Fluorescent intensity in 3D Cal33 spheroids from (A) Ch-1 Hoechst; (B) Ch-2 FITC; (C) Ch-3 TRITC.</i>	<i>52</i>
<i>Figure 23 Selected grayscale and color composite images of 2D Cal33 HNSCC cell culture + Hoechst staining for indicated exposure time. (A) Greyscale images of Hoechst 33342-stained nuclei (Ch 1) and color composite images of Ch 1, Ch 2 and Ch 3 Cal33 HNSCC cells.</i>	<i>54</i>
<i>Figure 24 Greyscale and color composite images of 2D Cal33 HNSCC cell culture + ellipticine treatment for indicated exposure time. (A) Greyscale images in Ch 1, greyscale images of ellipticine-treated in Ch 2 and color composite images of Ch 1, Ch 2 and Ch 3 Cal33 HNSCC cells.</i>	<i>55</i>
<i>Figure 25 Grayscale and color composite images of 2D Cal33 HNSCC cell culture + idarubicin treatment for indicated exposure time. (A) Greyscale images of Hoechst 33342-stained nuclei (Ch 1), greyscale images of idarubicin-treated (Ch 2 and Ch 3) and color composite images of Ch 1 and Ch 2 Cal33 HNSCC cells.</i>	<i>56</i>
<i>Figure 26 Selected grayscale and color composite images of 2D Cal33 HNSCC cell culture + daunorubicin treatment for indicated exposure time. (A) Greyscale images of Hoechst 33342-stained nuclei (Ch 1), greyscale images of daunorubicin-treated (Ch 2 and Ch 3) and color composite images of Ch 1 and Ch 2 Cal33 HNSCC cells.</i>	<i>58</i>
<i>Figure 27 Selected grayscale and color composite images of 2D Cal33 HNSCC cell culture + doxorubicin treatment for indicated exposure time. (A) Greyscale images of Hoechst 33342-</i>	

stained nuclei (Ch 1), greyscale images of doxorubicin-treated (Ch 2 and Ch 3) and color composite images of Ch 1 and Ch 2 Cal33 HNSCC cells..... 59

Figure 28 Quantifying 2D Cal33 microplate time course assay by MWCS image analysis. (A) Total cell counts of Cal33 HNSCC cells treated with ellipticine, idarubicin, daunorubicin and doxorubicin; Mean stain integrated intensity of (B) ellipticine and idarubicin in FITC filter (ch-2) for indicated exposure time. (C) idarubicin, daunorubicin and doxorubicin in TRITC filter (ch-3) for indicated exposure time..... 61

Figure 29 Selected grayscale and color composite images of 3D Cal33 HNSCC tumor spheroids + ellipticine treatment for indicated exposure time. (A) Greyscale images of Hoechst 33342-stained nuclei (Ch 1), greyscale images of ellipticine-treated (Ch 2 and Ch 3) and color composite images of Ch 1 and Ch 2 Cal33 HNSCC cells..... 63

Figure 30 Selected grayscale and color composite images of 3D Cal33 HNSCC tumor spheroids + idarubicin treatment for indicated exposure time. (A) Greyscale images of Hoechst 33342-stained nuclei (Ch 1), greyscale images of idarubicin-treated (Ch 2 and Ch 3) and color composite images of Ch 1 and Ch 2 Cal33 HNSCC cells..... 64

Figure 31 Selected grayscale and color composite images of 3D Cal33 HNSCC tumor spheroids + daunorubicin treatment for indicated exposure time. (A) Greyscale images of Hoechst 33342-stained nuclei (Ch 1), greyscale images of daunorubicin-treated (Ch 2 and Ch 3) and color composite images of Ch 1 and Ch 2 Cal33 HNSCC cells..... 65

Figure 32 Selected grayscale and color composite images of 3D Cal33 HNSCC tumor spheroids + doxorubicin treatment for indicated exposure time. (A) Greyscale images of Hoechst 33342-stained nuclei (Ch 1), greyscale images of daunorubicin-treated (Ch 2 and Ch 3) and color composite images of Ch 1 and Ch 2 Cal33 HNSCC cells..... 66

Figure 33 Quantifying 3D Cal33 tumor spheroid time course assay by MWCS image analysis. (A) Total cell counts of Cal33 HNSCC cells treated with ellipticine, idarubicin, daunorubicin and doxorubicin; Mean stain integrated intensity of (B) ellipticine and idarubicin in FITC filter (ch-2) for indicated exposure time. (C) idarubicin, daunorubicin and doxorubicin in TRITC filter (ch-3) for indicated exposure time. 67

Figure 34 Greyscale and color composite of 2D Cal33 cell cultures exposed to 10µM idarubicin at 5000, 10000 and 20000 cells/well. (A) Images of idarubicin treatment on 2D Cal33 cell culture from ch-1 hoechst, ch-2 FITC and color composite. 69

Figure 35 Greyscale and color composite of 2D Cal33 cell cultures exposed to 10µM daunorubicin at 5000, 10000 and 20000 cells/well. (A) Images of daunorubicin treatment on 2D Cal33 cell culture from ch-1 hoechst, ch-2 FITC and color composite. 70

Figure 36 Greyscale and color composite of 2D Cal33 cell cultures exposed to 10µM ellipticine at 5000, 10000 and 20000 cells/well. (A) Images of ellipticine treatment on 2D Cal33 cell culture from ch-1 hoechst, ch-2 FITC and color composite. 72

Figure 37 Fluorescent intensity of 2D Cal33 cells seeded at different densities and exposed to 10 µM of the 4 compounds. Fluorescent intensity in 2D cell cultures from (A) Average cell count of Cal33 cells of 2 10X images; (B) Ch-1 Hoechst; (C) Ch-2 FITC; (D) Ch-3 TRITC. 74

Figure 38 Greyscale and color composite of 3D Cal33 spheroids exposed to 10µM idarubicin at 5000, 10000 and 20000 cells/well. (A) Images of idarubicin treatment on 3D Cal33 spheroids from ch-1 hoechst, ch-2 FITC and color composite. 76

Figure 39 Greyscale and color composite of 3D Cal33 spheroids exposed to 10µM daunorubicin at 5000, 10000 and 20000 cells/well. (A) Images of daunorubicin treatment on 3D Cal33 spheroids from ch-1 hoechst, ch-2 FITC and color composite. 77

Figure 40 *Greyscale and color composite of 3D Cal33 spheroids exposed to 10 μ M doxorubicin at 5000, 10000 and 20000 cells/well. (A) Images of doxorubicin treatment on 3D Cal33 spheroids from ch-1 hoechst, ch-2 FITC and color composite. 78*

Figure 41 *Greyscale and color composite of 3D Cal33 spheroids exposed to 10 μ M ellipticine at 5000, 10000 and 20000 cells/well. (A) Images of ellipticine treatment on 3D Cal33 spheroids from ch-1 hoechst, ch-2 FITC and color composite. 79*

Figure 42 *Fluorescent intensity of 3D Cal33 spheroids seeded at different densities and exposed to 10 μ M of the 4 compounds. Fluorescent intensity in 3D Cal33 spheroids from (A) Ch-1 Hoechst; (B) Ch-2 FITC; (C) Ch-3 TRITC. 81*

Figure 43 *Pseudo-color images of Cal33 HNSCC cells in 2D cultures and 3D tumor spheroids exposed to 10 μ M ellipticine at 5,000, 10,000 and 20,000 cells/well. (A) Pseudocolor images from ch-2 FITC in 2D cell cultures; (B) Pseudocolor images from ch-2 FITC in 3D tumor spheroids. 82*

Figure 44 *Pseudo-color images of Cal33 HNSCC cells in 2D cultures and 3D tumor spheroids exposed to 10 μ M idarubicin at 5,000, 10,000 and 20,000 cells/well. (A) Pseudocolor images from ch-2 FITC in 2D cell cultures; (B) Pseudocolor images from ch-2 FITC in 3D tumor spheroids. 83*

Figure 45 *Pseudo-color images of Cal33 HNSCC cells in 2D cultures and 3D tumor spheroids exposed to 10 μ M daunorubicin at 5,000, 10,000 and 20,000 cells/well. (A) Pseudocolor images from ch-2 FITC in 2D cell cultures; (B) Pseudocolor images from ch-2 FITC in 3D tumor spheroids. 84*

Figure 46 *Pseudo-color images of Cal33 HNSCC cells in 2D cultures and 3D tumor spheroids exposed to 10 μ M doxorubicin at 5,000, 10,000 and 20,000 cells/well. (A) Pseudocolor images*

from ch-2 FITC in 2D cell cultures; (B) Pseudocolor images from ch-2 FITC in 3D tumor spheroids. 85

Figure 47 *Grayscale and color composite images of 3D FADU HNSCC tumor spheroids + ellipticine treatment. (A) Greyscale and color composite images of ellipticine-treated (Ch 2) and pseudo-color images of 3D FADU HNSCC spheroids; (B) Color range of pseudo-color images. 87*

Figure 48 *Grayscale and color composite images of 3D FADU HNSCC tumor spheroids + idarubicin treatment. (A) Greyscale and color composite images of ellipticine-treated (Ch 3) and pseudo-color images of 3D FADU HNSCC spheroids; (B) Color range of pseudo-color images. 88*

Figure 49 *Fluorescent intensity of 3D FADU spheroids seeded at different densities and exposed to 10 uM of the 4 compounds. Fluorescent intensity in 3D FADU spheroids from (A) Ch-1 Hoechst; (B) Ch-2 FITC; (C) Ch-3 TRITC. 90*

PREFACE

I would like to express my gratitude to my supervisor Dr. Paul A. Johnston for the guidance, patience and deep insights through the learning process of this master degree. His guidance helped me in all the time of research and writing of this master thesis. I could not have imagined having a better advisor for my master study.

Furthermore, I would like to thank Dr. Barry Gold for accepting me into this program and generous support and help in these two years.

I would like to thank Dr. Shilpa Sant for being my committee member, giving instructive suggestions on my thesis.

In addition, I like to thank my lab mates: David A Close, Ashley T. Fancher, Yun Hua, Stanton J. Kochanek and Daniel P. Camarco for your kind help and support on my researches and master thesis.

I would like to thank my family: my parents Zhibin Shen, Guoqi Shan and my girlfriend Yafei Lyu. Your support throughout my life is my motivation to move forward.

1.0 INTRODUCTION

1.1 DRUG DEVELOPMENT AND DRUG RESISTANCE

In the late 1980s, the National Cancer Institute (NCI) developed a panel of 60 well-characterized cancer cell lines from diverse tumor types, which have been used as a standard platform for screening drugs against heterogeneous cancer subtypes. It includes cell lines from the 9 most frequent cancer lineage types: leukemia, colon, lung, CNS, renal, melanoma, ovarian, breast and prostate.[1] This screening model was developed to supplant murine neoplasms with cell lines from human solid tumors and to become an efficient tool for identifying compounds with anticancer growth-inhibitory or toxic effects. The pattern of growth inhibition in the NCI 60 cell line panel was similar for compounds of similar mechanism and the development of the COMPARE algorithm provided a method to infer the mechanisms of action of novel compounds based on the similarity of their growth inhibition profiles to known drugs.[2] Previous studies in the NCI60 cell line panel have accumulated large amounts of compound screening data and multi-level omics data, which include genome-wide genetic alterations, gene expression and protein regulation information.[3] These NCI60 datasets were widely utilized for establishing linear correlation patterns in order to identify relationship among chemical responses, genetic alterations, mRNA expression and protein regulations in the NCI60 cell line panel[4]. There are two main methods used for the identification of anti-cancer agents. In the classic approach, compounds from

different sources are tested against a panel of cancer cell lines to identify agents that inhibit cell growth[5]. If a compound shows growth inhibitory activity *in vitro*, it's *in vivo* tumor efficacy will be evaluated in mice. Novel targeted approaches develop specific drugs against oncogenic proteins and signaling pathways. Computer-assisted drug design and high throughput screens are commonly utilized to identify compounds with anti-cancer activity. An evaluation of antitumor activities and determination of the mechanism(s) of action are necessary for further development.[5] However, most preclinical *in vitro* drug discovery studies employ growth inhibition assays and genetic alteration studies conducted in two-dimensional (2D) cell culture models[6]. In addition, the NCI 60 panel does not include cell lines derived from some common forms of human cancer, including head and neck squamous cell carcinoma (HNSCC).

Drug resistance in tumors is a major problem in current cancer drug development. Resistance to chemotherapy can be divided into two categories: intrinsic and acquired.[7] Intrinsic drug resistance is caused by molecular and genetic heterogeneity, cancer stem cells components of tumors, and the tumor microenvironment. Thus, the intrinsic drug resistance pre-exists in tumor cells and prevents chemotherapeutics from being effective. Moreover, tumor resistance can be acquired by tumors exposed to anticancer drugs: (i) mutations to target proteins during treatment that alter drug binding, (ii) increased expression of the therapeutic target, and (iii) activation of alternative compensatory signaling pathways.[7, 8] Multiple resistance mechanisms may cooperate to account for the failure of cancer drugs in response to therapy. One major multidrug resistance (MDR) mechanism in cancer cells is the elevated expression of efflux transporters, which causes both intrinsic and acquired drug resistance. The ATP-binding cassette (ABC) transporter family regulates the passage of drugs, nutrients and other important molecules across the plasma and intracellular membranes. Multi-drug resistance protein 1 (also known as P-gp,

ABCB1), MDR-associated protein 1 (also known as MRP1, ABCC1) and breast cancer resistance protein (BCRP) are found widely expressed in many human cancers, including pancreatic cancer, ovarian cancer and lymphoma cancer. These proteins promote the elimination of various hydrophobic anti-cancer compounds, including topoisomerase inhibitors and taxanes [8-10].

Other mechanisms of drug resistance include adaptive responses to tumor treatment. Pro-survival adaptive responses triggered by exposure to antitumor agents can alter tumor cell morphology and induce autophagy to reduce the effectiveness of tumor apoptosis [11]. The pro-survival adaptive responses are also well known as one of the hallmarks of cancer [12]. Mutations, amplifications and chromosomal translocations of anti-apoptotic BCL-2 family members [13], inhibitor of apoptosis proteins (IAPs) [14], and the caspase 8 inhibitors FLIP [15], are tightly associated with the adaptive resistance of tumors to chemotherapies. BCL-2 family proteins are known to be important gatekeepers of the apoptotic response that mainly reside in mitochondria, interact with pro-apoptotic effectors and activators directly, and protect these organelles from mitochondrial membrane permeabilization (MMP), which is one of the rate-limiting events of apoptosis induction [16].

Limited penetration of anticancer drugs in solid tumors also contributes to the low efficiency of some anticancer drugs [17]. In solid tumors, cancer cells grow in contact with each other, stromal cells and the ECM. The uncontrolled proliferation of tumor cells forces blood vessels apart, reduces vascular density and creates a population of cells distant (>100 μ m) from blood vessels [18]. Since systemic antitumor drugs gain access to cancer cells via by the blood circulation, the increased distance between tumor cells and blood vessels can hamper the penetration of chemotherapeutic agents into the cancer cells [19]. Furthermore, the poor vascular organization of solid tumors also causes increased extracellular pH and decreased oxygen levels

inside tumors [20, 21]. A number of studies indicate that therapeutic agents are less effective in the hypoxic and acidic microenvironments of cells in solid tumors [22, 23]. The cell-cell adhesion, cell-cell interactions, and extracellular matrix (ECM) of solid tumors forms a physical barrier to drug penetration and when combined with the increased distance from blood vessels slows down the distribution and movement of chemotherapeutic agents and prevents them achieving effective concentrations [24]. The effectiveness of antitumor agents is compromised if the drugs cannot gain access to all of the cells in a solid tumor and/or cannot achieve effective concentrations [17, 24, 25].

Although two-dimensional (2D) cell culture models have been used widely in preclinical studies for decades, they do not adequately reflect the microenvironment of solid tumors. First, one of the most evident differences between 2D and three-dimensional (3D) cell cultures is the dissimilarity of morphology and architecture.[26] Cells growing on the flat monolayers can freely adhere and spread on the x-y plane, but there is no support for cells in the vertical dimension. 2D culture conditions induces a forced apical-basal polarity, which is the main difference between epithelial cells and mesenchymal cells.[26]Moreover, tumor cells cultured on 2D flat surfaces do not experience the gradients of nutrients, oxygen and waste products that are observed in solid tumors.[19] 2D monolayer cell cultures are exposed to a uniform environment and drug concentrations that do not mimic the complex and dynamic gradients that exist in solid tumors.[18] Limitations to drug penetration in solid tumors has not received sufficient attention in anti-cancer drug development. In addition, the gene expression patterns and mutation profiles of tumor cell lines can be significantly different to those observed in patient tumors[27, 28], suggesting that cell lines may not be totally representative of human cancers. 3D tumor cell models have been developed to overcome some of the limitations of 2D cell cultures because they more closely

resemble the mechanical and physiological microenvironments of the cells in solid tumors. Moreover, drug penetration can be assessed quantitatively in 3D tumor models.[29] Our goal is to investigate drug penetration in 2D & 3D HNSCC tumor cell culture models, to determine whether differences in drug penetration contributes to the differences in drug responses observed between the two culture models.

1.2 WHY MIGHT 3D TUMOR CELL CULTURES PROVIDE BETTER MODELS FOR CANCER DRUG DISCOVERY?

Although investment in the development of anticancer drugs has increased considerably, <5% of potential anticancer drug candidates show sufficient efficacy and safety in clinical trials to be approved by the FDA and make it to the market. By contrast, the overall clinical success rate for developing new drugs in other therapeutic areas is on average 11%, and reaches 20% for cardiovascular diseases.[30] There are several factors that potentially contribute to the limited effectiveness of anti-cancer drug development, including insufficient translational research and a lack of adequate preclinical models that recapitulate the complexity and molecular heterogeneity of cancer. More predictive preclinical models for testing cancer drug efficacy and safety is one strategy with potential to significantly improve success rates.[5, 31]

The overwhelming majority of cell culture studies, including those used for cancer drug discovery, are performed in 2D cell cultures grown on surfaces such as micro-well plates and tissue culture flasks made from polystyrene or glass. However, it is generally recognized that the flat and hard plastic substrates used for 2D cell culture are not representative of either the cellular

environment or the adhesive, topographical, and mechanical forces experienced by cells in solid tumors.[26, 32] In contrast to tumor cells grown in 2D cultures, 3D tumor cell cultures exhibit many aspects of similarity to the cells in solid tumors. 3D tumor cell cultures are compact aggregates of tumor cells with increased cell-cell interactions, ECM-to-cell signaling.[33] Furthermore, large 3D tumor spheroid structures exhibit a necrotic core surrounded by an inner layer of quiescent viable cells and an outer layer of proliferating cells, which more closely recapitulates solid tumor architecture and biology to provide better *in vitro* preclinical models for cancer drug discovery than traditional 2D monolayer cell cultures.[34] The structure and architecture of 3D tumor cell cultures results in decreasing nutrient concentrations from the exterior to the center of the 3D cell mass.[35, 36] Moreover, 3D cell culture models can mimic the conditions of insufficient mass transport and limited diffusion in solid tumors, which not only produce gradients of O₂, nutrients, pH and waste products like CO₂[37], but also exhibits decreased drug penetration within the 3D tumor cell cultures.[38, 39]

1.3 WAYS TO FORM 3D SPHEROIDS:

Three-dimensional tumor spheroid cultures are either anchorage-dependent or anchorage-independent cell cultures. The scaffolds typically used in anchorage-dependent 3D cell cultures include polymeric hard scaffolds, biological scaffolds, and micro-patterned surface microplates.[40] A number of biological materials have been used to provide support and mimic and/or maintain the microenvironment of cells growth outside of the body, such as poly glycolic acid (PGA), poly lactic acid (PLA) and collagen. The scaffolds need to be degradable and nontoxic to cells. Whole organism models such as *drosophila melanogaster* (fruit fly), zebra fish and mouse

embryos models have been developed when there is a requirement for tissue-specific information.[41] Anchorage independent 3D cell cultures created without the use of scaffolds can be generated in hanging drop microplates, microplates coated with ultra-low attachment (ULA) surfaces, and in microfluidic devices.[32]

The wells of ULA microplates have a covalently bonded hydrogel surface that is hydrophilic and neutrally charged and effectively prohibits cellular attachment cues.[42] In the wells of ULA microplates cell-cell interactions predominate and many tumor cell lines seeded into ULA microplates will spontaneously self-assemble to form spheroids at the center of well over time. ULA microplates have been used to generate tumor spheroids using variety of different cell lines and different cancer types.[43-47] Delyan P. Ivanov et al.[48] developed a brain tumor co-culture models by means of ULA 96-well plates to assess drug delivery strategies. Toshiyoki Tsunoda et al.[49] established 3D culture models to screen drugs targeting KRAS-mediated signaling molecules on the ULA plate platforms. Our lab has previously developed a hydrogel microwell array method to generate size controlled 3D microtumors spheroids in head and neck squamous cell carcinoma (HNSCC) cell lines [50]. We have also developed CellTiter-Glo Luminescent (Promega) assays and image acquisition and analysis methods on the ImageXpress Micro (IXM) automated imaging platform (Molecular Devices, LLC) to measure and assess 3D tumor morphology, cell growth and viability [50]. We applied these methods and others that we developed during the course of this thesis project to the research studies described below.

1.4 HEAD AND NECK SQUAMOUS CELL CARCINOMA:

Head and neck squamous cell carcinoma (HNSCC) usually develops in the mucous membranes of the mouth, nose, and throat. HNSCC is the 6th most common non-skin cancer in the world, and 540,000 new HNSCC cases are diagnosed and 271,000 deaths are reported annually.[51] In addition to smoking, alcohol and genetics, human papillomavirus (HPV) infections, especially HPV-16, are risk factors for head and neck cancers.[52] The incidence of oropharyngeal cancers caused by HPV infection is increasing.[53] The FDA has approved six anticancer drugs for HNSCC therapy; methotrexate, 5-fluorouracil, bleomycin, cisplatin, docetaxel, and the molecularly targeted agent cetuximab. However, only 25% of HNSCC patients respond to these anti-cancer drugs, and despite their introduction, the overall cure rate and 5-year survival rate for head and neck cancer has remained at approximately 50% for over 30 years. In addition, patients with the recurrent/metastatic HNSCC have a median survival of only 6-12 months. There is therefore a need for new and effective therapies. Cal33 is a well- characterized head and neck cancer cell line model isolated from a squamous cell carcinoma of the tongue. It has been widely used in HNSCC cancer research including high-throughput screening[54, 55], cytogenetic analysis[56], and for gene mutation and copy number alteration studies[57].

1.5 DRUG PENETRATION IN 2D VS. 3D

Several techniques have been developed to investigate drug penetration in 3D tumor spheroids. C. Erlichman et. al. enabled to utilize sequential trypsinization method to test cytotoxicity of Adriamycin in MGH-U1 cells grown in monolayer cultures and 3D spheroids[58].

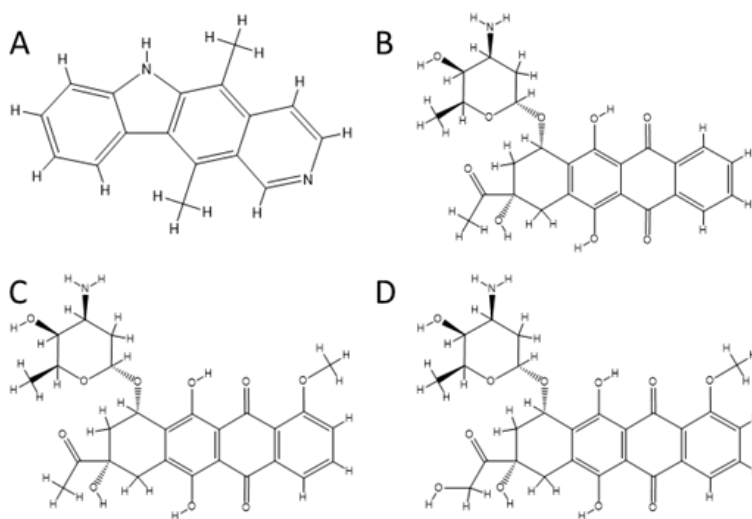
After the compound treatment, the 3D spheroids were trypsinized to cell suspensions and settled down again to monolayer cultures, then the colonies were counted using Model-F CoulterCounter.[58] Ralph E. Durand utilized hoechst 33342 to stain 3D tumor spheroids in order to form a concentration gradient from the outside to the center of the spheroids, and then the single cells within the spheroids could be sorted by fluorescence-activated cell sorting techniques[59]. This technique was used to selectively recover cells from a given subpopulation based on the diffusion gradient of Hoechst staining. Previous high-content screening studies in our lab have observed strong fluorescent signals in images acquired from U2OS cells treated with idarubicin and ellipticine in the 1.56–25 μM concentration range.[60, 61] Ellipticine produced strong fluorescent signals in the FITC channel and idarubicin produced strong fluorescent signals in the Texas red channel.[60] The fluorescent characteristics of these compounds have often been quantified and used to identify their localization in cells. [58, 59, 62, 63]

We selected ellipticine, idarubicin, daunorubicin and doxorubicin as our compound test set to measure drug penetration in 2D and 3D HNSCC models because of their fluorescent properties within cells. Figure 1 shows the chemical structures of the four compounds. Idarubicin, daunorubicin and doxorubicin belong to the class of anthracycline compounds, which were derived from the bacterium *Streptomyces Peucetius*. [64] These amphiphilic molecules possess a fluorescent hydroxyl-substituted anthraquinone chromophore and a hydrophilic aminoglycosidic side chain. The mechanisms of action (MOAs) of anthracycline compounds include (i) Intercalation of DNA/RNA for inhibiting DNA/RNA synthesis. (ii) Inhibition of topoisomerase II activity. (iii) Generation of free oxygen, leading to damage of DNA, proteins and membranes, etc.[65, 66] Anthracyclines are active against a wide variety of hematological and solid tumor

malignancies including acute leukemia, lymphomas, myeloma and neuroblastoma.[67]
Cardiotoxicity is the major side effect of anthracyclines.[68, 69]

Ellipticine is a polyaromatic small molecule isolated from apocyanaceae plants, and several of its derivatives exhibit significant antitumor and anti-HIV activities (Figure 1).[70] It is a potent antineoplastic agent that possesses high efficacy with relatively limited toxicity. Although not all of ellipticine's MOAs have been delineated yet, two prevalent MOAs include intercalation into DNA and inhibition of topoisomerase II[71]. In addition, several studies indicate that the formation of covalent DNA adducts mediated by cytochrome P450 (CYP) oxidized ellipticine metabolites and peroxidases might be another MOA of antitumor effects [72]. Previous preclinical trials have been undertaken to investigate the antitumor and anti-HIV activities of ellipticine.[73-75] Toxic side effects of ellipticine include nausea and vomiting, hypertension, muscular cramp, fatigue, mouth dryness, and mycosis of the tongue and esophagus.[76]

Figure 1 Chemical structures of (A) ellipticine, (B) idarubicin, (C) daunorubicin and (D) doxorubicin.



2.0 MATERIALS AND METHODS

2.1 COMPOUNDS AND REAGENTS

37% Formaldehyde (Cat. #252549) was purchased from Sigma Aldrich. Hoechst 33342 (Cat. #H1339) was purchased from Life Technologies. Dimethyl sulfoxide (DMSO) (99.9% high-performance liquid chromatography-grade) was obtained from Alfa Aesar (Ward Hill, MA). Dulbecco's Mg²⁺ and Ca²⁺-free phosphate-buffered saline (PBS) was purchased from Corning (Tewksbury, MA). L-glutamine (Cat. # SH30034.01) and Penicillin/Streptomycin (Cat. # SH30010) was purchased from Thermo Scientific. Fetal Bovine Serum (Cat. # NC0771932) was purchased from Fisher Scientific. CellTiter-Glo[®] luminescent cell viability assay reagent was purchased from Promega.

Stock solution aliquots of 20mM ellipticine (Tocris Bioscience Cat. #3357), 20mM idarubicin (Sigma Aldrich Cat. #H1349), 10 mM daunorubicin (From NCI60 stock, compound #10) and 10 mM doxorubicin (From NCI60 stock) were prepared in dimethyl sulfoxide (DMSO) and stored at -20°C. Prior to running experiments, the stocks of ellipticine and idarubicin were adjusted to 10 mM by dilution (1:2) in DMSO. The 10 mM stock solutions of the four compounds were then diluted 1:100 in serum-free DMEM to achieve an intermediate concentration of 100µM in 1% DMSO. For concentration response assays, the four compounds were then added to 2D and 3D cell culture assay plates resulting in a 1:4 dilutions and a final top concentration of 25µM and 0.25% DMSO. In time course experiments the final compound concentration was 10µM and 0.1% DMSO.

2.2 CELL CULTURES

The Cal33 HNSCC cell line was cultured in T75 tissue culture flasks and maintained in medium consisting of Dulbecco's Modified Eagle's Medium (DMEM) with 10% fetal bovine serum (FBS), 1% L-glutamine, and 1% penicillin/streptomycin (P/S). Cal33 HNSCC cells were passaged every 2 to 3 days and cultured in an incubator at 37°C and 5% CO₂ and 95% humidity. The FaDu HNSCC cell line was cultured in T75 tissue culture flasks and maintained in culture medium consisting of Dulbecco's Modified Eagle's Medium (DMEM) with 1% non-essential amino acids, 1% L-glutamine and 1% penicillin/streptomycin (P/S). FaDu HNSCC cells were passaged every 3 to 4 days and cultured in an incubator at 37°C in 5% CO₂ and 95% humidity. Cell suspensions for seeding assay plates were made by dissociating cells from flasks with trypsin, centrifugation of dissociated cells at 1200 rpm for 5 minutes at room temperature, and re-suspension in growth media. The number of trypan blue excluding viable cells in the cell suspension was counted using a hemocytometer.

2.2.1 Generation of 3D tumor spheroids and 2D cell cultures

For 3D spheroid generation, 384-well Ultra Low Attachment (ULA) Microplate (Corning Cat. # 4516) were rehydrated by adding 50µL of complete media to each well and placement the tissue culture incubator for ~0.5h. The rehydration media was removed from the ULA microplates and 45µL of the Cal33 cell suspension at different cell densities (625, 1250, 2500, 5000, 10000 and 20000 cells/well) were seeded into each well using matrix pipette (Thermo Scientific Inc.).

384-well ULA microplates containing cell suspensions were then centrifuged at 100 rpm for 1 minute. After the centrifugation, 3D HNSCC spheroids formed spontaneously over time when the plates were placed in incubator at 37°C and 5% CO₂ and 95% humidity.

For 2D cell culture assay plates, 45µL of the desired densities of Cal33 cell suspension were seeded into 384-well tissue culture treated microplates (Greiner Cat. # 781091). The 384-well plates were centrifuged at 100 rpm for 1 minute and incubated overnight at 37°C and 5% CO₂ and 95% humidity.

2.3 2D&3D HNSCC GROWTH INHIBITORY 50 CONCENTRATION (GI₅₀) ASSAY

For HNSCC cell line GI₅₀ assays, Cal33 cells were harvested, counted, and seeded into an uncoated, white, opaque 384-well assay plate for 2D assays (Greiner Bio-one Cat # 781080) or into ULA 384-well assay plate for 3D assays on day 1. For 2D assays, Cal33 cells were seeded at 1,000 cells per well in 45µL of tissue culture media into the wells of the 384-well assay plates, and for 3D assays Cal33 cells were seed at 5,000 cells per well in 45µL of tissue culture media into the wells of ULA 384-well microplates. The plates were then cultured overnight at 37°C, 5% CO₂, and 95% humidity. On day 2, 5µL of 4 compounds (ellipticine, idarubicin, daunorubicin and doxorubicin) at the indicated concentrations in serum-free media were transferred into the test wells of the 2D and 3D assay plates on the Janus MDT automated liquid handler equipped with a 384-well transfer head. Also, 5µL of 5% DMSO and 5µL of 2mM doxorubicin were added to the minimum and maximum control wells (n=32 each). The compound-treated plates were then

cultured for 72 h in an incubator at 37°C, 5% CO₂, and 95% humidity. We used the Cell-Titer Glo® (CTG) reagent which generates a luminescent signal (RLUs) that is directly proportional to the concentration of ATP ([ATP]) released by viable cells lysed in detergent to measure cell growth and viability (insert Johnston et al, STAT3 AD & HCS manuscript references- earlier). On day 5, 25µL of the Cell-Titer Glo® (CTG) cell viability detection reagent was dispensed into compound and control wells of 2D and 3D assay plates using a matrix pipette, and the plates were incubated for 15 min. The luminescence signals were then captured on the M5e micro-titer plate reader platform. For the HNSCC GI₅₀ assays, we used the DMSO and Doxorubicin control data from 2D and 3D microplates to normalize the growth inhibition of each compound and expressed it as percentage of controls. The DMSO and 200µM doxorubicin controls were used to calculate the S: B ratios and Z'-factor coefficient statistics for the assay signal windows.

2.4 DRUG PENETRATION CONCENTRATION-RESPONSE, TIME-COURSE AND SEEDING DENSITY ASSAYS

The penetration of ellipticine, idarubicin, daunorubicin and doxorubicin into HNSCC tumor cells in 2D cultures and 3D tumor spheroids were investigated at different drug concentrations, compound exposure times, and cell seeding densities.

In concentration response assays, 5µL of serial dilutions of the four compounds were added to replicate (n=3) wells of the 2D and 3D assay plates. The final concentrations of the test compounds in the wells were 25, 12.5, 6.25, 3.125, 1.5625 and 0.78125µM. After a 15 min incubation at 37°C, 5% CO₂, and 95% humidity, the 2D and 3D ULA microplates were then fixed and stained with Hoechst by the addition of 50µL of fixative solution to each well and a 30 min

incubation at room temperature in the dark. The fixative solution was prepared in PBS, and contained 37% Formaldehyde and Hoechst 33342 in a ratio of 400:100:1. The compounds, media and fixative mixture was aspirated using the Janus MDT automated liquid handler and the plates were washed 3 times with PBS. 50 μ L of PBS was then added to each well after washing and the plates were then sealed with aluminum foil. 2D and 3D assay plates were imaged and analyzed on the IXM automated high-content imaging platform as described below.

In time-course assays, 5 μ L of the four test compounds (10 μ M final) were transferred into replicate (n=3) wells and incubated at 37°C, 5% CO₂, and 95% humidity for the indicated time periods: 0, 2.5, 5, 10, 15, 30 and 45 min. The 2D and 3D assay plates were fixed, stained with Hoechst, and washed as described above, and then imaged and analyzed on the IXM automated high-content imaging platform as described below.

In cell density assays, Cal33 and FADU HNSCC cell lines were seeded into 384-well 2D and 3D assay plates, at seeding densities of 625, 1,250, 2,500, 5,000, 10,000 and 20,000 cells per well. 5 μ L of the four compounds (10 μ M final) were added to replicate (n=3) wells and incubated at 37°C, 5% CO₂ and 95% humidity for 15 minutes. The 2D and 3D assay plates were fixed, stained with Hoechst, and washed as described above, and the plates were then imaged and analyzed on the IXM automated high-content imaging platform as described below.

2.5 IMAGE ACQUISITION

The ImageXpress® Micro (IXM) XLS System is a wide-field automated high-content imaging platform (Molecular Devices, LLC) capable transmitted light, and fluorescent imaging of fixed- or live-cell assays, tissues and small organisms. Combined with the MetaXpress image

analysis software, it can both acquire and analyze images. The IXM high-content analysis system consists of a 1.4 megapixel cooled CCD camera (standard model). The IXM has a transmitted light module and is equipped with the following ZPS filter sets for fluorescent imaging: DAPI, FITC/ALEXA 488, CY3 (TRITC), CY5, and Texas Red. Images of Cal33 microtumors were acquired using either a 4x or 10x objective in both the transmitted light and fluorescent acquisition modes. The infrared laser autofocus was used to detect the bottom of the plate and well, and then a series of 10-20 Z-stack images were acquired, each separated by a step size of 20 μ m in a range equally distributed above and below a set Z-position. A journal was then used to collapse all of the images in the Z-stack to generate a single maximum projection image.

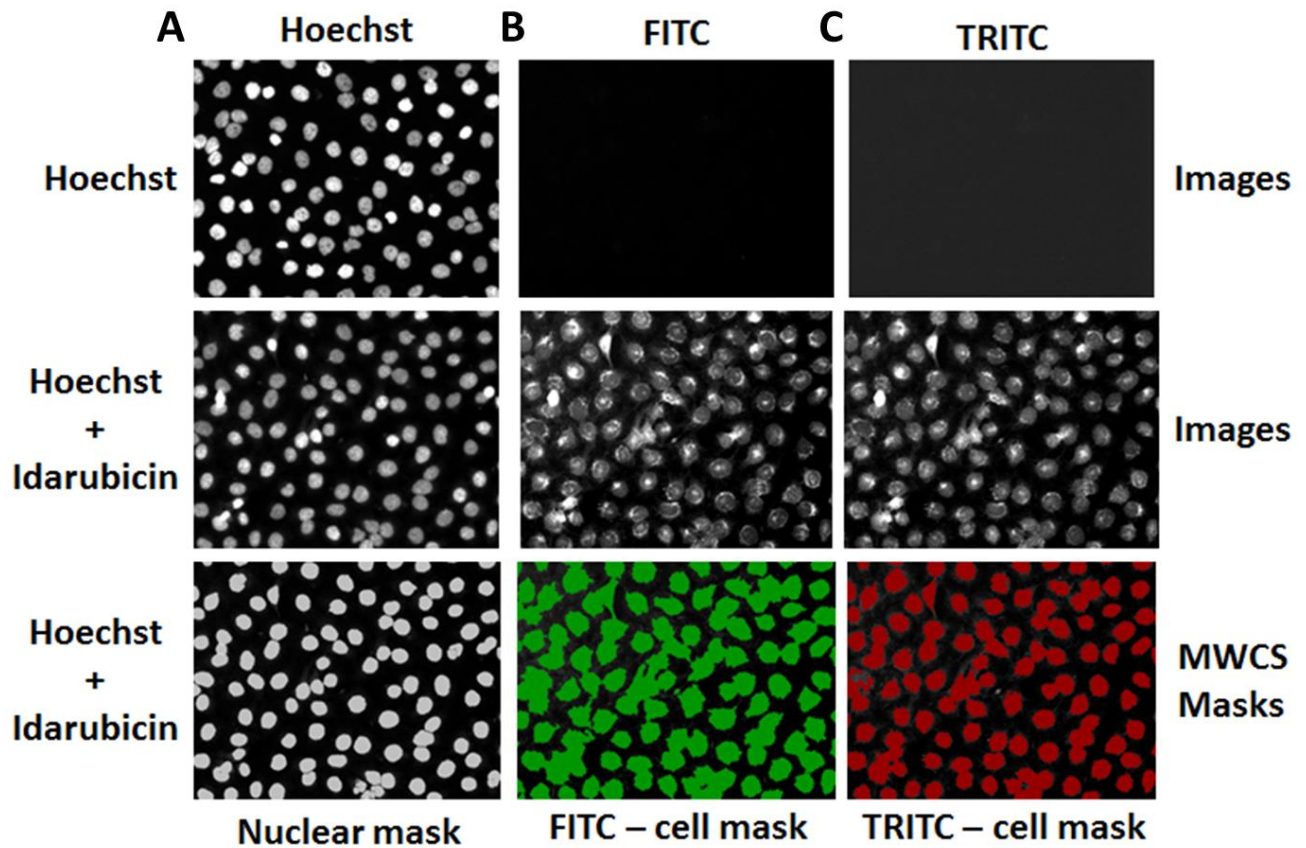
2.6 MULTI-WAVELENGTH CELL SCORING (MWCS)

We used the multi-wavelength cell scoring (MWCS) image analysis module to quantify the integrated fluorescent intensities of the 4 compounds in the digital images of the 2D and 3D HNSCC cultures acquired on the IXM as described above.

The MWCS module image segmentation identified and classified Hoechst 33342 stained fluorescent objects in Ch1 that exhibited appropriate fluorescent intensities above background and size (width, length, and area) characteristics of Cal33 nuclei and used these objects to create nuclear masks for each cell. For 2D Cal33 cell cultures we defined the approximate minimum width of Hoechst stained nuclei to be 8 μ m and the approximate maximum width to be 30 μ m, and the threshold intensity above local background to be 5 (Figure 2).

After applying user defined background average intensity thresholds, typically 200 in both Ch2 (FITC) and Ch3 (TRITC), the MWCS module image segmentation then creates cell masks for each cell. The nuclear mask from Ch1 was then used to quantify the integrated fluorescence intensity of Hoechst within the nuclear region of Cal33 cells and also to count the number of cells per image. The derived Cal33 cell masks from Ch2 and Ch3 were then used to quantify the integrated fluorescence intensity of the compounds in the FITC (Ch2) and TRITC (Ch3) channels (Figure 2). The MWCS image analysis module outputs quantitative data including: The W1 mean stain integrated fluorescent intensities of the Hoechst stained objects (compartments) in Ch1; the number of compartments or total cell count in Ch1; the W2 and W3 mean stain integrated fluorescent intensities of the Ch2 and Ch3 signals in whole cells. Positive W1/W2/W3 Mean Stain Integrated Intensity is the total pixel intensity of the W1/W2/W3 stain over the stained area in W1/W2/W3 positive cells, divided by the number of cells positive for W1/W2/W3.

Figure 2 2D Cal33 Cultures: MWCS Nuclear & cellular Masks. Fluorescent images of Cal33 cells in 2D cell cultures \pm 12.5 μ M idarubicin in (A)Ch1 Hoechst; (B) Ch2 FITC and (C) Ch3 TRITC.



Normal tissue culture microplates were seeded by 1000 Cal33 HNSCC cells per well as previously described. 5 μ L of idarubicin were added into wells with indicated concentration. After 15 min incubation at 37°C, 5% CO₂ The 2D microplate was fixed and stained in 3.7% formaldehyde containing Hoechst-33342. The 2D microplates were washed by PBS for three times after the 45-min fixation. Images were then acquired on the IXM High-Content Analysis System and analyzed using the MWCS image analysis module. The images presented are representative of similar images obtained in at least 3 independent experiments.

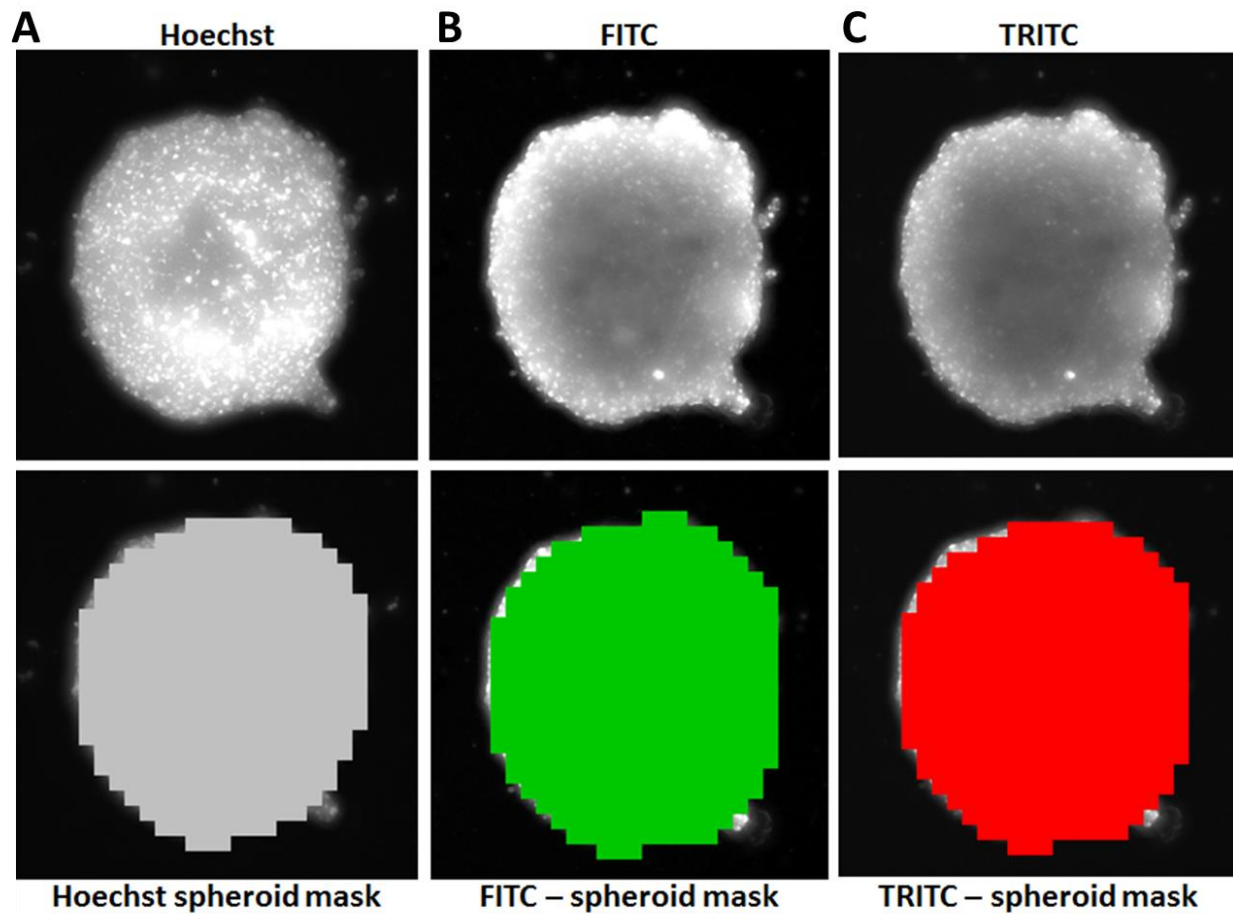
For 3D Cal33 or FADU spheroids we defined the approximate minimum width of Hoechst stained nuclei in the whole spheroid to be 150 μm and the approximate maximum width to be 550 μm , and the threshold intensity above local background to be 70 (Figure 3). After applying user defined background average intensity thresholds, typically 50-70 in both Ch2 (FITC) and Ch3 (TRITC), the MWCS module image segmentation then created masks for each spheroid. The spheroid mask from Ch1 was used to quantify the integrated fluorescence intensity of Hoechst within the Cal33 spheroid and to count the number of spheroids per image (Figure 3). The derived Cal33 spheroid masks from Ch2 and Ch3 were used to quantify the integrated fluorescence intensity of the compounds in the FITC (Ch2) and TRITC (Ch3) channels (Figure 3). The MWCS image analysis module outputs quantitative data including: The W1 mean stain integrated fluorescent intensities of the Hoechst stained spheroids in Ch1; the number of spheroids in Ch1; the W2 and W3 mean stain integrated fluorescent intensities of the Ch2 and Ch3 signals in the spheroids.

2.7 DATA PROCESSING AND CURVE FITTING

For the HNSCC growth inhibition GI_{50} assays, we used the DMSO control wells (Max controls $n=32$) to represent uninhibited growth and 200 μM Doxorubicin control wells (Min controls, $n=32$) to represent 100% of tumor cell cytotoxicity respectively. We then used the mean maximum and minimum plate controls to normalize the data from the compound treated wells as

% of controls. Also, the DMSO and 200 μ M Doxorubicin control wells were used to calculate signal: background ratios and Z'-factor coefficient assay performance statistics for the growth inhibition assay signal windows. GI₅₀ curves were fitted in a non-linear sigmoidal log(inhibitor) vs. normalized response model –using the variable slope equation in the GraphPad Prism 6 software: $Y=100/(1+10^{((\text{LogIC}_{50}-X) * \text{Hillslope}))})$, where y was the percent inhibition and x was the corresponding log₁₀ of the compound concentration. The GI₅₀ is the concentration of compound that gives a 50% response, half way between 0% and 100%. The Hillslope describes the steepness of the curve.

Figure 3 3D Cal33 Cultures: MWCS Spheroid Masks. Fluorescent images of Cal33 cells in 3D tumor spheroids + 12.5 μ M idarubicin in (A)Ch1 Hoechst; (B) Ch2 FITC and (C) Ch3 TRITC.



384-well ULA microplates were seeded by 5000 cells per well of Cal33 HNSCC cells. 5 μ L of idarubicin were added into wells with indicated concentration. After 15 min incubation at 37 $^{\circ}$ C, 5% CO₂ The 2D microplate was fixed and stained in 3.7% formaldehyde containing Hoechst-33342. The ULA microplates were washed by PBS for three times after the 45-min fixation. Images were then acquired on the IXM High-Content Analysis System and analyzed using MWCS image analysis module. The images are presented are representative of similar images obtained in at least 3 independent experiments.

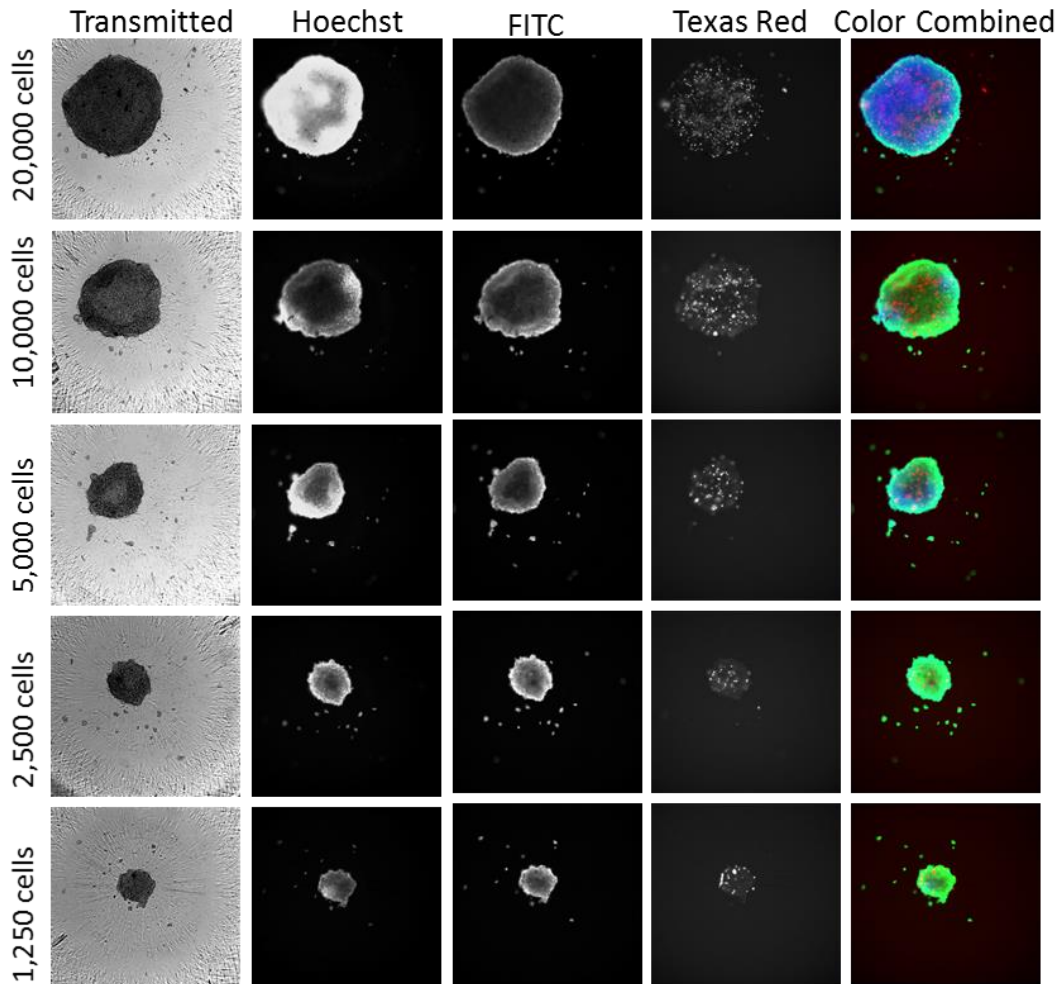
3.0 RESULTS AND DISCUSSION

3.1 2D & 3D HNSCC GROWTH INHIBITORY 50 CONCENTRATION (GI₅₀)

To determine and compare the growth inhibitory actions of ellipticine, idarubicin, daunorubicin and doxorubicin in 2D and 3D HNSCC cell cultures, the Cell Titer Glo® (CTG, Promega) detection assay was utilized to measure cell growth and viability in 2D and 3D HNSCC cultures. We began with the 2D CTG HNSCC growth inhibition assays that our lab has established previously[54, 55] and conducted experiments to determine if those methods could be transferred into 384-well ULA microplates to measure 3D HNSCC spheroid growth and viability. The CTG luminescent cell viability assay is a homogeneous method of determining the number of viable cells based on the quantification of ATP present, which is directly proportional to the number of cells in cultures[77]. Cal33 HNSCC cells that had been seeded into 384-well ULA microplates in serum-containing medium at the indicated cell densities were cultured overnight in an incubator. The cells were then stained with the live cell reagent Calcein AM and the dead cell reagent ethidium homodimer-1, then fixed in 3.7% formaldehyde containing Hoechst-33342. The Hoechst-33342 DNA dye was utilized to stain the nuclei of the Cal33 cells. Calcein AM is a cell permeant dye that can stain live cells. The non-fluorescent Calcein AM is converted to a green-fluorescent calcein after the acetoxymethyl ester hydrolysis by intracellular esterase. Ethidium homodimer-1 (EthD-1) can be used to detect dead cells by binding to DNA and emit red fluorescence when the membrane is disrupted in dead cells, Ethidium homodimer is impermeable to the intact membrane of live cells, it can only stain the DNA of dead cells with disrupted plasma membranes. We then utilized the IXM automated imaging platform to sequentially acquire images

for transmitted light along with the Hoechst (Ch 1), FITC (Ch 2) and Texas Red (Ch 3) fluorescent channels. The transmitted light and fluorescent images of Hoechst-stained indicated that the size of 3D tumor spheroids increased when more cell were seeded into the 384-well ULA microplates (Figure 4). Fluorescent images of Cal33 HNSCC cells stained with calcein AM and EthD-1 indicated that the vast majority of the Cal33 cells in the 3D tumor spheroids formed were alive after the 24-hour incubation period (Figure 4). The color composite overlays of the Ch1, Ch 2 and Ch 3 fluorescent images also indicates that the majority of Cal33 cells in different sized 3D tumor spheroids are viable and only a few dead cells stained by EthD-1 were apparent in the core of the 3D tumor spheroids. These images demonstrate that Cal33 cells seeded in ULA plates spontaneously form 3D tumor spheroids when they are deprived of cell attachment cues and because the cells remain viable under these conditions they should be amenable to the development of 3D tumor model growth inhibition assays (Figure 4).

Figure 4 *Generation of size-controlled 3D Cal33 HNSCC spheroids. (A) fluorescent images of Hoechst stained in Ch 1, calcein AM stained in Ch 2, ethidium homodimer-1 stained in Ch 3 and color composite of three fluorescent channels.*



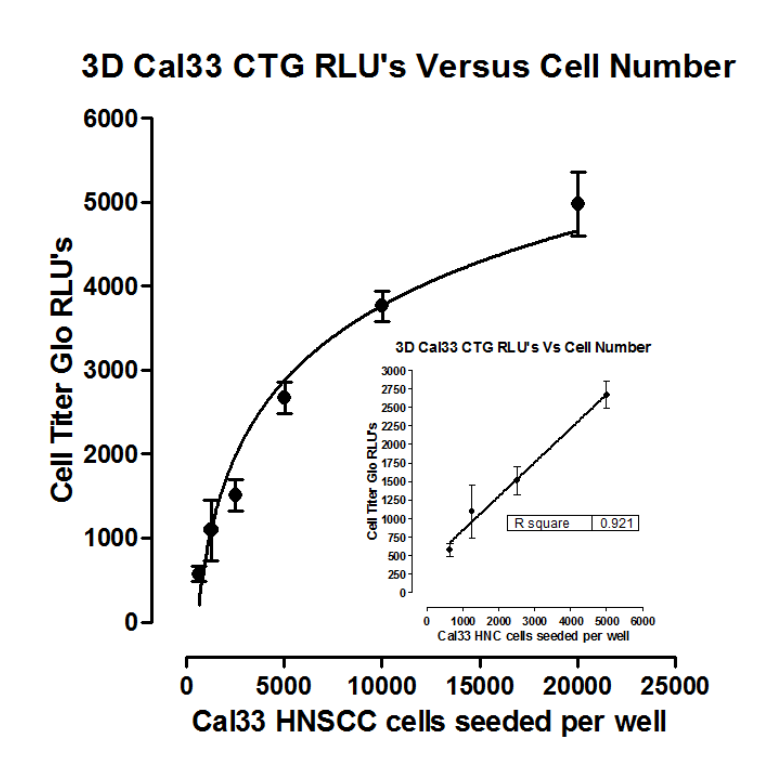
Cal33 HNSCC cells were seeded in 3D 384-well ULA microplates with a serial seeding density of 1250, 2500, 5000, 10000 and 20000 cells per well. Live–dead staining by calcein AM and ethidium homodimer -1 was added after 24 hours, which indicated the cell viability in 3D spheroids. Images of transmitted light, ch-1 hoechst, ch-2 FITC, ch-3 Texas Red and color combined were captured on ImageXpress Micro (IXM) automated imaging system. The images presented are representative of similar images obtained in 3 independent experiments.

To determine if our 2D CTG assay would be transferable to our 3D Cal33 spheroids formed in ULA microplates we added the CTG reagent to Cal33 HNSCC spheroids formed at the indicated cell seeding densities after 24-hours in culture. Figure 5 demonstrates that the relative luminescent units (RLU's) increased in a linear fashion in spheroids formed by 625 up to 5000 cells per well (Figure 5), and although the RLU's continue to increase thereafter with more cells added, the rate of increase was no longer linear with respect to cell number. The data represent the mean \pm SD of triplicates and the experiments were repeated independently on at least 3 occasions. Based on these data, we selected 5000 cells per well as a suitable cell seeding density for the 3D HNSCC growth inhibition GI50 assays.

To define the assay signal window or dynamic range of the 2D and 3D HNSCC growth inhibition assays, we used the 0.5% DMSO control wells to represent uninhibited growth (Max controls n=32), and 200 μ M Doxorubicin + 0.5% DMSO control wells to represent 100% of tumor cell cytotoxicity (Min controls, n=32) respectively (Figure 6). We also used the DMSO and 200 μ M Doxorubicin control wells to calculate signal: background ratios and Z'-factor coefficient performance statistics for the 2D (Figure 6) and 3D (Figure 6) growth inhibition assays. In addition, we used the mean maximum and minimum plate controls to normalize the data from compound treated wells as % of controls. Figure 6 indicates that the 2D and 3D HNSCC assay plate controls exhibited a robust and reproducible separation between the 200 μ M doxorubicin responses and 0.5% DMSO signals. In Cal33 HNSCC 2D cultures and 3D tumor spheroids, the S:B ratios were 223.6-fold and 22.1-fold, respectively. The Z'-factor coefficients for the 2D and 3D HNSCC growth inhibition assays were 0.45 and 0.51, respectively (Figure 6). These data indicate that the plate controls for the 2D and 3D HNSCC growth inhibition assays performed

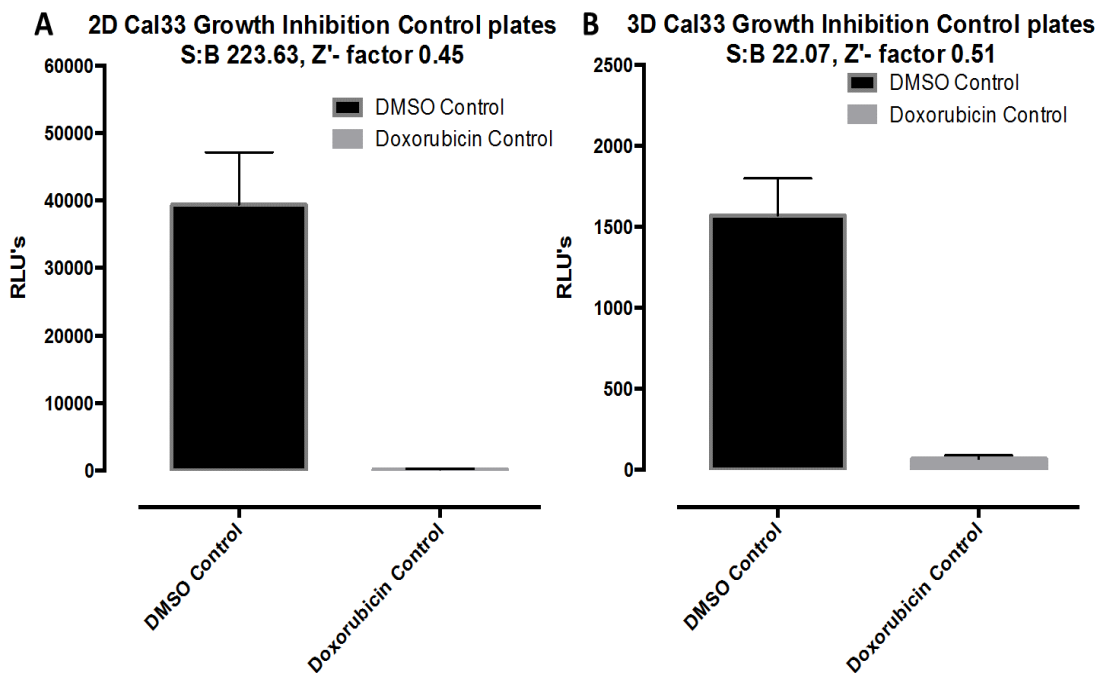
very well and provide a robust and reproducible dynamic range in which to measure the effects of compounds.

Figure 5 CellTiter-Glo (CTG) cell viability assay on 3D 384-well ULA microplate.



CellTiter-Glo (CTG) detection reagent was added to quantify the cellular ATP levels in order to measure viable cells numbers. 25 μ L of CellTiter-Glo reagent was added to each well. The plate was then incubated on a shaking platform for 15 min at room temperature. Relative luminescence (RLUs) units were captured using a SpectraMax M5e Multi- Mode Microplate Reader (Molecular Devices, LLC). The data represent the mean \pm SD ($n=3$) of triplicates determinations from one of three independent experiments.

Figure 6 Signal to background ratios (*S: B*) and *z*'- factor of (A)2D cultures & (B) 3D ULA micro plates.



DMSO and 200μM doxorubicin controls were used to calculate the signal: background ratios and Z'-factor coefficient statistics for the assay signal window. S: B ratio = Mean of DMSO controls/ Mean of 2mM doxorubicin. Z'-factor = 1 - ((3(SD of 2mM doxorubicin + SD of DMSO controls))/(Mean of DMSO controls - 2mM doxorubicin)). Each of DMSO and 2mM doxorubicin controls were repeated in 32 wells.*

Based on these data, we proceeded to evaluate and compare the ability of ellipticine, idarubicin, daunorubicin and doxorubicin to inhibit the growth of Cal33 HNSCC cells in 2D and 3D cell cultures (Figure 7 &

	Replicate Experiments					Replicate Experiments					GI50 Ratio 3D/2D
	1	2	3	GI50 (μM)		1	2	3	GI50 (μM)		
Compound	3D	3D	3D	Mean	SDM	2D	2D	2D	Mean	SDM	
Ellipticine	>10 0	7.46	50.86	29.160	30.688	4.623	1.32	7.295	4.413	2.993	6.6
Idarubicin	3.78 3	0.596	0.9457	1.775	1.748	0.0040	0.006	0.2282	0.079	0.129	22.3
Daunorubicin	140 2	0.925	2.628	1.777	1.204	0.0292	0.057	0.6567	0.248	0.355	7.2
Doxorubicin	1.08 7	0.297	0.7268	0.704	0.395	0.0064	0.016	0.1825	0.068	0.099	10.3

Table 1). Cal33 spheroids were significantly (>5-fold) more resistant than the corresponding 2D Cal33 cultures to growth inhibition by all four cancer drugs (Figure 7).

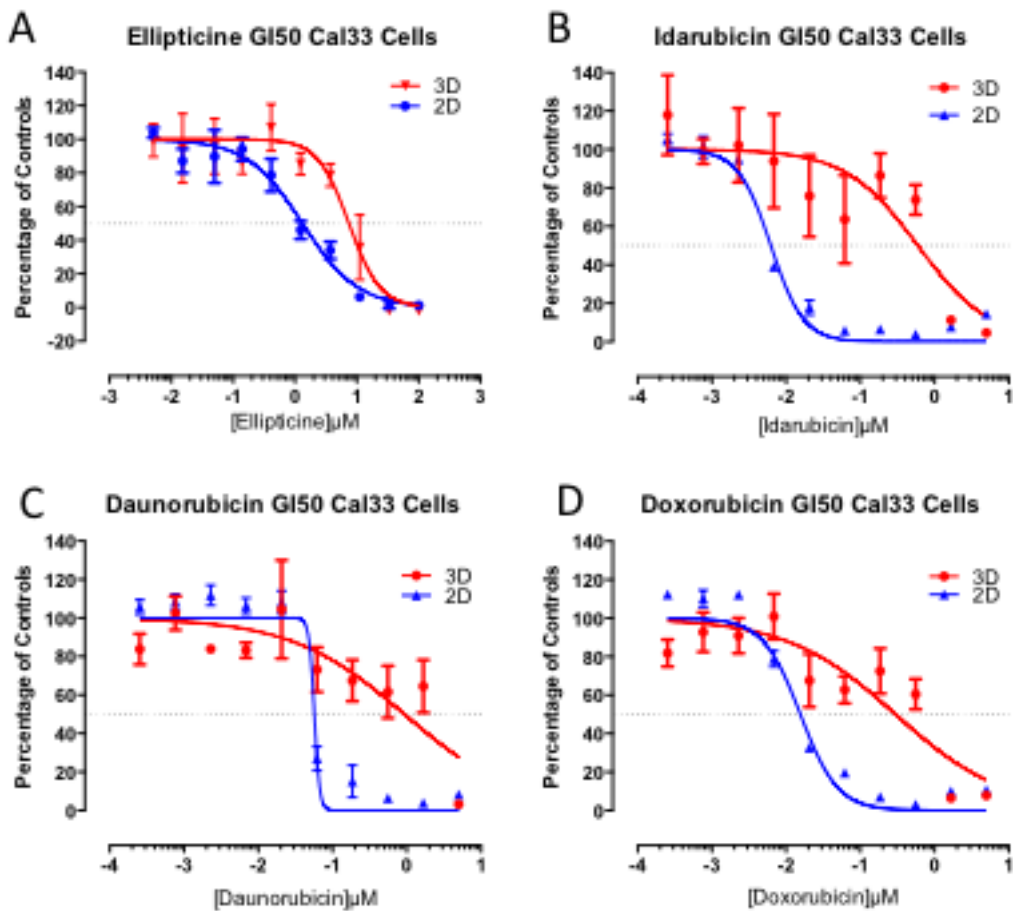
	Replicate Experiments					Replicate Experiments					GI50 Ratio 3D/2D
	1	2	3	GI50 (μM)		1	2	3	GI50 (μM)		
Compound	3D	3D	3D	Mean	SDM	2D	2D	2D	Mean	SDM	
Ellipticine	>10 0	7.46	50.86	29.160	30.688	4.623	1.32	7.295	4.413	2.993	6.6
Idarubicin	3.78 3	0.596	0.9457	1.775	1.748	0.0040	0.006	0.2282	0.079	0.129	22.3
Daunorubicin	140 2	0.925	2.628	1.777	1.204	0.0292	0.057	0.6567	0.248	0.355	7.2
Doxorubicin	1.08 7	0.297	0.7268	0.704	0.395	0.0064	0.016	0.1825	0.068	0.099	10.3

Table 1 *GI50 values of ellipticine, idarubicin, daunorubicin and doxorubicin in 2D and 3D cell cultures.* lists the individual and mean GI_{50} values for ellipticine, idarubicin, daunorubicin, and doxorubicin in 2D and 3D culture models that were obtained in three independent growth inhibition experiments. After excluding two apparent 3D GI_{50} outlier values from experiment 1 (

	Replicate Experiments					Replicate Experiments					GI50 Ratio 3D/2D
	1	2	3	GI50 (μM)		1	2	3	GI50 (μM)		
Compound	3D	3D	3D	Mean	SDM	2D	2D	2D	Mean	SDM	
Ellipticine	>10 0	7.46	50.86	29.160	30.688	4.623	1.32	7.295	4.413	2.993	6.6
Idarubicin	3.78 3	0.596	0.9457	1.775	1.748	0.0040	0.006	0.2282	0.079	0.129	22.3
Daunorubicin	140 2	0.925	2.628	1.777	1.204	0.0292	0.057	0.6567	0.248	0.355	7.2
Doxorubicin	1.08 7	0.297	0.7268	0.704	0.395	0.0064	0.016	0.1825	0.068	0.099	10.3

Table 1, highlighted in orange), the 3D:2D GI₅₀ ratios for ellipticine, idarubicin, daunorubicin, and doxorubicin were 6.6-fold, 22.3-fold, 7.2-fold and 10.3-fold respectively, indicating that Cal33 spheroids were significantly more resistant to growth inhibition than 2D cultures. There are several factors that could contribute to the enhanced drug resistance of 3D HNSCC spheroids. Reduced penetration of drugs into cells in different regions or zones of 3D spheroid cultures (surface layers, intermediate layers, and interior core) might lead to non-uniform drug exposure levels in cells in these different regions such that compounds might fail to achieve efficacious concentrations [37]. All four compounds are topoisomerase II inhibitors that induce apoptosis in proliferating tumor cells by inhibiting the DNA synthesis[65, 66]. Cells in different regions of 3D spheroids exhibit differential rates of cellular proliferation such that the cells that are in quiescent (intermediate layers) or dormant (interior core) zones might be less sensitive to the effects of antiproliferative agents[34]. The necrotic core and the inner layers of quiescent viable cells inside 3D spheroids might revert to proliferating cells if the outer layer of actively proliferating cells are killed by antitumor compounds[34]. To investigate whether the increased resistance of 3D HNSCC spheroids to growth inhibition by ellipticine, idarubicin, daunorubicin, and doxorubicin might be due to differences in drug penetration between 2D and 3D HNSCC cultures, we conducted a series of experiments to define the concentration, time, and cell density dependent penetration of these compounds in 2D and 3D cell culture models.

Figure 7 2D & 3D Cal33 HNSCC GI₅₀ assays. GI₅₀ assay on 2D cell cultures and 3D tumor spheroids treated with (A) Ellipticine; (B) Idarubicin; (C) Daunorubicin; (D) Doxorubicin.



1000 Cal33 HNSCC cells were seeded into 2D 384-well assay plates and 5000 Cal33 HNSCC cells were seeded into 3D 384-well ULA microplates, incubated at 37°C, 5% CO₂, and 95% humidity. After 24 hours, indicated concentration of compounds was transferred by Janus MDT automated liquid handler into the testing wells of 2D and 3D plates. Controls well received DMSO and 2mM doxorubicin respectively and the plates were incubated for additional 72 hours. On day 5, 25μL of the CellTiter Glo (CTG) cell viability detection reagent was dispensed into compound wells of 2D and 3D microplates by matrix pipette. The plates were then incubated on a shaking platform for 15 min at room temperature. Relative luminescence (RLUs) units were captured using a SpectraMax M5e Multi-Mode Microplate Reader (Molecular Devices, LLC). For the 2D & 3D HNSCC IC₅₀ assays, DMSO controls were used to normalize as 0% and 2mM doxorubicin was used to normalize as 100% inhibition. The data represent the mean ± SD (n=3) of triplicates determination from one of 3 independent experiments.

Table 1 GI50 values of ellipticine, idarubicin, daunorubicin and doxorubicin in 2D and 3D cell cultures.

Compound	Replicate Experiments			GI50 (μM)		Replicate Experiments			GI50 (μM)		GI50 Ratio
	1	2	3	Mean	SDM	1	2	3	Mean	SDM	3D/2D
Ellipticine	>10 0	7.46	50.86	29.160	30.688	4.623	1.32	7.295	4.413	2.993	6.6
Idarubicin	3.78 3	0.596	0.9457	1.775	1.748	0.0040	0.006	0.2282	0.079	0.129	22.3
Daunorubicin	140 2	0.925	2.628	1.777	1.204	0.0292	0.057	0.6567	0.248	0.355	7.2
Doxorubicin	1.08 7	0.297	0.7268	0.704	0.395	0.0064	0.016	0.1825	0.068	0.099	10.3

GI50 data of 2D and 3D GI50 assays presented in table was generated in three independent experiments.

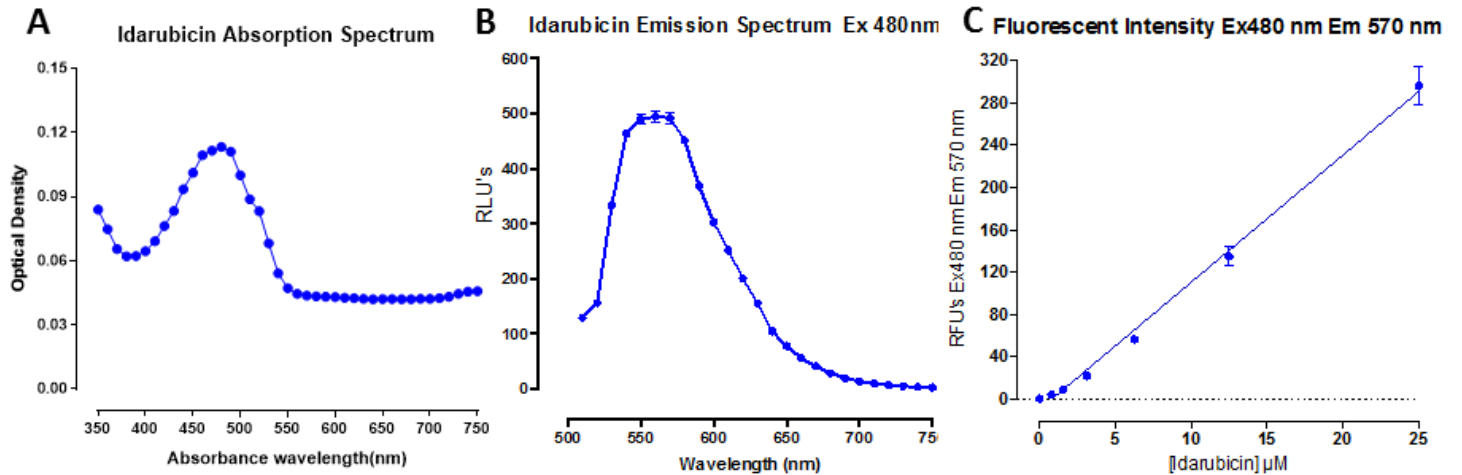
Each of the maximum (200 μM doxorubicin) and minimum (0.5% DMSO) plate controls conducted on the same assay microplates. The present the mean \pm SD ($n=3$) of triplicates of these three independent experiments.

3.2 ABSORPTION AND EMISSION SPECTRUM OF COMPOUNDS IN SOLUTION

Fluorescent molecules absorb radiation at specific wavelengths to reach excited states and after energy is dissipated by the system, the molecule releases energy as a longer wavelength fluorescence emission. To determine the optimal excitation (Ex) and emission (Em) wavelengths of ellipticine, idarubicin, daunorubicin and doxorubicin, we dissolved the compounds in PBS and performed 10 nm wavelength scans to measure their absorption and emission spectra on the M5e plate reader. The absorption spectra of the 4 compounds dissolved in PBS at 25 μM were measured to select a suitable excitation wavelength for each compound (Figure 8, Figure 9, Figure 10 & Figure 11). The three structurally related anthracycline compounds idarubicin, daunorubicin and doxorubicin (Figure 1) had very similar absorption spectra with a broad absorption peak between 400 and 550 nm (Figure 8, Figure 9 & Figure 10). In contrast, ellipticine did not exhibit an obvious

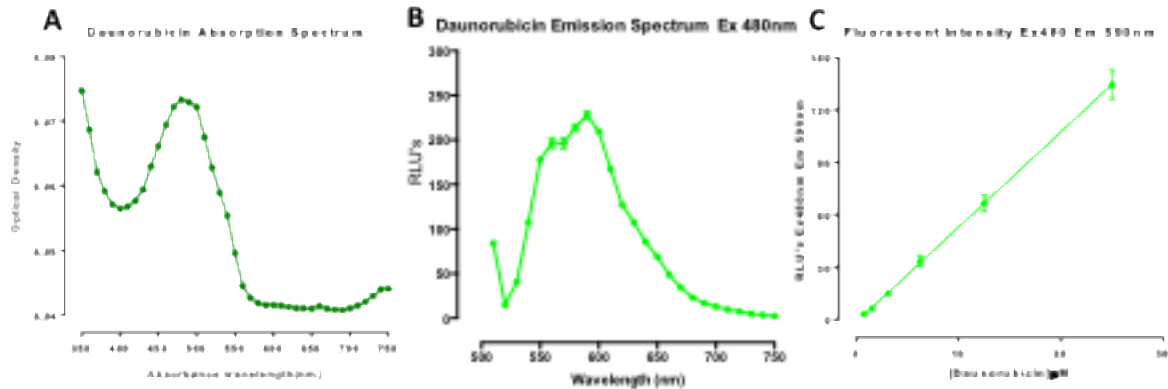
absorption peak between 350 and 750 nm (Figure 11). Based on the absorption spectra of idarubicin, daunorubicin and doxorubicin we selected an Ex wavelength of 480 nm to perform a 10nm fluorescence emission spectral scan for these compounds (Figure 8, Figure 9 & Figure 10). When excited at 480 nm all three structurally related anthracycline compounds idarubicin, daunorubicin and doxorubicin (Figure 1) produced very similar emission spectra with a broad emission peak between 520 and 650 nm (Figure 8, Figure 9 & Figure 10). Consistent with its lack of absorption at 480 nm, ellipticine failed to produce a fluorescent emission spectrum when excited at 480 nm (Figure 11). The relative fluorescent intensity values (RFUs) of idarubicin (Ex 480, Em 570 nm), daunorubicin (Ex 480, Em 590 nm), and doxorubicin (Ex 480, Em 590 nm) increased linearly with respect to compound concentration (Figure 8, Figure 9 & Figure 10). In contrast, the relative fluorescent intensity values (RFUs) of ellipticine (Ex 480, Em 590 nm) were zero at all concentrations (Figure 11). Based on the linear relationship between the fluorescent intensity RFUs produced by idarubicin, daunorubicin and doxorubicin and their concentrations in solution, we conclude that the fluorescent intensity values of these 3 compounds can be used to infer the relative concentrations of these drugs within cells.

Figure 8 Idarubicin (A) Absorption spectrum of 20 μ M idarubicin in PBS; (B) Fluorescent emission spectrum of 20 μ M idarubicin in PBS Ex. 480 nm; (C) Fluorescent intensity of different concentrations of idarubicin in PBS, Ex 480 nm & Em. 570 nm.



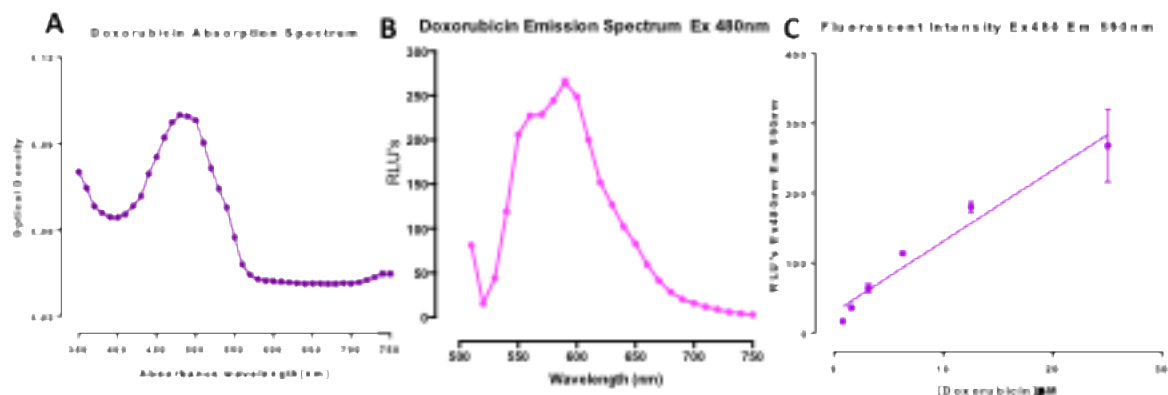
(A) 20 μ M of idarubicin was added to the wells of a 384-well assay microplate in 50 μ L PBS per well, and the absorption spectrum was acquired on a SpectraMax® M5e multi-mode microplate reader. (B) Using an excitation wavelength of 480 nm the fluorescence emission spectrum was then acquired on the M5e. (C) The relative fluorescence intensity units (RFU's) of 25, 12.5, 6.25, 3.125, 1.5625 and 0.78125 μ M idarubicin at Ex. 480 nm and Em 570 nm was then acquired on the M5e. There were three replicate wells (n=3) for each idarubicin concentration and the mean RFU's \pm SD of the triplicates are presented.

Figure 9 *Daunorubicin* (A) Absorption spectrum of 20 μ M daunorubicin in PBS; (B) Fluorescent emission spectrum of 20 μ M daunorubicin in PBS Ex. 480 nM; (C) Fluorescent intensity of different concentrations of daunorubicin in PBS, Ex 480 nm & Em. 590 nm.



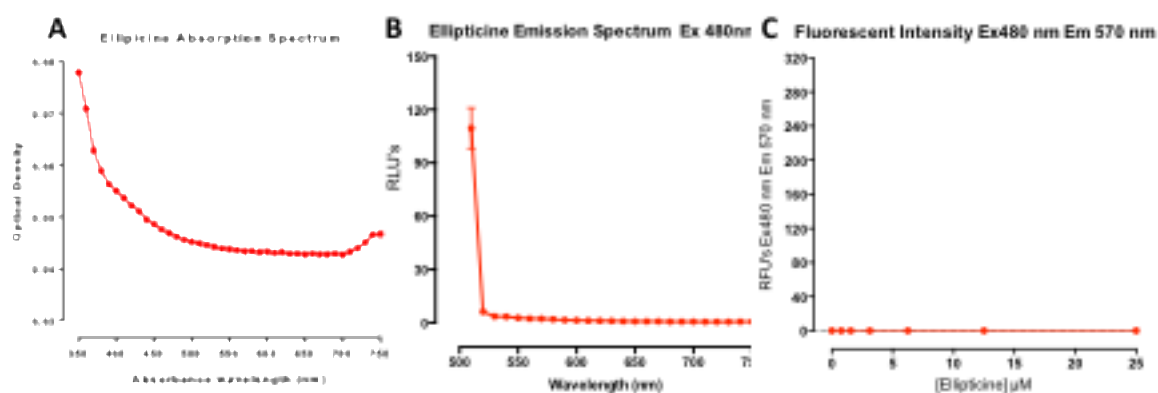
(A) 20 μ M of daunorubicin was added to the wells of a 384-well assay microplate in 50 μ L PBS per well, and the absorption spectrum was acquired on a SpectraMax® M5e multi-mode microplate reader. (B) Using an excitation wavelength of 480 nm the fluorescence emission spectrum was then acquired on the M5e. (C) The relative fluorescence intensity units (RFU's) of 25, 12.5, 6.25, 3.125, 1.5625 and 0.78125 μ M daunorubicin at Ex. 480 nm and Em 590 nm was then acquired on the M5e. There were three replicate wells (n=3) for each daunorubicin concentration and the mean RFU's \pm SD of the triplicates are presented.

Figure 10 Doxorubicin (A) Absorption spectrum of 20 μ M doxorubicin in PBS; (B) Fluorescent emission spectrum of 20 μ M doxorubicin in PBS Ex. 480 nm; (C) Fluorescent intensity of different concentrations of doxorubicin in PBS, Ex 480 nm & Em. 590 nm.



(A) 20 μ M of doxorubicin was added to the wells of a 384-well assay microplate in 50 μ L PBS per well, and the absorption spectrum was acquired on a SpectraMax® M5e multi-mode microplate reader. (B) Using an excitation wavelength of 480 nm the fluorescence emission spectrum was then acquired on the M5e. (C) The relative fluorescence intensity units (RFU's) of 25, 12.5, 6.25, 3.125, 1.5625 and 0.78125 μ M doxorubicin at Ex. 480 nm and Em 590 nm was then acquired on the M5e. There were three replicate wells (n=3) for each doxorubicin concentration and the mean RFU's \pm SD of the triplicates are presented.

Figure 11 Ellipticine (A) Absorption spectrum of 20 μ M ellipticine in PBS; (B) Fluorescent emission spectrum of 20 μ M ellipticine in PBS Ex. 480 nm; (C) Fluorescent intensity of different concentrations of ellipticine in PBS, Ex 480 nm & Em. 570 nm.



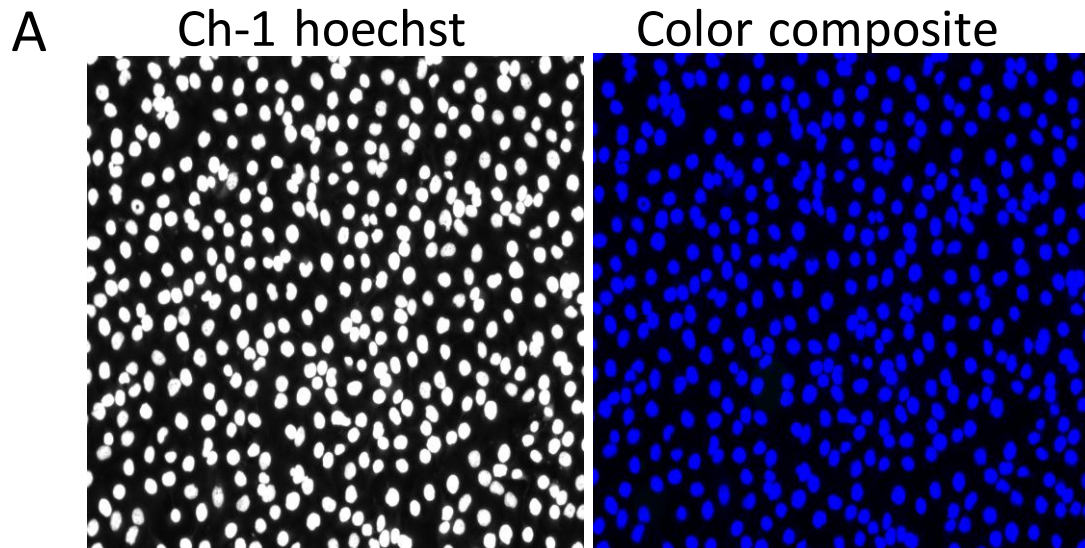
(A) 20 μ M of ellipticine was added to the wells of a 384-well assay microplate in 50 μ L PBS per well, and the absorption spectrum was acquired on a SpectraMax® M5e multi-mode microplate reader. (B) Using an excitation wavelength of 480 nm the fluorescence emission spectrum was then acquired on the M5e. (C) The relative fluorescence intensity units (RFU's) of 25, 12.5, 6.25, 3.125, 1.5625 and 0.78125 μ M ellipticine at Ex. 480 nm and Em 570 nm was then acquired on the M5e. There were three replicate wells (n=3) for each ellipticine concentration and the mean RFU's \pm SD of the triplicates are presented.

3.3 COMPOUND PENETRATION IN 2D AND 3D CAL33 HNSCC CELL CULTURE MODELS

3.3.1 IMAGES AND CONCENTRATION DEPENDENT PENETRATION OF 2D AND 3D CULTURES

We first investigated the concentration dependent penetration of ellipticine, idarubicin, daunorubicin and doxorubicin into 2D Cal33 cell cultures. Cal33 cells that had been seeded into normal tissue culture assay plates were cultured overnight and then exposed to the indicated concentrations of the 4 compounds for 15-min. The 2D cell cultures were then fixed in 3.7% formaldehyde containing Hoechst-33342 for 45 min, and then washed by repeated aspiration and rinsing with PBS. We then utilized the IXM automated imaging system to acquire images sequentially in Ch 1 Hoechst (blue), Ch 2 FITC (green) and Ch 3 TRITC (red) fluorescent channels. Hoechst 33342 DNA staining in Ch 1 was used to identify the nuclei of Cal33 cells in 2D cell cultures. The color composite overlays of the Ch 1, Ch 2 and Ch 3 fluorescent images of Hoechst stained nuclei are predominantly blue, which indicates that the Hoechst staining only fluoresces in Ch 1 (Figure 12).

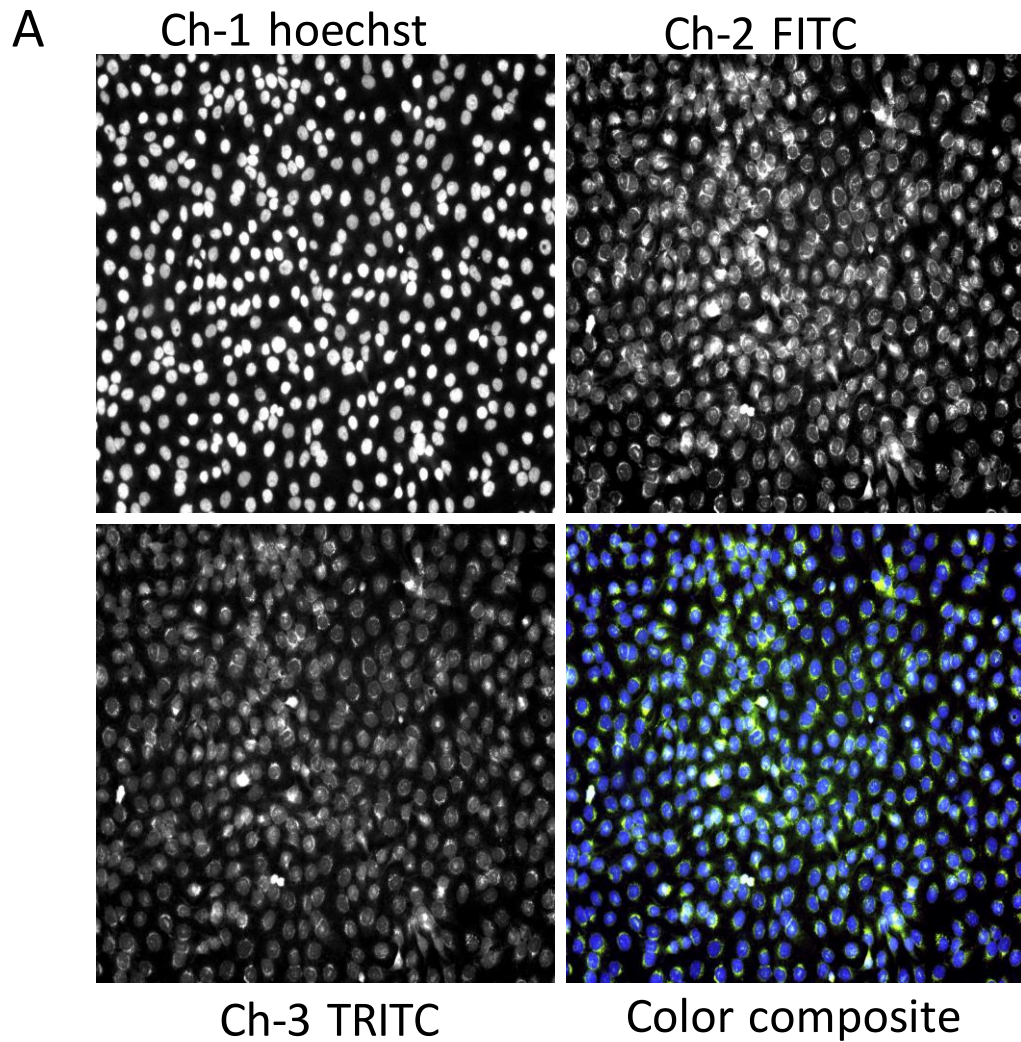
Figure 12 *Grayscale and color composite images of 2D Cal33 HNSCC cells stained with Hoechst 33342. (A) Greyscale images of Hoechst 33342-stained nuclei (Ch 1), greyscale images of idarubicin-treated (Ch 2, Ch 3) and color composite images of Ch 1, Ch 2 and Ch 3 Cal33 HNSCC cells.*



Normal tissue culture microplates were seeded by 1000 Cal33 HNSCC cells per well as previously described. The 2D microplate was fixed and stained in 3.7% formaldehyde containing Hoechst- and then washed by repeated aspiration and rinsing with PBS after the 45-min fixation. Images were then acquired on the IXM High-Content Analysis System and analyzed using the MWCS image analysis module. The images presented are representative of similar images obtained in at least 3 independent experiments.

Fluorescent images in Ch2 (FITC) and Ch3 (TRITC) of 2D Cal33 cell cultures exposed to idarubicin produced strong fluorescent signals, and the color composite images showed a combination of blue (Hoechst staining), together with strong green and red signals that was predominantly yellow (Figure 13).

Figure 13 Grayscale and color composite images of 2D Cal33 HNSCC cells + idarubicin treatment. (A) Grayscale images of Hoechst 33342-stained nuclei (Ch 1), grayscale images of idarubicin-treated (Ch 2, Ch 3) and color composite images of Ch 1, Ch 2 and Ch 3 Cal33 HNSCC cells.

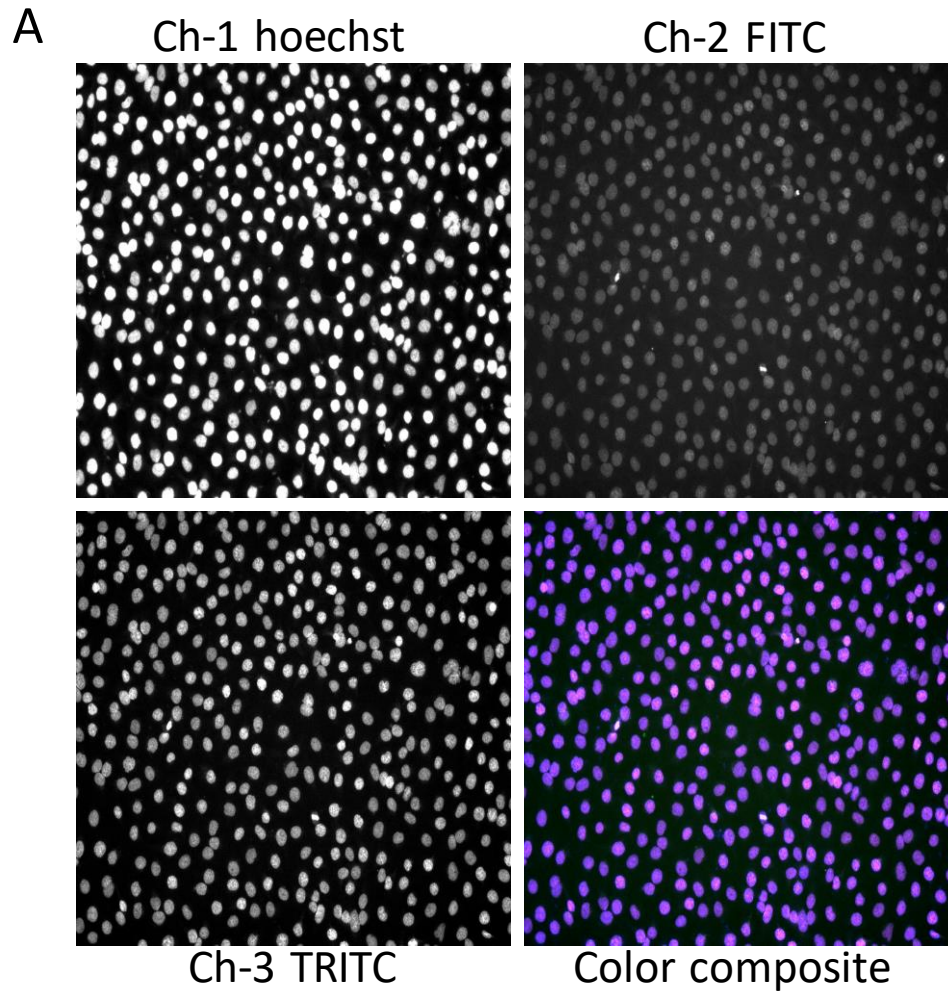


Normal tissue culture microplates were seeded by 1000 Cal33 HNSCC cells per well as previously described. 5 μ L of idarubicin were added into wells with indicated concentration. After 15 min incubation at 37 $^{\circ}$ C, 5% CO₂ The 2D microplate was fixed and stained in 3.7% formaldehyde containing Hoechst-33342. The 2D microplates were

washed by PBS for three times after the 45-min fixation. Images were then acquired on the IXM High-Content Analysis System and analyzed using the MWCS image analysis module. The images presented are representative of similar images obtained in at least 3 independent experiments.

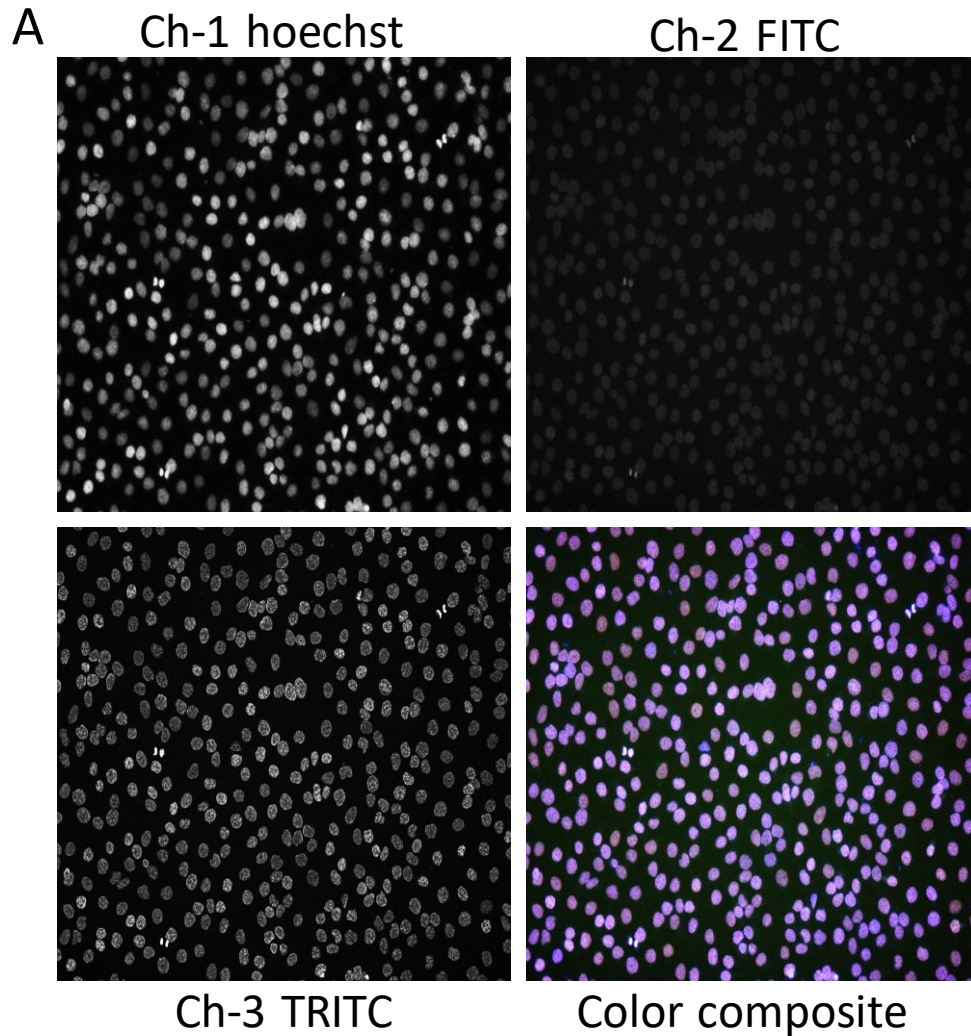
The images indicate that idarubicin fluorescence can be detected in 2D Cal33 cells in both the green (Ch 2) and red (Ch 3) channels and that the Hoechst fluorescent signal (Ch1) appeared to be significantly less intense than in cells that were not exposed to compounds (Compare Figure 13 to Figure 12). Daunorubicin and doxorubicin-exposed cells were also fluorescent in the images from the green (Ch 2) and red (Ch 3) channels but the red signal predominates making the color composite image purple due to the blue (Hoechst staining) and strong red signal (Figure 14 & Figure 15). The Hoechst fluorescent signal (Ch1) appeared to be significantly less intense in 2D Cal33 cells that were exposed to daunorubicin and doxorubicin compared to cells that were not exposed to compounds (Compare Figure 14 & Figure 15 to Figure 12).

Figure 14 Grayscale and color composite images of 2D Cal33 HNSCC cells + daunorubicin treatment. (A) Greyscale images of Hoechst 33342-stained nuclei (Ch 1), greyscale images of daunorubicin-treated (Ch 2, Ch 3) and color composite images of Ch 1, Ch 2 and Ch 3 Cal33 HNSCC cells.



Normal tissue culture microplates were seeded by 1000 Cal33 HNSCC cells per well as previously described. 5 μ L of daunorubicin were added into wells with indicated concentration. After 15 min incubation at 37°C, 5% CO₂ The 2D microplate was fixed and stained in 3.7% formaldehyde containing Hoechst-33342. The 2D microplates were washed by PBS for three times after the 45-min fixation. Images were then acquired on the IXM High-Content Analysis System and analyzed using the MWCS image analysis module. The images presented are representative of similar images obtained in at least 3 independent experiments.

Figure 15 Grayscale and color composite images of 2D Cal33 HNSCC cells + doxorubicin treatment. (A) Greyscale images of Hoechst 33342-stained nuclei (Ch 1), greyscale images of doxorubicin-treated (Ch 2, Ch 3) and color composite images of Ch 1, Ch 2 and Ch 3 Cal33 HNSCC cells.

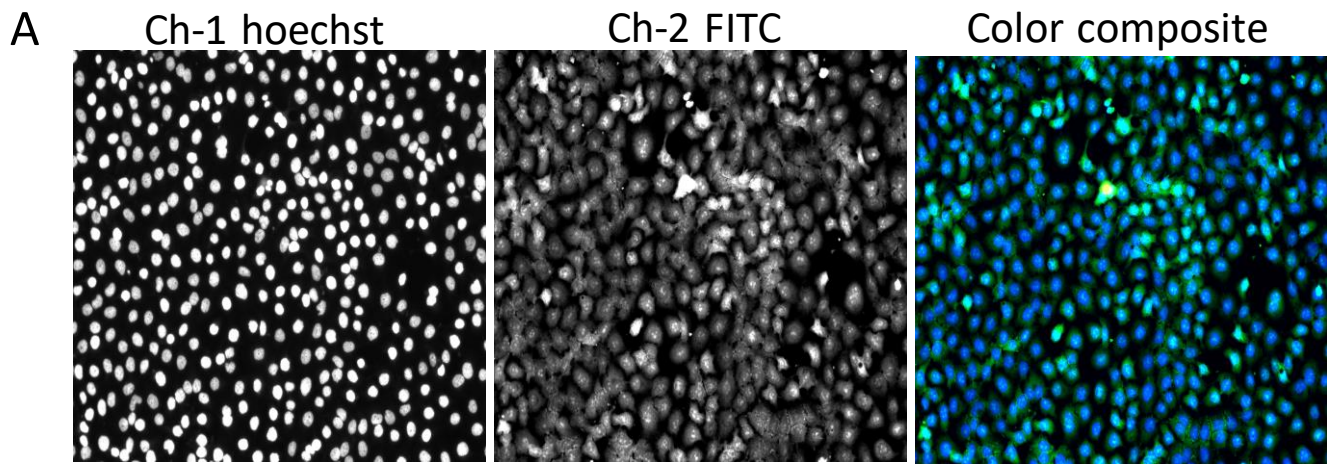


Normal tissue culture microplates were seeded by 1000 Cal33 HNSCC cells per well as previously described. 5 μ L of doxorubicin were added into wells with indicated concentration. After 15 min incubation at 37°C, 5% CO₂ The 2D microplate was fixed and stained in 3.7% formaldehyde containing Hoechst-33342. The 2D microplates were washed by PBS for three times after the 45-min fixation. Images were then acquired on the IXM High-Content Analysis System and analyzed using the MWCS image analysis module. The images presented are representative of similar images obtained in at least 3 independent experiments.

In addition to inhibition of topoisomerase II activity, the anthracycline compounds intercalate with DNA/RNA and it may be that they compete with Hoechst for the same DNA binding sites and thereby reduce the Hoechst fluorescent signal relative to cells that were not exposed to compounds. For idarubicin, daunorubicin and doxorubicin the location of the fluorescent signal is predominantly nuclear, although idarubicin also appears to have a strong perinuclear distribution (Figure 13, Figure 14 & Figure 15)

Interestingly, although the fluorescence of ellipticine cannot be detected directly when dissolved in PBS, the compound has previously been shown to be fluorescent within cells[60, 61] (Figure 16). It may be that ellipticine becomes fluorescent after it intercalates with DNA or ellipticine-DNA adducts are formed. Fluorescent images of 2D Cal33 exposed to ellipticine exhibited strong fluorescent signals in the green channel (Ch2, FITC), and the color composite images showed a combination of blue (Hoechst staining) together with a strong green signal (Figure 16). Interestingly the ellipticine fluorescence was located throughout the cells and the Hoechst-33342 stained DNA images were similar to cells not exposed to compounds (*Compare Figure 16 to Figure 12*).

Figure 16 *Grayscale and color composite images of 2D Cal33 HNSCC cells + ellipticine treatment. (A) Grayscale images of Hoechst 33342-stained nuclei (Ch 1), grayscale images of ellipticine-treated (Ch 2) and color composite images of Ch 1 and Ch 2 Cal33 HNSCC cells.*

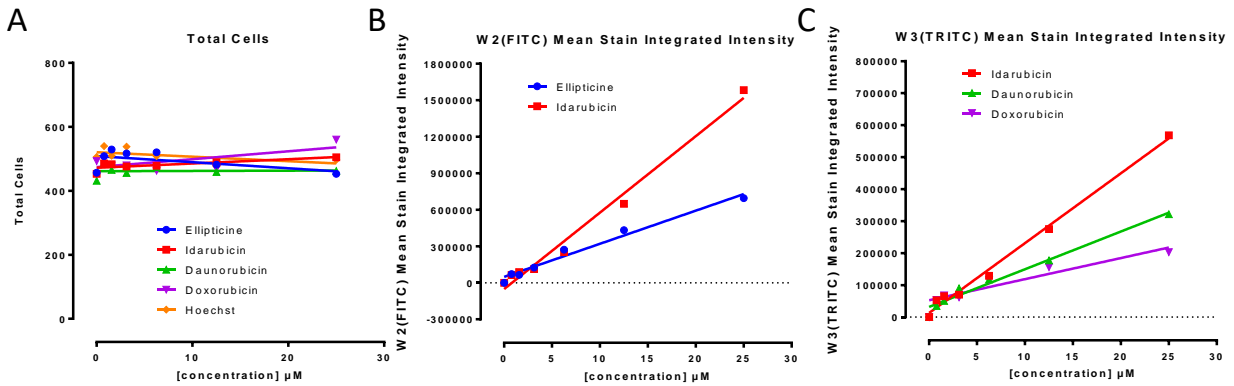


Normal tissue culture microplates were seeded by 1000 Cal33 HNSCC cells per well as previously described. 5 μ L of ellipticine were added into wells with indicated concentration. After 15 min incubation at 37 °C, 5% CO₂ The 2D microplate was fixed and stained in 3.7% formaldehyde containing Hoechst-33342. The 2D microplates were washed by PBS for three times after the 45-min fixation. Images were then acquired on the IXM High-Content Analysis System and analyzed using the MWCS image analysis module. The images presented are representative of similar images obtained in at least 3 independent experiments.

To extract and analyze quantitative data from the digital images, we utilized the multi-wavelength cell scoring (MWCS) image analysis module of the MetaXpress software on the IXM platform. The algorithm uses the Hoechst DNA stain to identify cell nuclei, create a nuclear mask, and count cells. The algorithm then uses the nuclear mask and user set thresholds in the FITC (Ch2, green) and TRITC (Ch3, red) channels to create a cell mask and outputs the average and integrated fluorescent intensity signals from within the cell masks. Figure 17 portrays the

integrated fluorescent intensity measurements obtained in 2D Cal33 cell cultures exposed to the indicated concentrations of ellipticine, idarubicin, daunorubicin, and doxorubicin for 15 min. We used the number of Hoechst stained objects in Ch1 to count the number of cells that were analyzed in the acquired images and demonstrated that the cell counts were consistent for 2D Cal33 cultures exposed to the indicated concentrations of the 4 compounds (up to 25 μ M), and that the fluorescent signals obtained were from the same cell numbers (Figure 17). *Figure 17B* shows the integrated fluorescent intensities (RFUs) extracted from Ch2 (FITC, green) images of 2D Cal33 cultures after exposure to the indicated concentrations of ellipticine or idarubicin. The integrated RFUs for ellipticine and idarubicin increased linearly with respect to compound concentration. Figure 17 shows the integrated (RFUs) extracted from Ch3 (TRITC, red) images of 2D Cal33 cultures after exposure to the indicated concentrations of idarubicin, daunorubicin and doxorubicin. The RFUs for idarubicin, daunorubicin and doxorubicin increased linearly with respect to compound concentration. The linear correlation of the RFUs with the concentrations of idarubicin, daunorubicin and doxorubicin (Figure 17), is consistent with the linear correlation observed between the RFU's and compound concentrations in solution (Figure 8, Figure 9 & Figure 10).

Figure 17 Fluorescent intensity of 2D Cal33 cells seeded at 1000 cells/well and exposed to the indicated concentrations of the 4 compounds. Fluorescent intensity in 2D cell cultures from (A) Ch-1 Hoechst; (B) Ch-2 FITC; (C) Ch-3 TRITC.

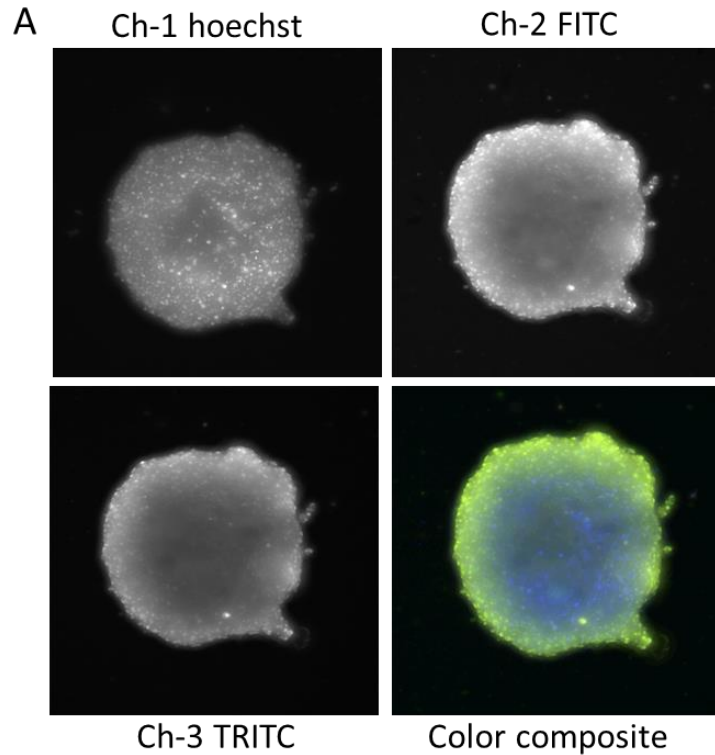


Normal tissue culture microplates were seeded at 1000 cells/well of Cal33 HNSCC cells. Cell monolayers were exposed to the indicated concentrations of ellipticine, idarubicin, daunorubicin and doxorubicin for 15 min. 2D Cal33 monolayers were fixed and stained in 3.7% Formaldehyde and Hoechst 33342. Fluorescent intensities of 4 compounds were acquired on IXM and analyzed using the MWCS image analysis module. Each concentration well was in triplicates and the assay was repeated at least three times. R-square of linear regression for ellipticine and idarubicin in Ch 2 is 0.7489 and 0.9546, respectively. R-square of linear regression for idarubicin, daunorubicin and doxorubicin in Ch 3 is 0.9744, 0.9726 and 0.7998, respectively. The data represent the mean \pm SD of triplicates determination from one of these independent experiments,

Then we conducted experiments to determine the concentration dependent penetration of ellipticine, idarubicin, daunorubicin and doxorubicin into 3D Cal33 tumor spheroids. Cal33 cells that had been seeded into 384-well ULA microplates were cultured overnight and then exposed to the indicated concentrations of the 4 compounds for 15-min. The 3D tumor spheroids were then fixed in 3.7% formaldehyde containing Hoechst-33342 for 45 min, and then washed by repeated

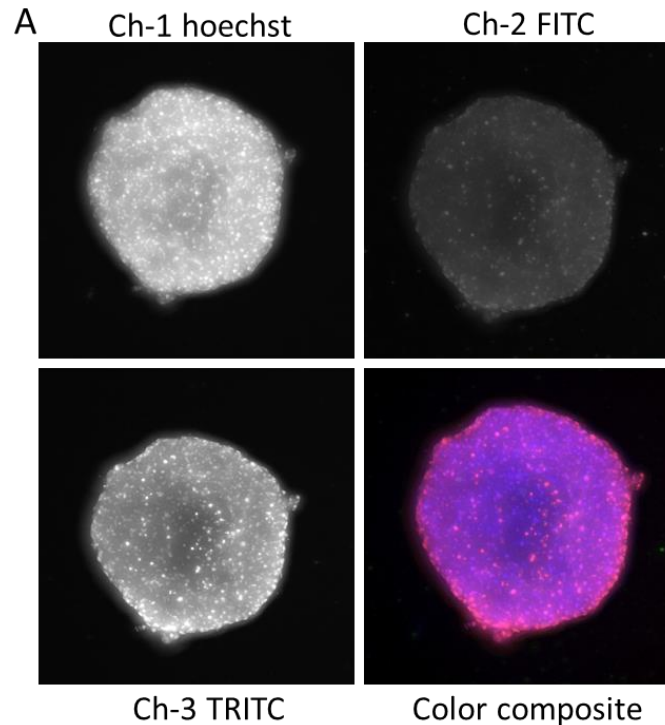
aspiration and rinsing with PBS on JANUS MDT automated lipid handling workstation. We then utilized the IXM automated imaging system to acquire images sequentially in Ch 1 Hoechst (blue), Ch 2 FITC (green) and Ch 3 TRITC (red) fluorescent channels. Hoechst 33342 DNA staining in Ch 1 was used to identify the nuclei of Cal33 cells and to define a mask of the in 3D tumor spheroids. Similar to the results in 2D cell cultures, fluorescent images in Ch2 (FITC) and Ch3 (TRITC) of 2D Cal33 cell cultures exposed to idarubicin produced strong fluorescent signals in Ch2 and Ch3, and the color composite images showed a combination of blue (Hoechst staining), together with strong green and red signals that were predominantly yellow (Figure 18).

Figure 18 Grayscale and color composite images of 3D Cal33 HNSCC tumor spheroids + idarubicin treatment. (A) Greyscale images of Hoechst 33342-stained nuclei (Ch 1), greyscale images of idarubicin-treated (Ch 2 and Ch 3) and color composite images of Ch 1, Ch 2 and Ch 3 Cal33 HNSCC cells.



384-well ULA microplates were seeded by 5000 cells per well of Cal33 HNSCC cells. 5 μ L of idarubicin were added into wells with indicated concentration. After 15 min incubation at 37°C, 5% CO₂ The 2D microplate was fixed and stained in 3.7% formaldehyde containing Hoechst-33342. The ULA microplates were washed by PBS for three times after the 45-min fixation. Images were then acquired on the IXM High-Content Analysis System and analyzed using MWCS image analysis module. The images are presented are representative of similar images obtained in at least 3 independent experiments.

Figure 19 Grayscale and color composite images of 3D Cal33 HNSCC tumor spheroids + daunorubicin treatment. (A) Greyscale images of Hoechst 33342-stained nuclei (Ch 1), greyscale images of daunorubicin-treated (Ch 2 and Ch 3) and color composite images of Ch 1, Ch 2 and Ch 3 Cal33 HNSCC cells.



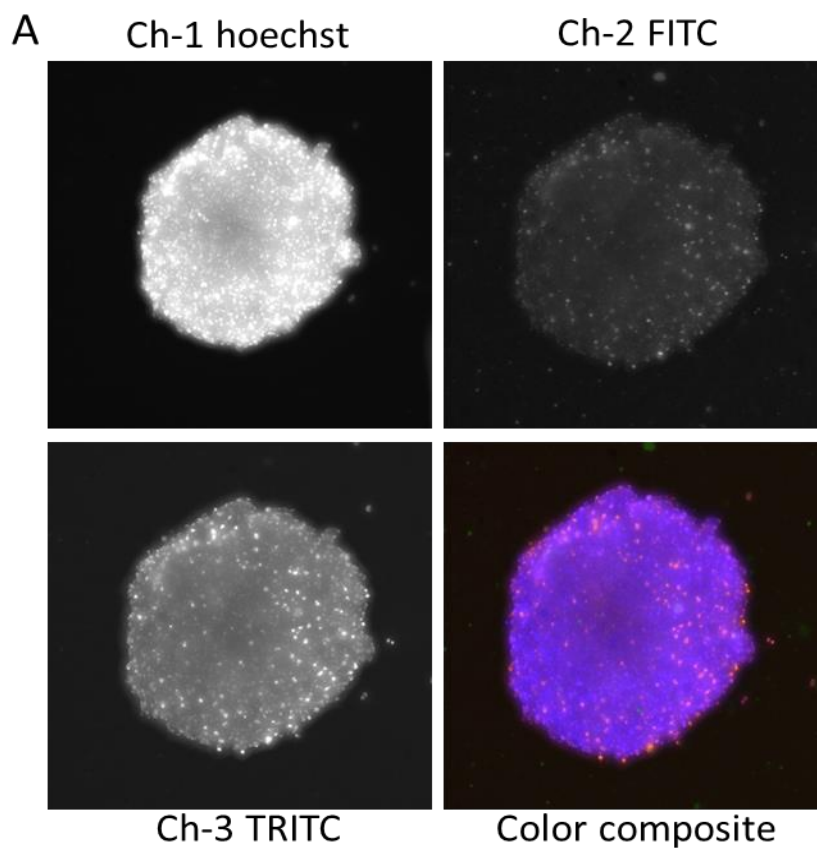
384-well ULA microplates were seeded by 5000 cells per well of Cal33 HNSCC cells. 5 μ L of daunorubicin were added into wells with indicated concentration. After 15 min incubation at 37 $^{\circ}$ C, 5% CO₂ The 2D microplate was fixed and stained in 3.7% formaldehyde containing Hoechst-33342. The ULA microplates were washed by PBS for three times after the 45-min fixation. Images were then acquired on the IXM High-Content Analysis System and analyzed using MWCS image analysis module. The images are presented are representative of similar images obtained in at least 3 independent experiments.

Daunorubicin and doxorubicin-exposed 3D tumor spheroids were also fluorescent in the images from the green (Ch 2) and red (Ch 3) channels but the red signal predominates making the

color composite images of the spheroids purple due to the blue (Hoechst staining) and strong red signal (Figure 19 & Figure 20).

Figure 20 *Grayscale and color composite images of 3D Cal33 HNSCC tumor spheroids + doxorubicin treatment.*

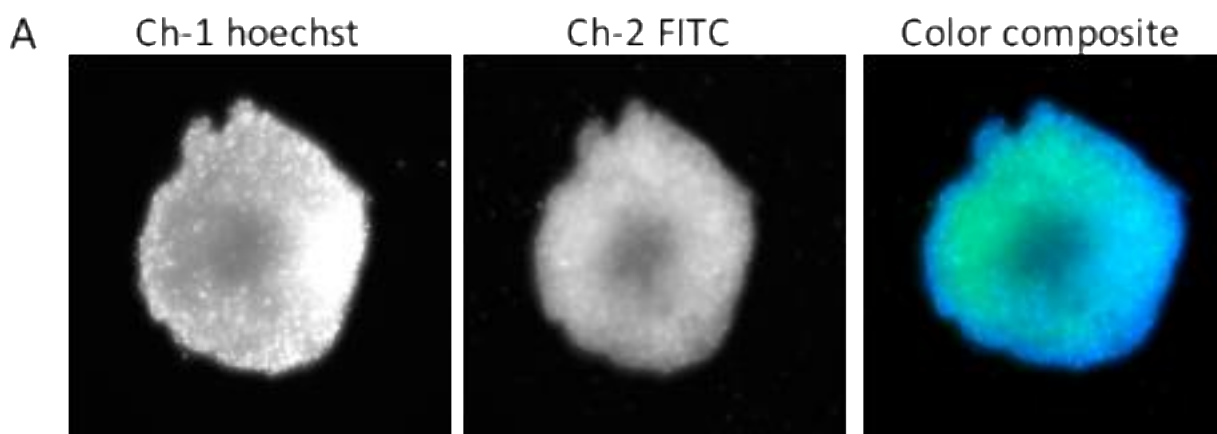
(A) Greyscale images of Hoechst 33342-stained nuclei (Ch 1), greyscale images of doxorubicin-treated (Ch 2 and Ch 3) and color composite images of Ch 1, Ch 2 and Ch 3 Cal33 HNSCC cells.



384-well ULA microplates were seeded by 5000 cells per well of Cal33 HNSCC cells. 5 μ L of doxorubicin were added into wells with indicated concentration. After 15 min incubation at 37 $^{\circ}$ C, 5% CO₂ The 2D microplate was fixed and stained in 3.7% formaldehyde containing Hoechst-33342. The ULA microplates were washed by PBS for three times after the 45-min fixation. Images were then acquired on the IXM High-Content Analysis System and analyzed using MWCS image analysis module. The images are presented are representative of similar images obtained in at least 3 independent experiments.

Also, the fluorescence images of 3D tumor spheroids exposed to ellipticine are shown in Figure 21. These images exhibited strong fluorescent signals in the green channel (Ch2, FITC), and the color composite images showed a combination of blue (Hoechst staining) together with a strong green signal (Figure 21).

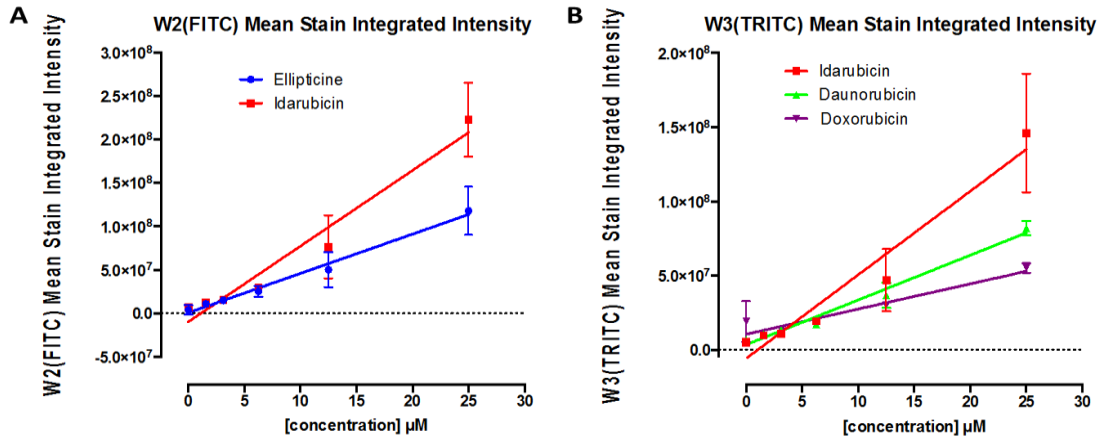
Figure 21 *Grayscale and color composite images of 3D Cal33 HNSCC tumor spheroids + ellipticine treatment. (A) Grayscale images of Hoechst 33342-stained nuclei (Ch 1), grayscale images of ellipticine-treated (Ch 2) and color composite images of Ch 1 and Ch 2 Cal33 HNSCC cells.*



384-well ULA microplates were seeded by 5000 cells per well of Cal33 HNSCC cells. 5 μ L of ellipticine were added into wells with indicated concentration. After 15 min incubation at 37 °C, 5% CO₂ The 2D microplate was fixed and stained in 3.7% formaldehyde containing Hoechst-33342. The ULA microplates were washed by PBS for three times after the 45-min fixation. Images were then acquired on the IXM High-Content Analysis System and analyzed using MWCS image analysis module. The images are presented are representative of similar images obtained in at least 3 independent experiments.

Fluorescent intensity values were quantified from images of 3D Cal33 tumor spheroids exposed to the indicated concentrations of ellipticine, idarubicin, daunorubicin and doxorubicin. The algorithm uses the Hoechst DNA stain to create a spheroid mask in order to define the outline and area of the 3D spheroid. The algorithm then uses the spheroid mask and user set thresholds in the FITC (Ch2, green) and TRITC (Ch3, red) channels to create a spheroid mask in each channel and outputs the average and integrated fluorescent intensity signals from within the spheroid masks. Figure 22 portrays the integrated fluorescent intensity measurements obtained in the images of 3D tumor spheroids exposed to the indicated concentrations of ellipticine, idarubicin, daunorubicin, and doxorubicin for 15 min. These data show the integrated RFUs for ellipticine, idarubicin, daunorubicin and doxorubicin increased linearly with respect to compound concentration (Figure 22). The linear correlation of the RFUs and the concentrations of idarubicin, daunorubicin and doxorubicin added to 3D tumor spheroids (Figure 22), is consistent with the linear relationship observed in 2D cell cultures (Figure 17) and compounds in solution (Figure 8, Figure 9 & Figure 10).

Figure 22 Fluorescent intensity of 3D Cal33 spheroids seeded 5000 cells/well and exposed to the indicated concentrations of the 4 compounds. Fluorescent intensity in 3D Cal33 spheroids from (A) Ch-1 Hoechst; (B) Ch-2 FITC; (C) Ch-3 TRITC.

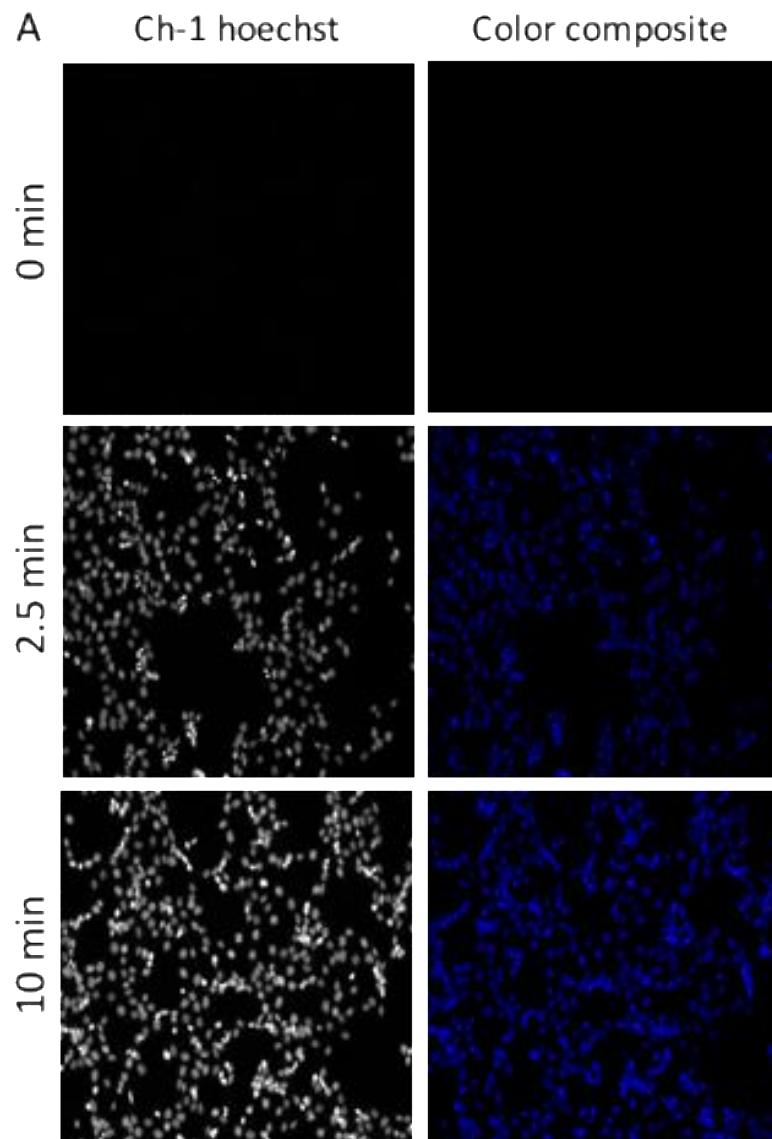


384-well ULA microplates were seeded by 5000 Cal33 HNSCC cells per well as previously described. 5 μL of ellipticine were added into wells with indicated concentration. After 15 min incubation at 37 $^{\circ}\text{C}$, 5% CO_2 The 3D microplate was fixed by adding 50 μL of 37% formaldehyde containing Hoechst-33342. The 3D microplates were washed by PBS for three times after the 45-min fixation. Images were then acquired on the ImageXpress Micro (IXM) High-Content Analysis System and analyzed. The images presented are representative of similar images obtained in at least 3 independent experiments. The quantitative data presented were extracted from the digital images using MWCS image analysis module. R-square of linear regression for ellipticine and idarubicin in Ch 2 is 0.9251 and 0.9199, respectively. R-square of linear regression for idarubicin, daunorubicin and doxorubicin in Ch 3 is 0.8908, 0.9710 and 0.8570, respectively. The data represent the mean \pm SD of triplicates determination from one of these independent experiments.

3.3.2 TIME DEPENDENT PENETRATION OF 2D AND 3D CULTURES

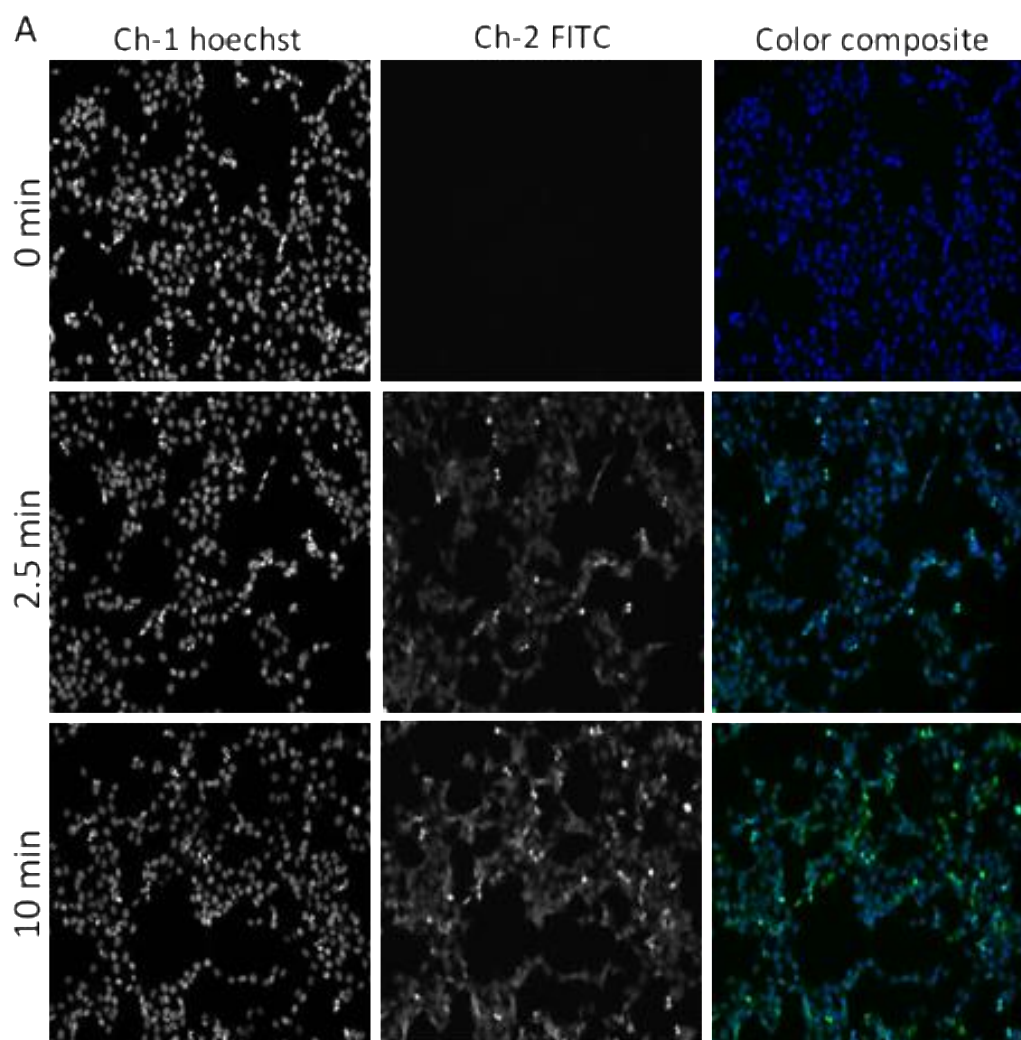
To evaluate the time dependent penetration of ellipticine, idarubicin, daunorubicin and doxorubicin in 2D cell cultures assays, we exposed Cal33 HNSCC cells seeded in 2D cell cultures to 10 μ M of four compounds for the indicated time period. The 2D cell cultures were then fixed in 3.7% formaldehyde containing Hoechst-33342 for 45 min, and then washed by repeated aspiration and rinsing with PBS. We then utilized the IXM automated imaging system to acquire images sequentially in Ch 1 Hoechst (blue), Ch 2 FITC (green) and Ch 3 TRITC (red) fluorescent channels. Hoechst 33342 DNA staining in Ch 1 was used to identify the nuclei of Cal33 cells in 2D cell cultures. The color composite overlays of the Ch 1, Ch 2 and Ch 3 fluorescent images of Hoechst stained nuclei are predominantly blue, which indicates that the Hoechst staining only fluoresces in Ch 1 (Figure 23).

Figure 23 Selected grayscale and color composite images of 2D Cal33 HNSCC cell culture + Hoechst staining for indicated exposure time. (A) Greyscale images of Hoechst 33342-stained nuclei (Ch 1) and color composite images of Ch 1, Ch 2 and Ch 3 Cal33 HNSCC cells.



Normal tissue culture microplates were seeded by 1000 Cal33 HNSCC cells per well as previously described. The 2D microplates were fixed in 3.7% formaldehyde. The 2D microplates were washed by PBS for three times after the 45-min fixation. Images were then acquired on the ImageXpress Micro (IXM) High-Content Analysis System and analyzed using MWCS image analysis module. The images presented are representative of similar images obtained in at least 3 independent experiments.

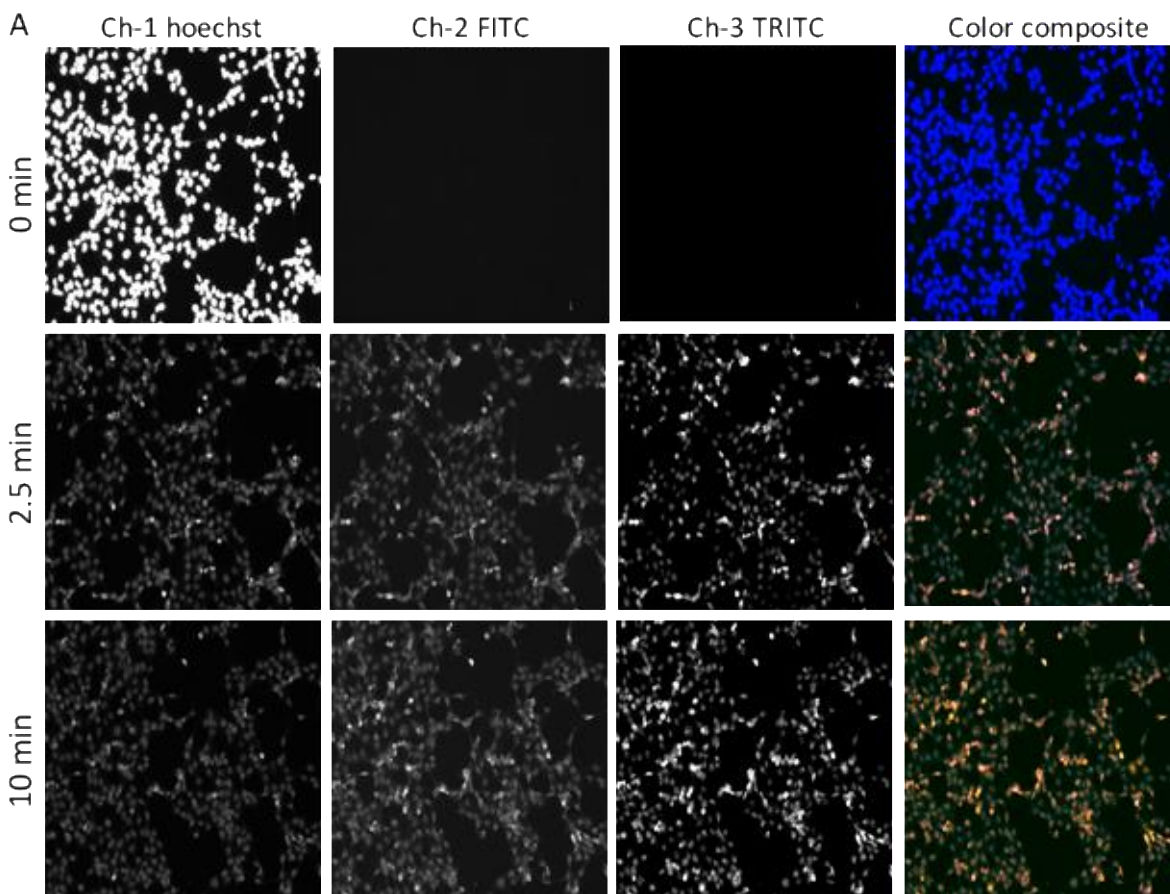
Figure 24 Greyscale and color composite images of 2D Cal33 HNSCC cell culture + ellipticine treatment for indicated exposure time. (A) Greyscale images in Ch 1, greyscale images of ellipticine-treated in Ch 2 and color composite images of Ch 1, Ch 2 and Ch 3 Cal33 HNSCC cells.



Normal tissue culture microplates were plated by Cal33 HNSCC cells as previously described. 5 μ L of ellipticine were added into wells at 0, 2.5 and 10 min time points. The 2D microplate was fixed and stained in 3.7% Formaldehyde and Hoechst. Images were acquired on the ImageXpress Micro(IXM) High-Content Analysis System and analyzed using MWCS image analysis module. Each concentration was in triplicates and the assay was repeated at least three times.

Fluorescent images in Ch2 of 2D Cal33 cell cultures exposed to ellipticine produced strong fluorescent signals, and the color composite images showed a combination of blue (Hoechst staining), together with strong green and red signals that was predominantly yellow (Figure 24).

Figure 25 *Grayscale and color composite images of 2D Cal33 HNSCC cell culture + idarubicin treatment for indicated exposure time. (A) Greyscale images of Hoechst 33342-stained nuclei (Ch 1), greyscale images of idarubicin-treated (Ch 2 and Ch 3) and color composite images of Ch 1 and Ch 2 Cal33 HNSCC cells.*

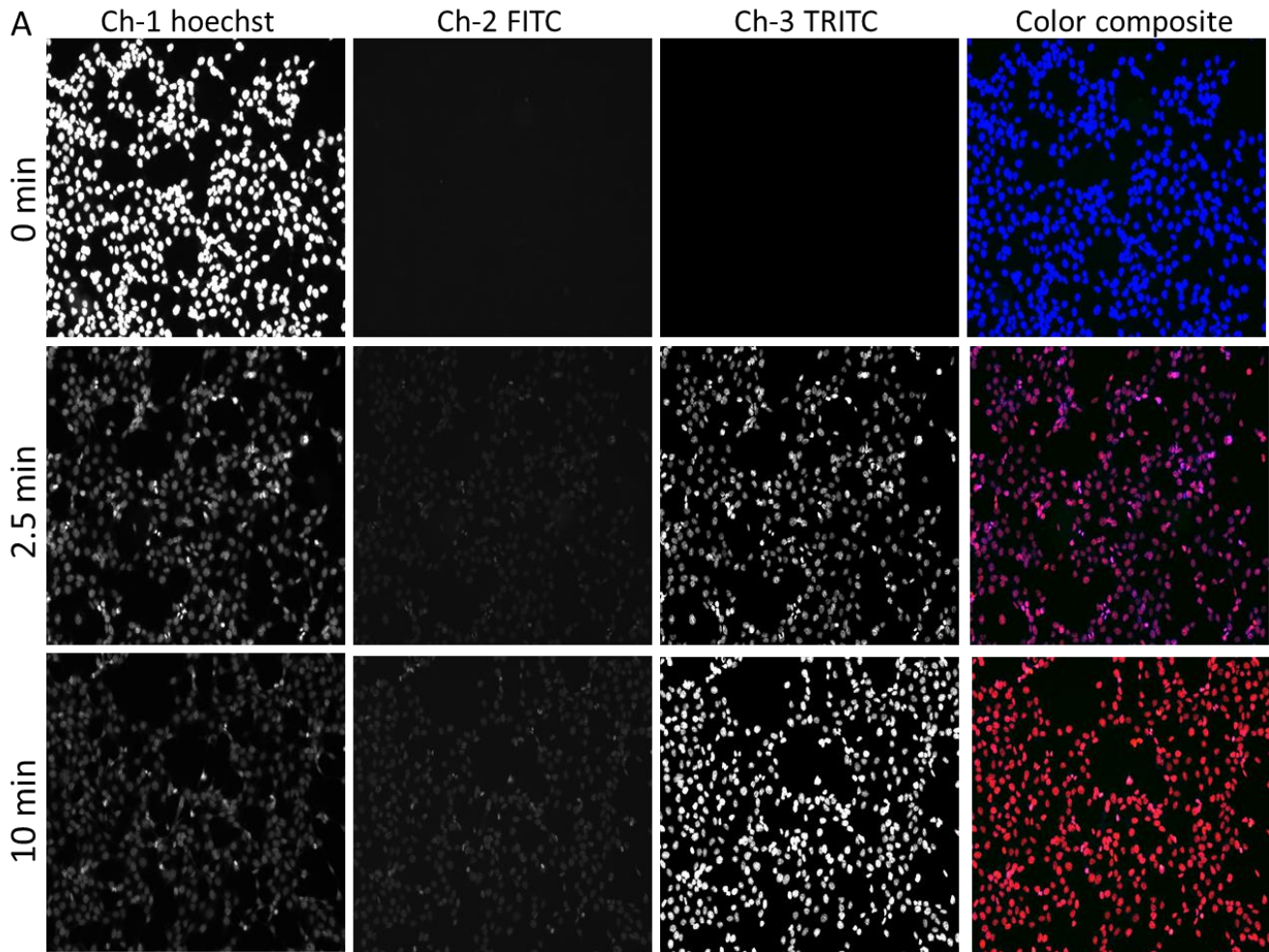


Normal tissue culture microplates were plated by Cal33 HNSCC cells as previously described. 5 μ L of idarubicin were added into wells at 0, 2.5 and 10 min time points. The 2D microplate was fixed and stained in 3.7% Formaldehyde and Hoechst. Images were acquired on the ImageXpress Micro(IXM) High-Content Analysis System and analyzed using MWCS image analysis module. Each concentration was in triplicates and the assay was repeated at least three times.

Fluorescent images in Ch2 (FITC) and Ch3 (TRITC) of 2D Cal33 cell cultures exposed to idarubicin produced strong fluorescent signals, and the color composite images showed a combination of blue (Hoechst staining), together with strong green and red signals that was predominantly yellow (Figure 25).

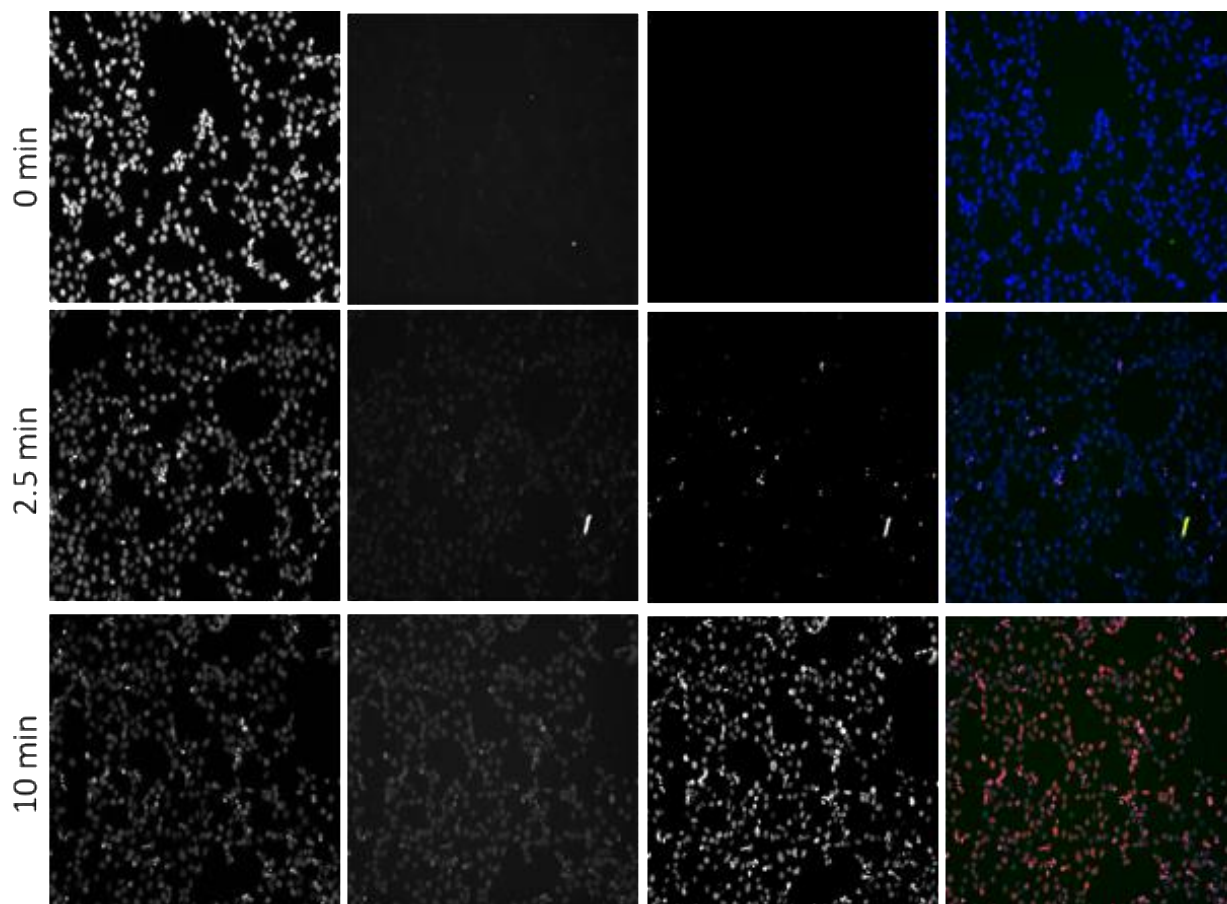
Daunorubicin and doxorubicin-exposed cells were also fluorescent in the images from the green (Ch 2) and red (Ch 3) channels but the red signal predominates making the color composite image purple due to the blue (Hoechst staining) and strong red signal (Figure 26 & Figure 27). The Hoechst fluorescent signal (Ch1) appeared to be significantly less intense in 2D Cal33 cells that were exposed to daunorubicin and doxorubicin compared to cells that were not exposed to compounds (Compare Figure 26 & Figure 27 to Figure 23).

Figure 26 Selected grayscale and color composite images of 2D Cal33 HNSCC cell culture + daunorubicin treatment for indicated exposure time. (A) Greyscale images of Hoechst 33342-stained nuclei (Ch 1), greyscale images of daunorubicin-treated (Ch 2 and Ch 3) and color composite images of Ch 1 and Ch 2 Cal33 HNSCC cells.



Normal tissue culture microplates were plated by Cal33 HNSCC cells as previously described. 5 μ L of daunorubicin were added into wells at 0, 2.5 and 10 min time points. The 2D microplates were fixed and stained in 3.7% Formaldehyde and Hoechst 33342. Images were acquired on the ImageXpress Micro(IXM) High-Content Analysis System and analyzed using MWCS image analysis module. Each concentration was in triplicates and the assay was repeated at least three times.

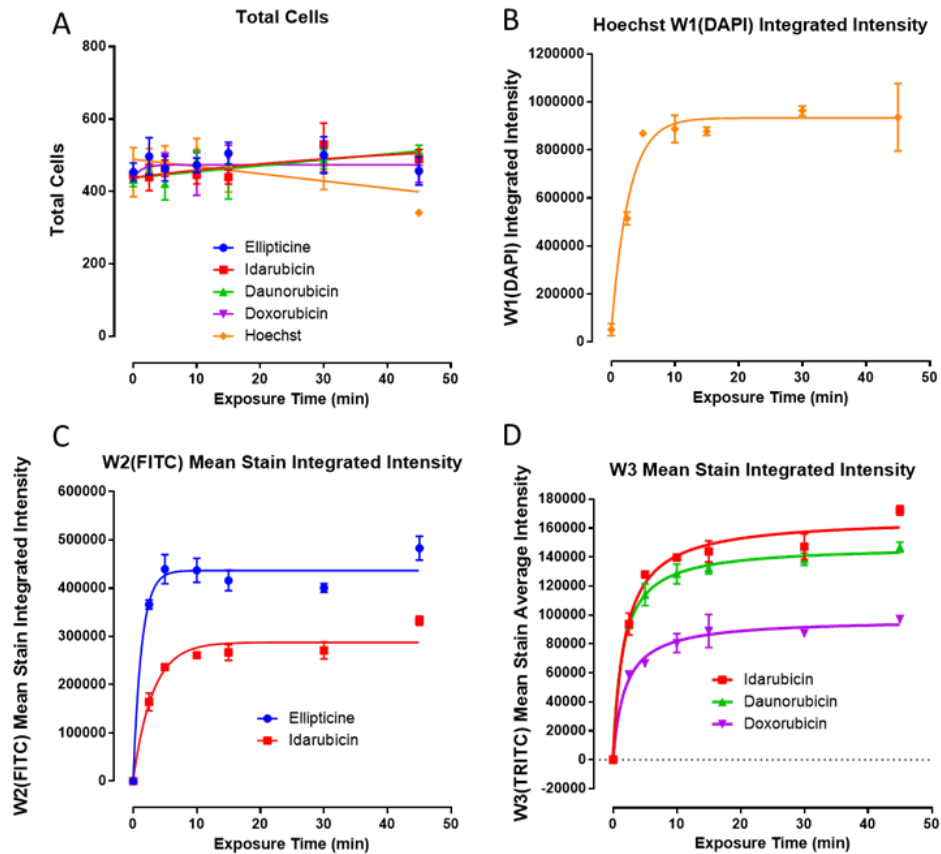
Figure 27 Selected grayscale and color composite images of 2D Cal33 HNSCC cell culture + doxorubicin treatment for indicated exposure time. (A) Greyscale images of Hoechst 33342-stained nuclei (Ch 1), greyscale images of doxorubicin-treated (Ch 2 and Ch 3) and color composite images of Ch 1 and Ch 2 Cal33 HNSCC cells.



Normal tissue culture microplates were plated by Cal33 HNSCC cells as previously described. 5 μ L of doxorubicin were added into wells at 0, 2.5 and 10 min time points. The 2D microplates were fixed and stained in 3.7% Formaldehyde and Hoechst 33342. Images were acquired on the ImageXpress Micro(IXM) High-Content Analysis System and analyzed using MWCS image analysis module. Each concentration was in triplicates and the assay was repeated at least three times.

Figure 28 portrays the integrated fluorescent intensity measurements obtained in 2D Cal33 cell cultures exposed to 10 μ M of the 4 drugs for up to 45 minutes. We used the number of Hoechst stained objects in Ch 1 to count the number of cells that were analyzed in the acquired images and demonstrated that the cell counts were consistent for 2D Cal33 cultures exposed to 10 μ M of the 4 compounds throughout the 45min time period (Figure 28). Figure 28 shows the integrated fluorescent intensities (RFUs) extracted from Ch 1 (DAPI, blue) images of 2D Cal33 cultures stained with Hoechst-33342 at periods throughout the 45 min time period. The integrated RFUs for Hoechst increased in a roughly linear fashion through 10 min of Hoechst exposure to reach a maximum plateau that was maintained through 45 min in the continuous presence of the dye (Figure 28). Figure 28 demonstrates that the RFUs extracted from Ch2 (FITC, green) images of 2D Cal33 cultures exposed to 10 μ M of ellipticine and idarubicin for indicated time periods. The time course of ellipticine and idarubicin accumulation in the Ch 2 FITC images of 2D Cal33 cells followed a very similar pattern to Hoechst, with a rapid initial linear uptake phase that reached a maximum plateau between 5-10 min and was maintained through 45 min. (Figure 28). Figure 26D shows the RFUs extracted from Ch3 (TRITC, red) images of 2D Cal33 cultures exposed to 10 μ M of idarubicin, daunorubicin and doxorubicin over 45 min. Again, the RFUs for idarubicin, daunorubicin and doxorubicin cellular accumulation increased linearly with respect to drug exposure time through 10 min and then reached a maximum plateau with continuous exposure (Figure 28).

Figure 28 Quantifying 2D Cal33 microplate time course assay by MWCS image analysis. (A) Total cell counts of Cal33 HNSCC cells treated with ellipticine, idarubicin, daunorubicin and doxorubicin; Mean stain integrated intensity of (B) ellipticine and idarubicin in FITC filter (ch-2) for indicated exposure time. (C) idarubicin, daunorubicin and doxorubicin in TRITC filter (ch-3) for indicated exposure time.



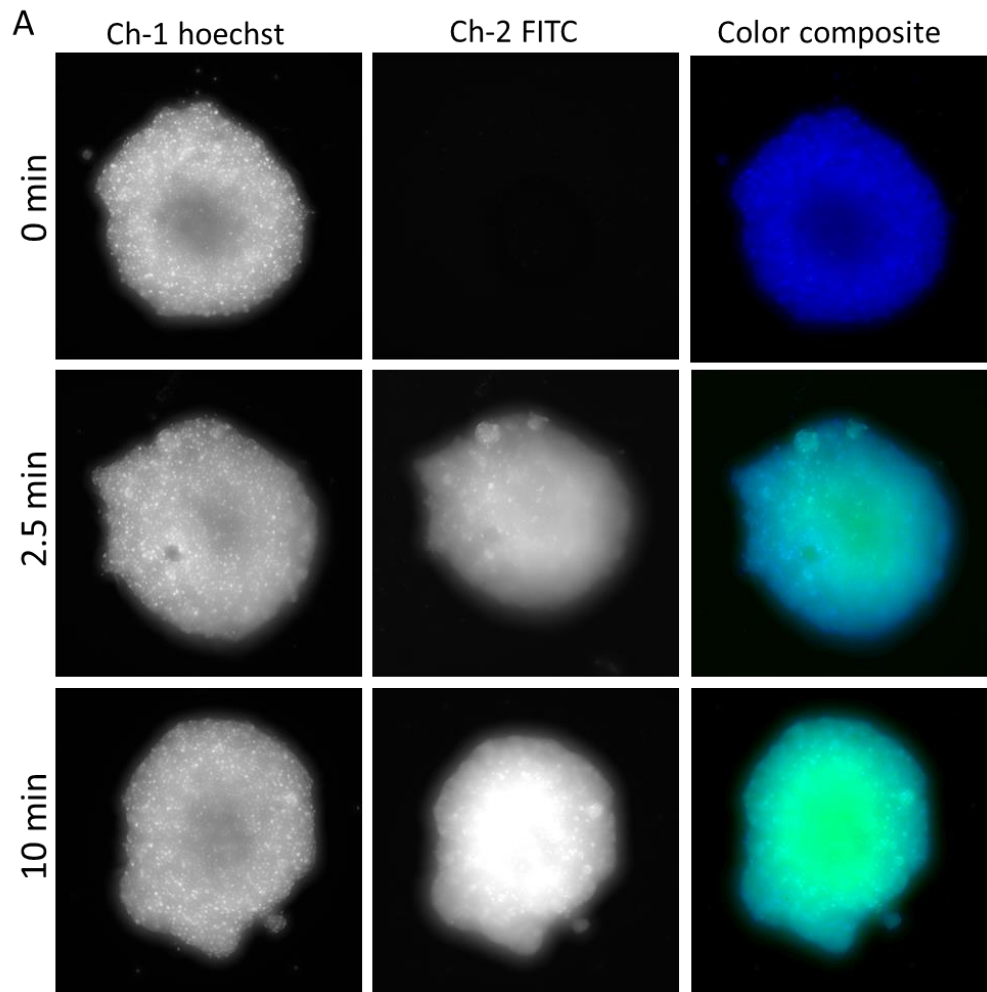
Normal tissue culture microplates were seeded by 1000 Cal33 HNSCC cells per well as previously described. 5 μ L of 4 compounds were added into wells for indicated exposure time. Then the 2D microplate was fixed and stained in 3.7% formaldehyde containing Hoechst-33342. The 2D microplates were washed by PBS for three times after the 45-min fixation. Images were then acquired on IXM High-Content Analysis System and analyzed. The images presented are representative of similar images obtained in at least 3 independent experiments. The quantitative data presented were extracted from the digital images using MWCS image analysis module. R-square of linear regression for Hoechst stained is 0.7752. R-square of linear regression for ellipticine and idarubicin in Ch 2 is 0.7434 and 0.8047, respectively. R-square of linear regression for idarubicin, daunorubicin and doxorubicin in Ch 3 is 0.8454,

0.8102, and 0.9268, respectively. The data represent the mean \pm SD of triplicates determination from one of these independent experiments.

We then conducted similar time course experiments to measure the accumulation of ellipticine, idarubicin, daunorubicin and doxorubicin into 3D Cal33 tumor spheroids. Cal33 cells that had been seeded into 384-well ULA microplates were cultured overnight and then exposed to 10 μ M of the 4 compounds for the indicated exposure times. The 3D tumor spheroids were then fixed in 3.7% formaldehyde containing Hoechst-33342, and washed by repeated aspiration and rinsing with PBS on JANUS MDT automated lipid handling workstation. We then utilized the IXM automated imaging system to acquire images sequentially in Ch 1 Hoechst (blue), Ch 2 FITC (green) and Ch 3 TRITC (red) fluorescent channels.

Similar to the results in 2D cell cultures, fluorescent images in Ch2 (FITC) of 2D Cal33 cell cultures exposed to ellipticine produced strong fluorescent signals in Ch2, and the color composite images showed a combination of blue (Hoechst staining) and green signals (Figure 29).

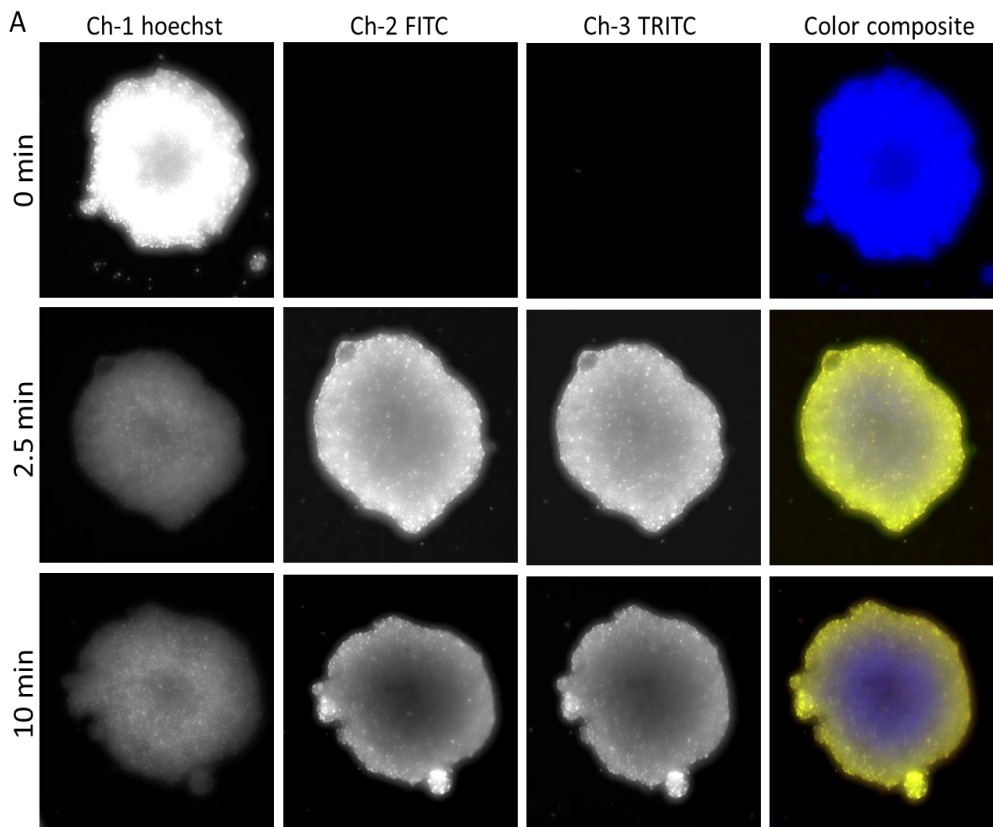
Figure 29 Selected grayscale and color composite images of 3D Cal33 HNSCC tumor spheroids + ellipticine treatment for indicated exposure time. (A) Greyscale images of Hoechst 33342-stained nuclei (Ch 1), greyscale images of ellipticine-treated (Ch 2 and Ch 3) and color composite images of Ch 1 and Ch 2 Cal33 HNSCC cells.



384-well ULA microplates were seeded by 5000 Cal33 HNSCC cells per well as previously described. 5 μ L of ellipticine was added into wells for indicated exposure time. The ULA microplates were then stained in 3.7% formaldehyde containing Hoechst-33342. Then the ULA microplates were washed by PBS for three times after the 45-min fixation. Images were acquired on the IXM High-Content Analysis System and analyzed using MWCS image

analysis module. The images presented are representative of similar images obtained in at least 3 independent experiments.

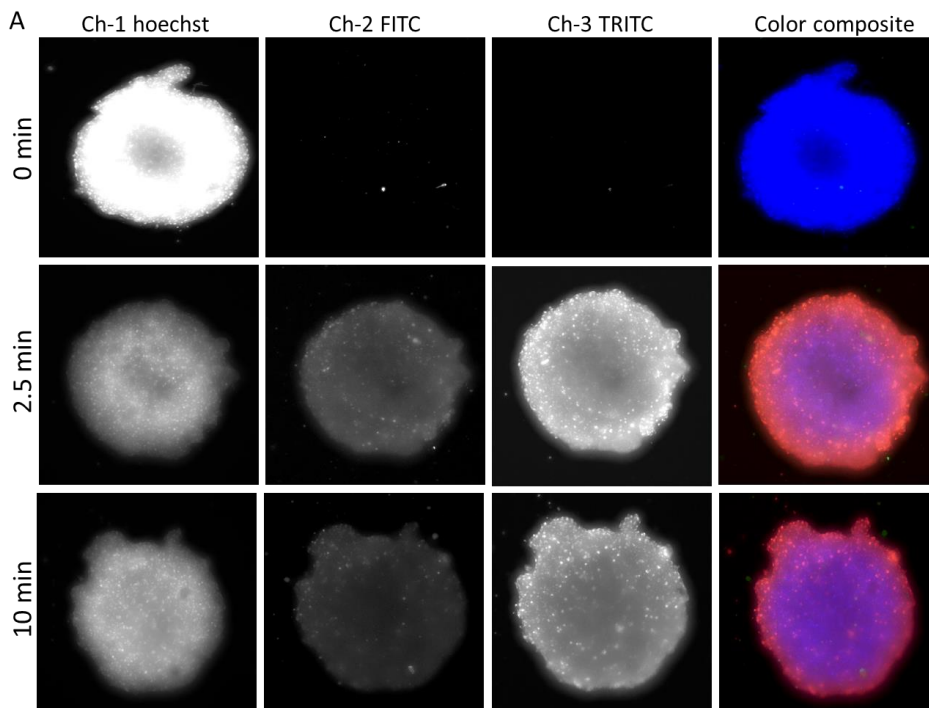
Figure 30 Selected grayscale and color composite images of 3D Cal33 HNSCC tumor spheroids + idarubicin treatment for indicated exposure time. (A) Greyscale images of Hoechst 33342-stained nuclei (Ch 1), greyscale images of idarubicin-treated (Ch 2 and Ch 3) and color composite images of Ch 1 and Ch 2 Cal33 HNSCC cells



384-well ULA microplates were seeded by 5000 Cal33 HNSCC cells per well as previously described. 5 μ L of idarubicin was added into wells for indicated exposure time. The ULA microplates were then and stained in 3.7% formaldehyde containing Hoechst-33342. Then the ULA microplates were washed by PBS for three times after the 45-min fixation. Images were acquired on the IXM High-Content Analysis System and analyzed using MWCS image analysis module. The images presented are representative of similar images obtained in at least 3 independent experiments.

Fluorescent images in Ch2 (FITC) and Ch3 (TRITC) of 2D Cal33 cell cultures exposed to idarubicin produced strong fluorescent signals in Ch2 and Ch3, and the color composite images showed a combination of blue (Hoechst staining), together with strong green and red signals that were predominantly yellow (Figure 30).

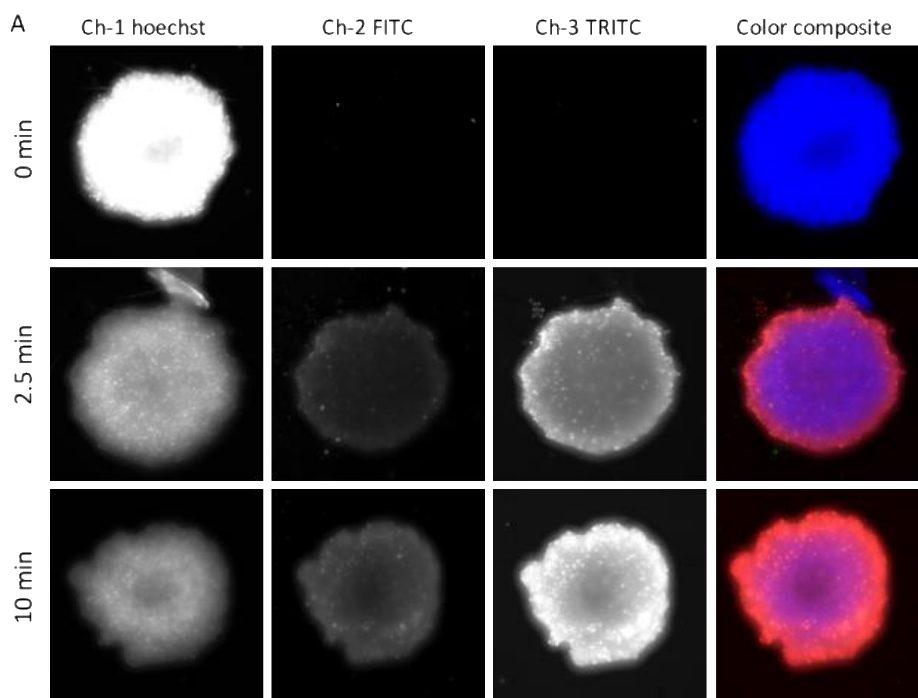
Figure 31 Selected grayscale and color composite images of 3D Cal33 HNSCC tumor spheroids + daunorubicin treatment for indicated exposure time. (A) Greyscale images of Hoechst 33342-stained nuclei (Ch 1), greyscale images of daunorubicin-treated (Ch 2 and Ch 3) and color composite images of Ch 1 and Ch 2 Cal33 HNSCC cells.



384-well ULA microplates were seeded by 5000 Cal33 HNSCC cells per well as previously described. 5 μ L of daunorubicin was added into wells for indicated exposure time. The ULA microplates were then and stained in 3.7% formaldehyde containing Hoechst-33342. Then the ULA microplates were washed by PBS for three times after the 45-min fixation. Images were acquired on the IXM High-Content Analysis System and analyzed using MWCS image analysis module. The images presented are representative of similar images obtained in at least 3 independent experiments.

Daunorubicin and doxorubicin-exposed 3D tumor spheroids were also fluorescent in the images from the green (Ch 2) and red (Ch 3) channels but the red signal predominates making the color composite images of the spheroids purple due to the blue (Hoechst staining) and strong red signals (Figure 31 & Figure 32).

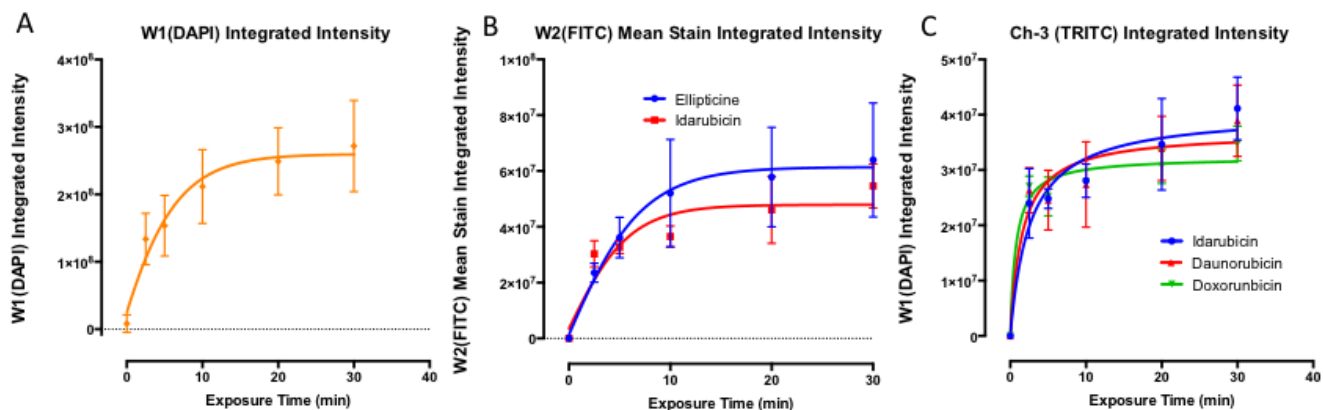
Figure 32 Selected grayscale and color composite images of 3D Cal33 HNSCC tumor spheroids + doxorubicin treatment for indicated exposure time. (A) Greyscale images of Hoechst 33342-stained nuclei (Ch 1), greyscale images of daunorubicin-treated (Ch 2 and Ch 3) and color composite images of Ch 1 and Ch 2 Cal33 HNSCC cells.



A 3D 384-well ULA microplate was seeded by 5000 Cal33 HNSCC cells per well as previously described. 5 μ L of doxorubicin was added into wells for indicated exposure time. The 3D microplate was then fixed by adding 50 μ L of 37% formaldehyde containing Hoechst-33342. Then the 3D microplate was washed by PBS for three times after the 45-min fixation. Images were acquired on the ImageXpress Micro (IXM) High-Content Analysis System and analyzed using MWCS image analysis module. The images presented are representative of similar images obtained in at least 3 independent experiments.

The time dependent accumulation of test compounds in 3D Cal33 HNSCC tumor spheroids (Figure 33) was consistent with the time dependent drug penetration observed in 2D cell cultures (Figure 33). The time course of drug accumulation in the Ch 2 FITC and Ch3 TRITC images of 3D Cal33 spheroids followed a very similar pattern to Hoechst, with a rapid initial linear uptake phase that reached a maximum plateau between 5-10 min and was maintained through 45 min.

Figure 33 Quantifying 3D Cal33 tumor spheroid time course assay by MWCS image analysis. (A) Total cell counts of Cal33 HNSCC cells treated with ellipticine, idarubicin, daunorubicin and doxorubicin; Mean stain integrated intensity of (B) ellipticine and idarubicin in FITC filter (ch-2) for indicated exposure time. (C) idarubicin, daunorubicin and doxorubicin in TRITC filter (ch-3) for indicated exposure time.



ULA microplates were seeded by 5000 Cal33 HNSCC cells per well as previously described. 5 μ L of 4 compounds were added into wells for indicated exposure time. Then the 3D microplate was fixed and stained in 3.7% formaldehyde containing Hoechst-33342. The 3D microplates were washed by PBS for three times after the 45-min fixation. Images were then acquired on the IXM High-Content Analysis System and analyzed. The images presented are representative of similar images obtained in at least 3 independent experiments. The quantitative data presented

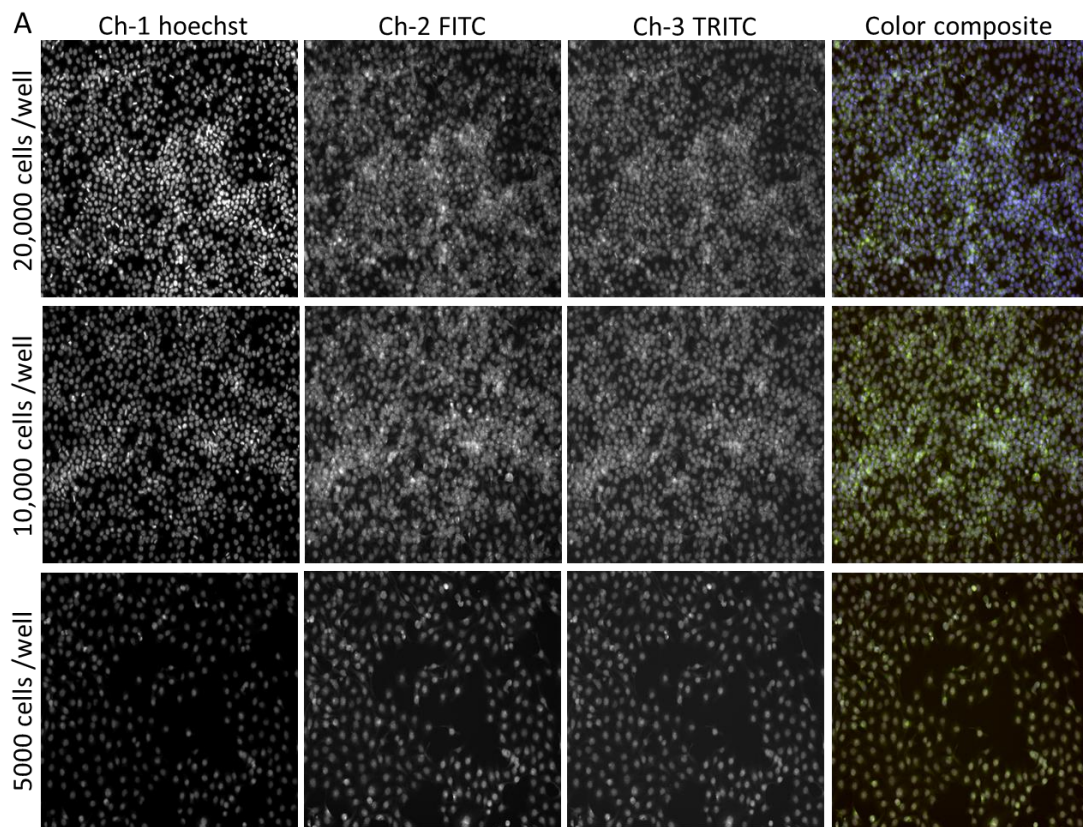
were extracted from the digital images using MWCS image analysis module as described in materials and methods. R-square of linear regression for Hoechst stained is 0.7752. R-square of linear regression for ellipticine and idarubicin in Ch 2 is 0.7434 and 0.8047, respectively. R-square of linear regression for idarubicin, daunorubicin and doxorubicin in Ch 3 0.8454, 0.8102 and 0.9268, respectively. The data represent the mean \pm SD of triplicates determination from one of these independent experiments.

3.3.3 Cal33 HNSCC 2D & 3D SEEDING DENSITY ASSAYS AND PSEUDOCOLOR IMAGES OF 2D&3D CULTURES

We conducted experiments to see if the cell density of our 2D and 3D HNSCC cultures would affect the drug penetration of ellipticine, idarubicin, daunorubicin and doxorubicin. Different cell numbers of Cal33 cells that had been seeded into normal tissue culture assay plates and were cultured overnight to form 2D monolayers were and then exposed to 10 μ M of the compounds for 15-min. These microplates were then fixed in 3.7% formaldehyde containing Hoechst-33342 for 45 min, and washed by repeated aspiration and rinsing with PBS. We then utilized the IXM automated imaging system to acquire images sequentially in Ch 1 Hoechst (blue), Ch 2 FITC (green) and Ch 3 TRITC (red) fluorescent channels. Hoechst 33342 DNA staining in Ch 1 was used to identify the nuclei of Cal33 cells in 2D cell cultures. Fluorescent images of 2D Cal33 cell cultures exposed to idarubicin in Ch2 (FITC) and Ch3 (TRITC) produced strong

fluorescent signals, and the color composite images showed a combination of blue, green and red signals in all of the indicated seeding densities (Figure 34).

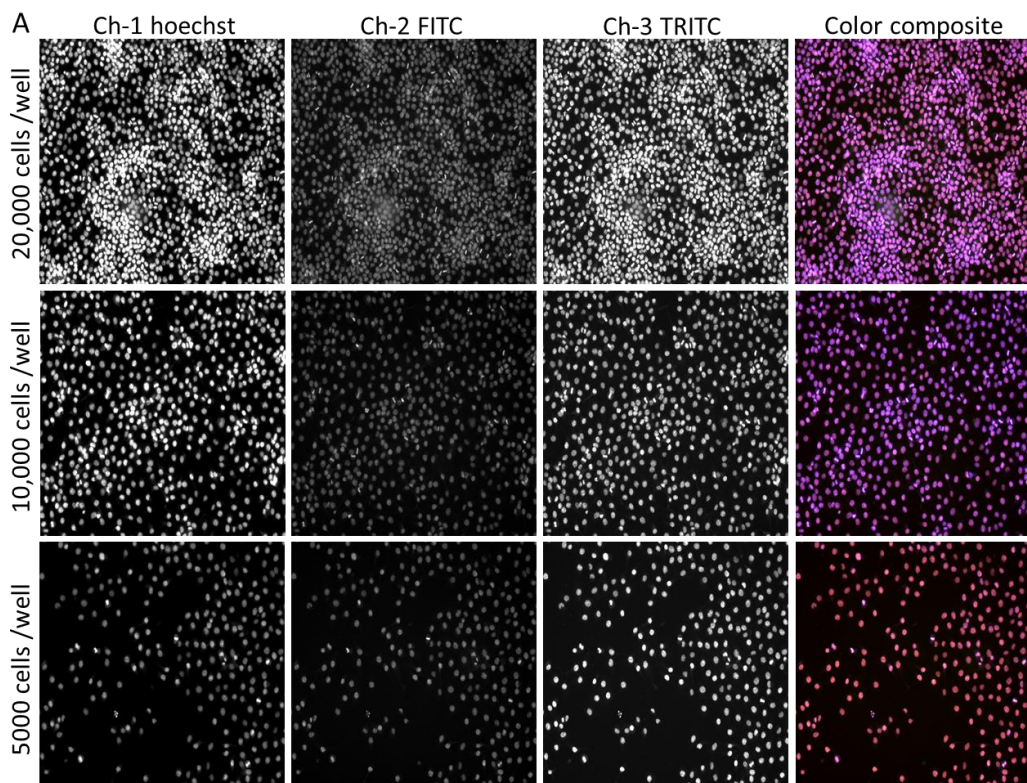
Figure 34 Greyscale and color composite of 2D Cal33 cell cultures exposed to 10 μ M idarubicin at 5000, 10000 and 20000 cells/well. (A) Images of idarubicin treatment on 2D Cal33 cell culture from ch-1 hoechst, ch-2 FITC and color composite.



Normal tissue culture microplates seeded by 5000, 10000 and 20,000 Cal33 HNSCC cells per well. 5 μ L of idarubicin was added into wells and incubated for 15 min. The final concentration in wells was 10 μ M as described in materials and methods section. The cells were fixed and stained in 3.7% Formaldehyde and Hoechst 33342. Images were acquired on IXM and analyzed using the MWCS image analysis module. Each concentration well was in triplicates and the assay was repeated at least three times.

Images of daunorubicin and doxorubicin-exposed Cal33 HNSCC cells seeded in normal tissue culture assay plates were also fluorescent in both the green (Ch 2) and red (Ch 3) channels at the indicated seeding densities (Figure 35) and the sub-cellular localization appeared to be predominantly nuclear co-localized with the Hoechst stained.

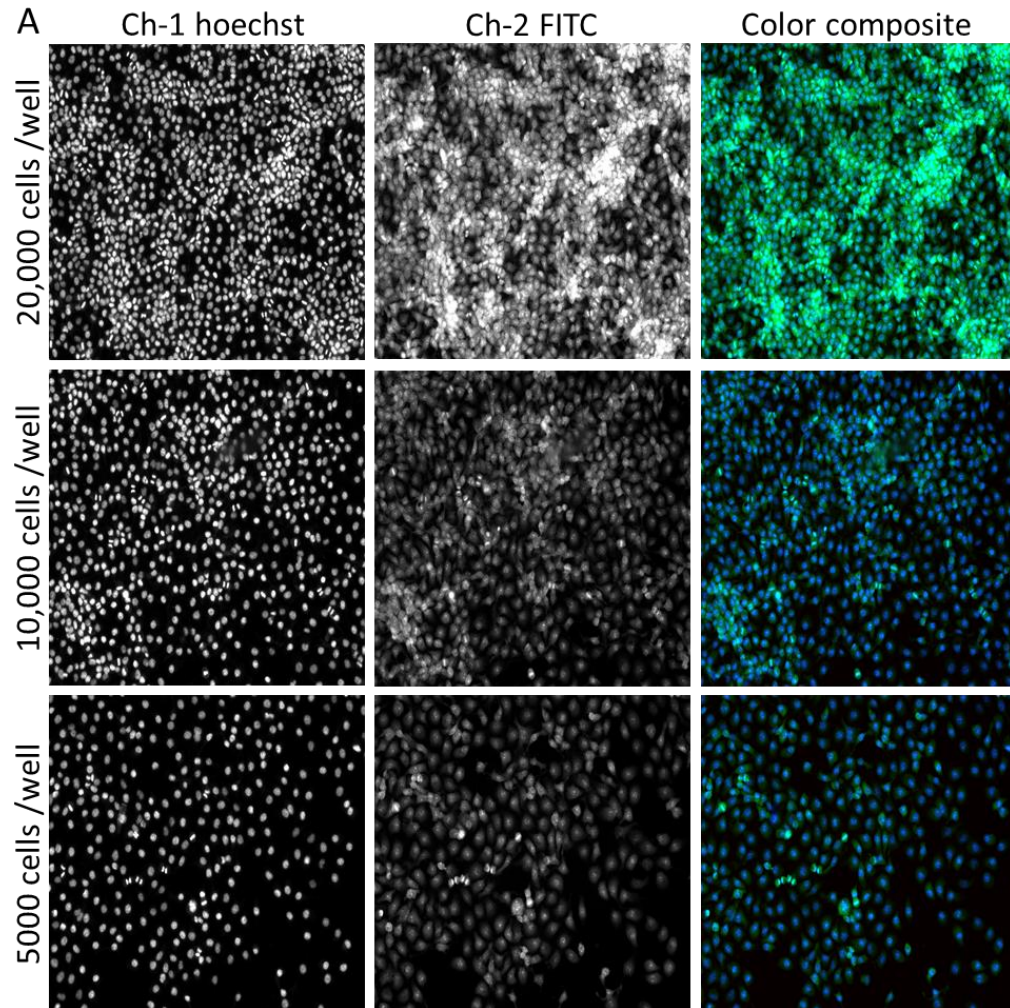
Figure 35 Greyscale and color composite of 2D Cal33 cell cultures exposed to 10 μ M daunorubicin at 5000, 10000 and 20000 cells/well. (A) Images of daunorubicin treatment on 2D Cal33 cell culture from ch-1 hoechst, ch-2 FITC and color composite.



Normal tissue culture microplates were seeded by 5000, 10000 and 20,000 Cal33 HNSCC cells per well. 5 μ L of daunorubicin was added into wells and incubated for 15 min. The final concentration in wells was 10 μ M as described in materials and methods section. The cells were fixed and stained in 3.7% Formaldehyde and Hoechst 33342. Images were acquired on IXM and analyzed using the MWCS image analysis module. Each concentration well was in triplicates and the assay was repeated at least three times.

The greyscale and color composite fluorescence images of 2D Cal33 cell cultures seeded at 5,000, 10,000 and 20,000 Cal33 cells per well and exposed to 10 uM ellipticine are shown *in* Figure 36). These images exhibited strong fluorescent signals in the green channel (Ch2, FITC), and the color composite images showed a combination of blue (Hoechst staining) together with a strong green signal (Figure 36). Similar images were observed in 2D Cal33 cell cultures exposed to different concentrations of the 4 drugs and for different time periods confirming that drug penetration of these fluorescent compounds can be evaluated 2D monolayer cultures seeded at different cell densities in normal tissue culture plates (Figure 26, Figure 27 & Figure 28).

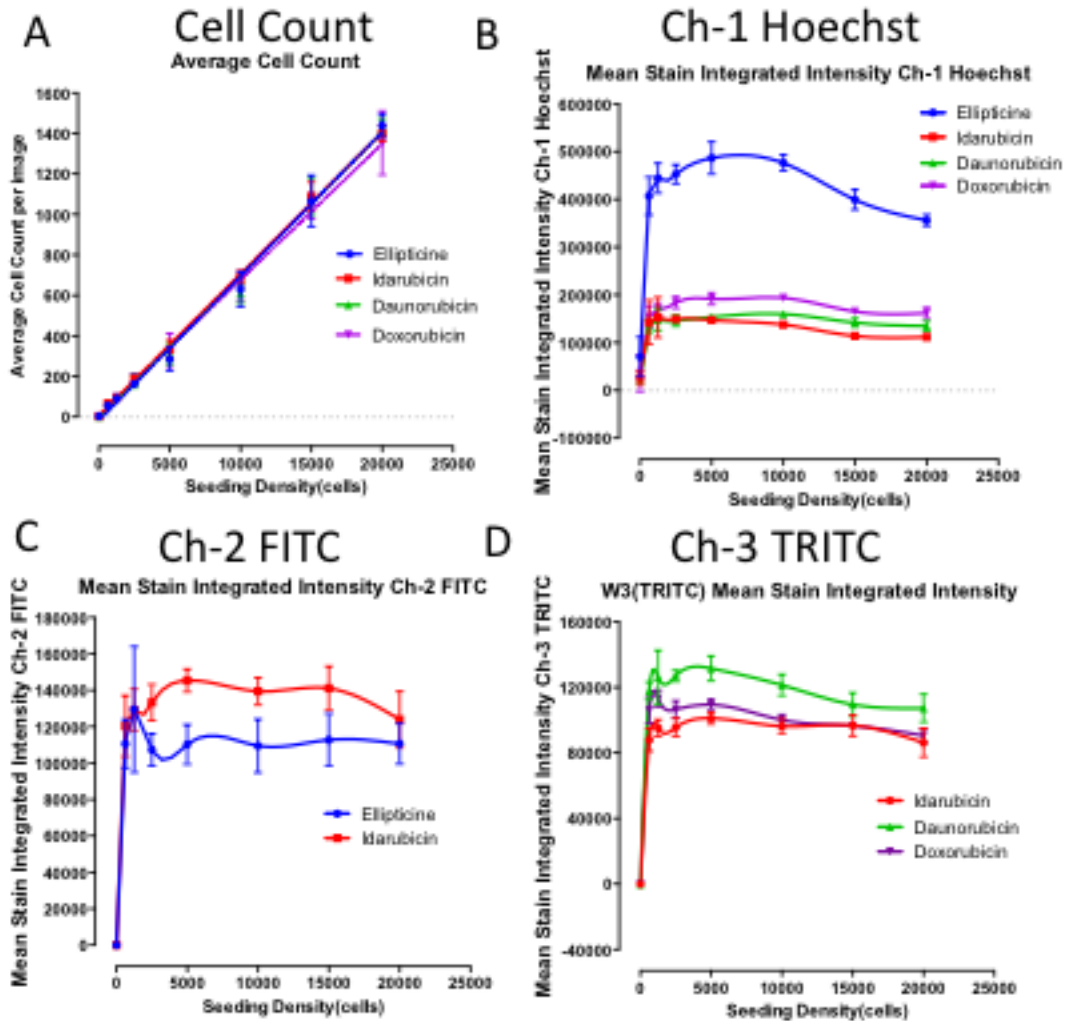
Figure 36 Greyscale and color composite of 2D Cal33 cell cultures exposed to 10 μ M ellipticine at 5000, 10000 and 20000 cells/well. (A) Images of ellipticine treatment on 2D Cal33 cell culture from ch-1 hoechst, ch-2 FITC and color composite.



Normal tissue culture microplates were seeded by 5000, 10000 and 20,000 Cal33 HNSCC cells per well. 5 μ L of ellipticine was added into wells and incubated for 15 min. The final concentration in wells was 10 μ M as described in materials and methods section. The cells were fixed and stained in 3.7% Formaldehyde and Hoechst 33342. Images were acquired on IXM and analyzed using the MWCS image analysis module. Each concentration well was in triplicates and the assay was repeated at least three times.

Quantitative data from the digital images were extracted and analyzed by same algorithm and analysis module used in 2D Cal33 HNSCC concentration response assays. Figure 37 portrays the integrated fluorescent intensity measurements obtained in 2D HNSCC cell cultures at the indicated cell seeding densities and exposed to 10 μ M of ellipticine, idarubicin, daunorubicin, and doxorubicin for 15 min. Although the absolute fluorescent intensity values for each compound are different, the integrated fluorescent intensities (RFUs) extracted from images of Cal33 cells exposed to compounds in Ch1, Ch2 and Ch3 fluorescent channels remained constant at all seeding densities suggesting that drug penetration and/or accumulation was independent of cell number (Figure 37). Consistent with our previous observations, exposure to idarubicin, daunorubicin or doxorubicin reduced the Hoechst RFU values suggesting that these compound may compete for the same DNA binding site as Hoechst. These data indicate that all four fluorescent compounds penetrated 2D Cal33 cell cultures uniformly at all seeding densities (Figure 37). Therefore, the drug penetration of 10 μ M ellipticine, idarubicin, daunorubicin, and doxorubicin for 15min exposure is not dependent on the cell numbers in 2D cell cultures.

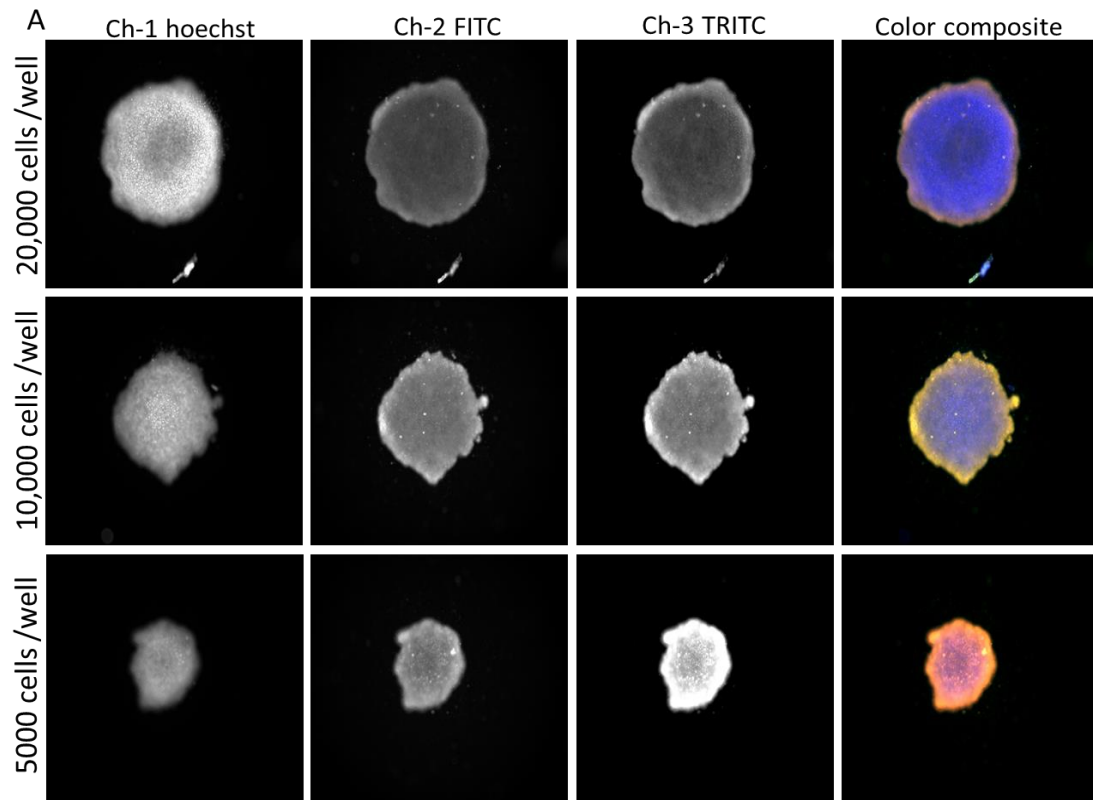
Figure 37 Fluorescent intensity of 2D Cal33 cells seeded at different densities and exposed to 10 μ M of the 4 compounds. Fluorescent intensity in 2D cell cultures from (A) Average cell count of Cal33 cells of 2 10X images; (B) Ch-1 Hoechst; (C) Ch-2 FITC; (D) Ch-3 TRITC.



Normal tissue culture microplates were seeded at the indicated seeding densities of Cal33 HNSCC cells. Cell monolayers were exposed to ellipticine, idarubicin, daunorubicin and doxorubicin for 15 min. The final concentration in wells was 10 μ M. 2D Cal33 monolayers were fixed and stained in 3.7% Formaldehyde and Hoechst 33342. Fluorescent intensities of 4 compounds were acquired on IXM and analyzed using the MWCS image analysis module. Each concentration well was in triplicates and the assay was repeated at least three times.

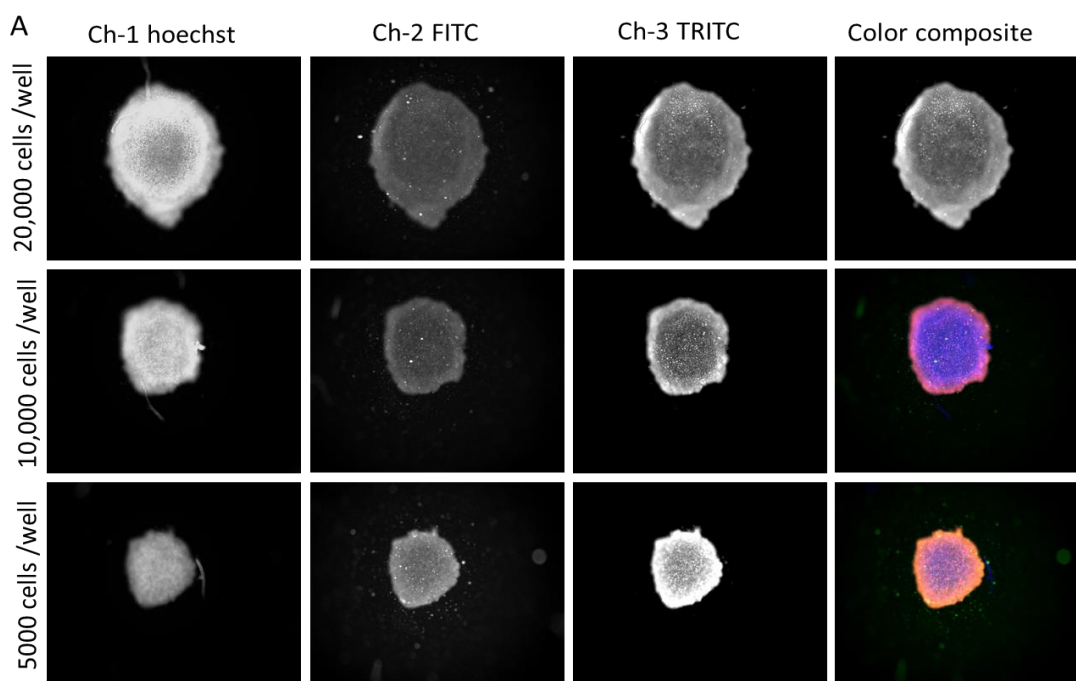
We used the same methods to investigate the drug penetration of ellipticine, idarubicin, daunorubicin and doxorubicin into different sized Cal33 HNSCC spheroids formed in ULA plates seeded at different cell seeding densities. Different numbers of Cal33 cells that had been seeded into spheroids 384-well ULA microplates were cultured overnight and then exposed to 10 μ M of the compounds for 15-min. These microplates were then fixed in 3.7% formaldehyde containing Hoechst-33342 for 45 min, and washed by repeated aspiration and rinsing with PBS. We then utilized the IXM to acquire images sequentially in Ch 1 Hoechst (blue), Ch 2 FITC (green) and Ch 3 TRITC (red) fluorescent channels. Hoechst 33342 DNA staining in Ch 1 was used to identify the nuclei of Cal33 cells in 3D cell cultures and create a spheroid mask to measure the integrated fluorescent intensities in Ch1, Ch2 and Ch3. Fluorescent images of 3D tumor spheroid exposed to idarubicin from Ch 2 and Ch 3 produced strong fluorescent signals, and the color composite images showed a combination of blue, green and red signals in differently sized spheroids formed from the indicated seeding densities (Figure 38).

Figure 38 Greyscale and color composite of 3D Cal33 spheroids exposed to 10 μ M idarubicin at 5000, 10000 and 20000 cells/well. (A) Images of idarubicin treatment on 3D Cal33 spheroids from ch-1 hoechst, ch-2 FITC and color composite.



384-well ULA microplates were seeded by 5000, 10000 and 20,000 Cal33 HNSCC cells per well. 5 μ L of idarubicin was added into wells and incubated for 15 min. The final concentration in wells was 10 μ M as described in materials and methods section. The cells were fixed and stained in 3.7% Formaldehyde and Hoechst 33342. Images were acquired on IXM and analyzed using the MWCS image analysis module. Each concentration well was in triplicates and the assay was repeated at least three times.

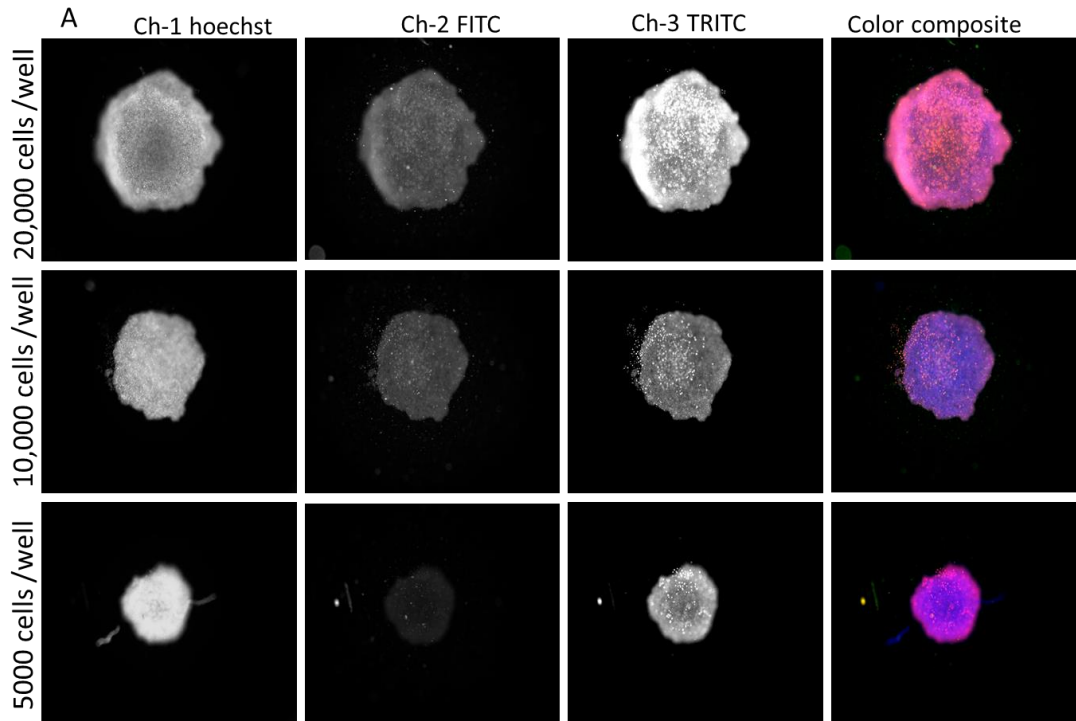
Figure 39 Greyscale and color composite of 3D Cal33 spheroids exposed to 10 μ M daunorubicin at 5000, 10000 and 20000 cells/well. (A) Images of daunorubicin treatment on 3D Cal33 spheroids from ch-1 hoechst, ch-2 FITC and color composite.



384-well ULA microplates were seeded by 5000, 10000 and 20,000 Cal33 HNSCC cells per well. 5 μ L of daunorubicin was added into wells and incubated for 15 min. The final concentration in wells was 10 μ M as described in materials and methods section. The cells were fixed and stained in 3.7% Formaldehyde and Hoechst 33342. Images were acquired on IXM and analyzed using the MWCS image analysis module. Each concentration well was in triplicates and the assay was repeated at least three times.

Images of daunorubicin or doxorubicin-treated Cal33 HNSCC cells seeded in 384-well ULA microplates were also fluorescent in both the green (Ch 2) and red (Ch 3) channels in indicated seeding densities (Figure 39 & Figure 40).

Figure 40 Greyscale and color composite of 3D Cal33 spheroids exposed to 10 μ M doxorubicin at 5000, 10000 and 20000 cells/well. (A) Images of doxorubicin treatment on 3D Cal33 spheroids from ch-1 hoechst, ch-2 FITC and color composite.

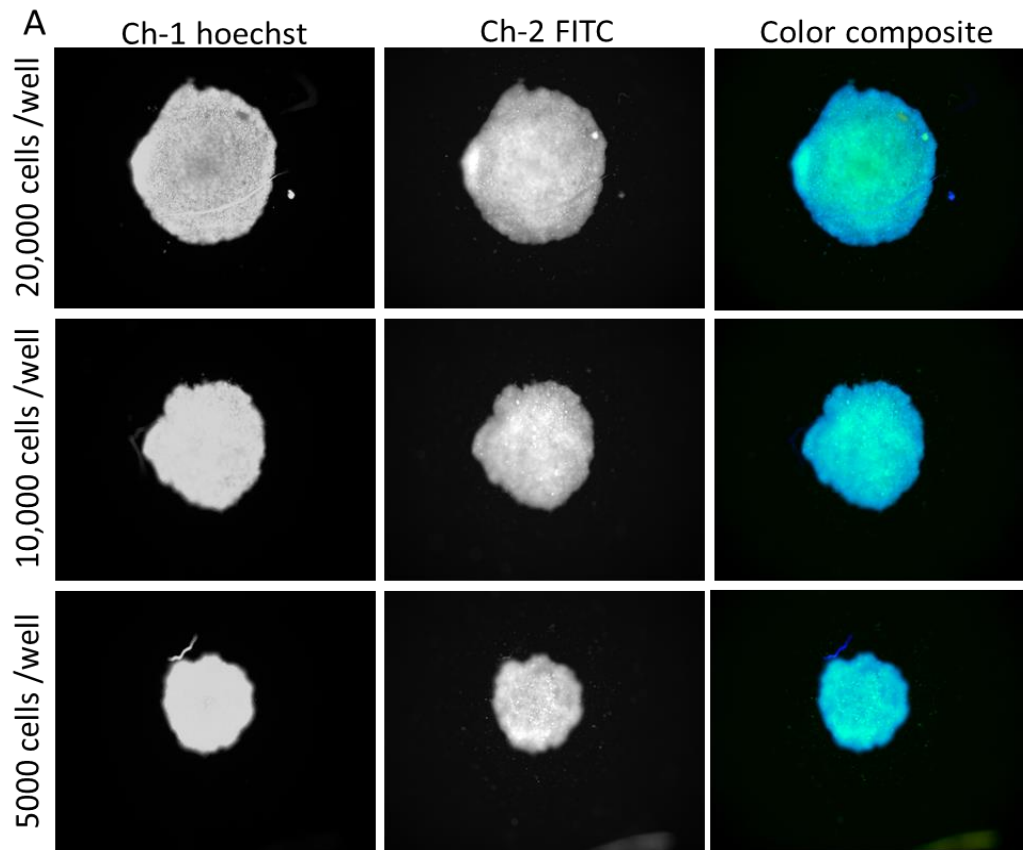


384-well ULA microplates were seeded by 5000, 10000 and 20,000 Cal33 HNSCC cells per well. 5 μ L of doxorubicin was added into wells and incubated for 15 min. The final concentration in wells was 10 μ M as described in materials and methods section. The cells were fixed and stained in 3.7% Formaldehyde and Hoechst 33342. Images were acquired on IXM and analyzed using the MWCS image analysis module. Each concentration well was in triplicates and the assay was repeated at least three times.

The fluorescence images of 3D cell cultures differently sized Cal33 spheroids formed in ULA plates seeded at 5,000, 10,000 and 20,000 Cal33 cells per well treated by ellipticine are shown in Figure 41. The images of Cal33 spheroids exposed to ellipticine exhibited strong

fluorescent signals in the green channel (Ch2, FITC), and the color composite images showed a combination of blue (Hoechst staining) together with a strong green signal (Figure 41).

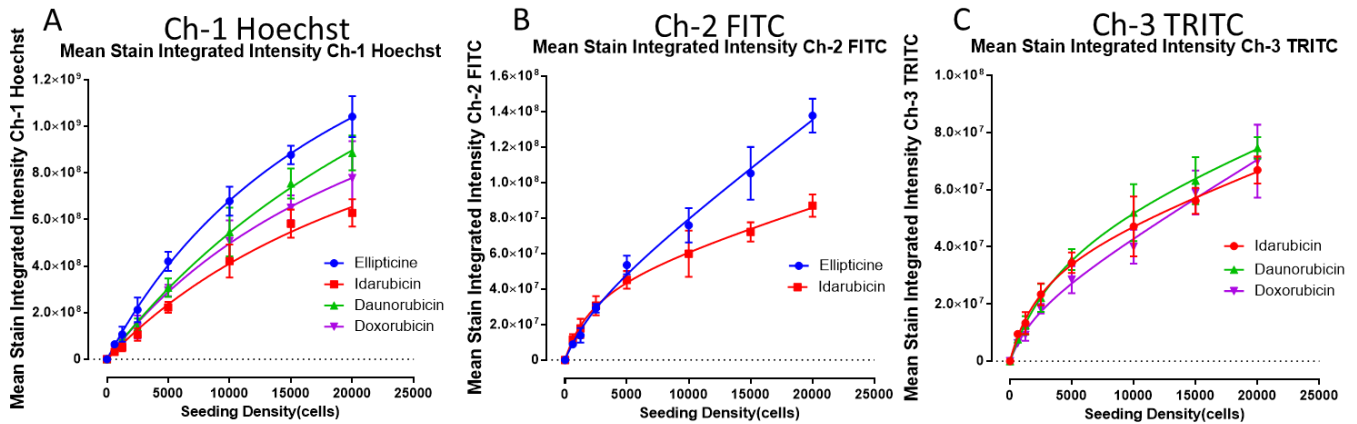
Figure 41 *Greyscale and color composite of 3D Cal33 spheroids exposed to 10 μ M ellipticine at 5000, 10000 and 20000 cells/well. (A) Images of ellipticine treatment on 3D Cal33 spheroids from ch-1 hoechst, ch-2 FITC and color composite.*



384-well ULA microplates were seeded by 5000, 10000 and 20,000 Cal33 HNSCC cells per well. 5 μ L of ellipticine was added into wells and incubated for 15 min. The final concentration in wells was 10 μ M as described in materials and methods section. The cells were fixed and stained in 3.7% Formaldehyde and Hoechst 33342. Images were acquired on IXM and analyzed using the MWCS image analysis module. Each concentration well was in triplicates and the assay was repeated at least three times.

In marked contrast to 2D Cal33 cell monolayers, the fluorescent signals were detected in 3D Cal33 spheroids when cells exposed to the four compounds exhibited a strong dependence of cell numbers and corresponding size of the spheroids produced. (Figure 42). The fluorescent intensities extracted from images of Cal33 3D tumor spheroids increased as the seeding densities (Figure 42). The data suggests that more compounds accumulated into the 3D Cal33 spheroids as the size of the 3D tumor spheroids formed increased. The images demonstrate that the size of the Cal33 tumor spheroids formed (width, area and volume) is dependent upon the number of cells added to the wells of the ULA plates and that the larger the spheroid the more drug accumulates (Figure 38, Figure 39, Figure 40 & Figure 41). Furthermore, the overall fluorescent intensities extracted from images of 3D tumor spheroids are >10-fold higher than for 2D cell cultures. Images of Cal33 HNSCC cells seeded into 2D assay plates indicate that even at higher densities the cal33 cells do not appear to form many cell-cell contacts (Figure 34, Figure 35, Figure 36, Figure 38, Figure 39, Figure 40 & Figure 41). Whereas, Cal33 tumor spheroids form a compact three-dimensional architecture of cells that are in direct contact with other cells (Figure 38, Figure 39, Figure 40 & Figure 41). These images and data demonstrate that the penetration of compounds may be hampered by the physical and physiological barrier of 3D tumor spheroids, which prevents drugs from getting into the spheroids. In contrast, the drugs can easily penetrate into the tumor cells in 2D cell cultures where cells grow without cell-cell contacts and three-dimensional architectures. (Figure 34, Figure 35 & Figure 36).

Figure 42 *Fluorescent intensity of 3D Cal33 spheroids seeded at different densities and exposed to 10 μ M of the 4 compounds. Fluorescent intensity in 3D Cal33 spheroids from (A) Ch-1 Hoechst; (B) Ch-2 FITC; (C) Ch-3 TRITC.*

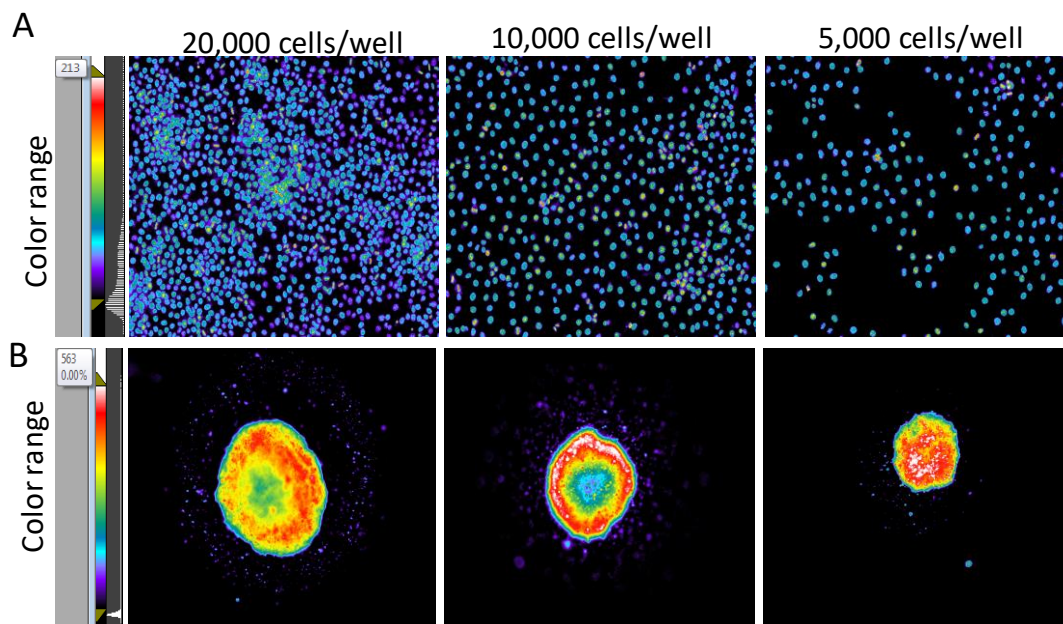


384-well ULA microplates were seeded at the indicated seeding densities of Cal33 HNSCC cells. 3D Cal33 spheroids were exposed to ellipticine, idarubicin, daunorubicin and doxorubicin for 15 min. The final concentration in wells was 10 μ M. 3D Cal33 spheroids were fixed and stained in 3.7% Formaldehyde and Hoechst 33342. Fluorescent intensities of 4 compounds were acquired on IXM and analyzed using the MWCS image analysis module. Each concentration well was in triplicates and the assay was repeated at least three times.

To evaluate drug penetration in 2D and 3D cultures, representative images are presented in pseudo-color format where the relative fluorescent intensities inside the 2D cell or 3D tumor spheroid are indicated by the different colors. “Hotter” and “brighter” colors (white, red, yellow) represent the higher intensity signals of compounds and blue or purple represent lower intensity signals. The same color range was set to apply for images of cells at different seeding densities. For all four drugs, the corresponding pseudo-color images at all seeding densities tested indicate that there is no significant drug penetration gradient in 2D cell cultures, and the fluorescent intensity measurements were constant at all densities, suggesting that drug penetration and/or accumulation

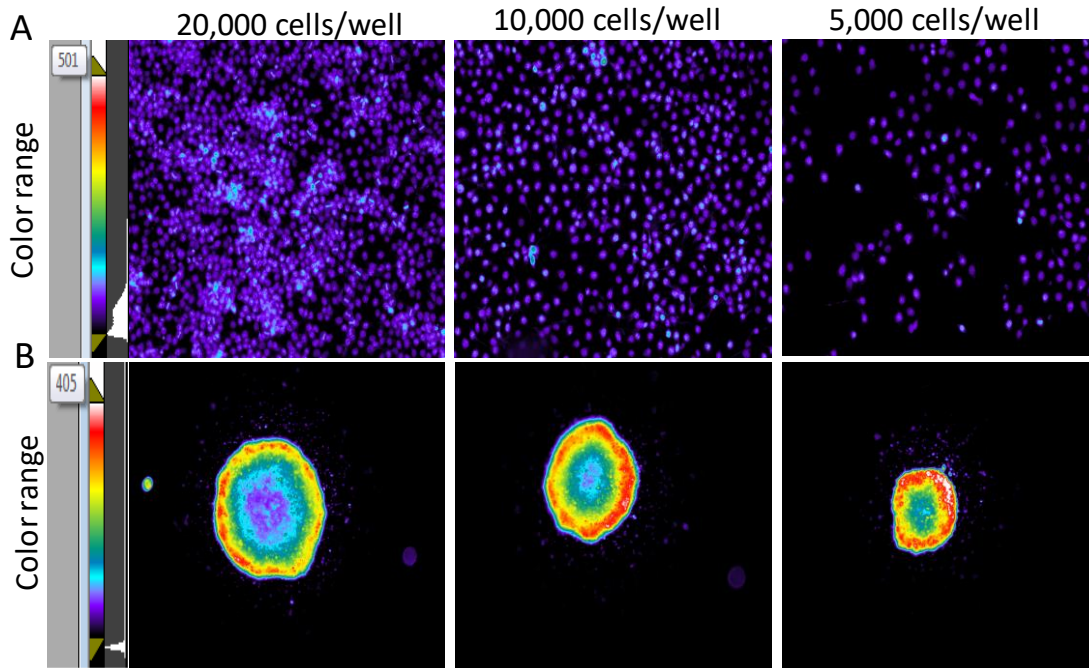
was independent of cell number. In marked contrast, rainbow-like color rings were observed in the pseudo-color images of Cal33 HNSCC cells in 3D tumor spheroids exposed to the 4 drugs. “Hotter” colors are present at the outer layers of the 3D tumor spheroids, and the temperature of the colors decrease towards the core of the spheroids. These images indicate that a significant drug penetration gradient with all four drugs in Cal33 HNSCC 3D tumor spheroids (Figure 43).

Figure 43 Pseudo-color images of Cal33 HNSCC cells in 2D cultures and 3D tumor spheroids exposed to 10 μ M ellipticine at 5,000, 10,000 and 20,000 cells/well. (A) Pseudocolor images from ch-2 FITC in 2D cell cultures; (B) Pseudocolor images from ch-2 FITC in 3D tumor spheroids.



Normal tissue culture microplates and 384-well ULA microplates were seeded by 5000, 10000 and 20,000 Cal33 HNSCC cells per well. 5 μ L of ellipticine was added into wells and incubated for 15 min. The final concentration of ellipticine in wells was 10 μ M

Figure 44 Pseudo-color images of Cal33 HNSCC cells in 2D cultures and 3D tumor spheroids exposed to 10 μ M idarubicin at 5,000, 10,000 and 20,000 cells/well. (A) Pseudocolor images from ch-2 FITC in 2D cell cultures; (B) Pseudocolor images from ch-2 FITC in 3D tumor spheroids.

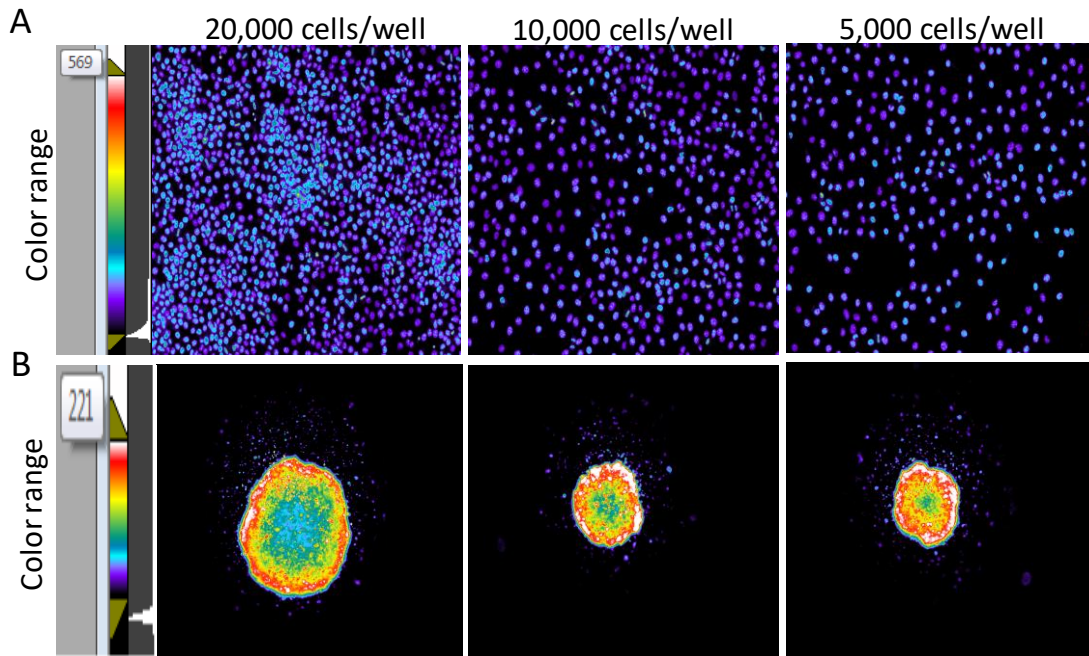


Normal tissue culture microplates and 384-well ULA microplates were seeded by 5000, 10000 and 20,000 Cal33 HNSCC cells per well. 5 μ L of idarubicin was added into wells and incubated for 15 min. The final concentration of ellipticine in wells was 10 μ M.

Similar phenomenon was also observed in images of Cal33 cells treated with idarubicin in 2D cell cultures and 3D tumor spheroids from Ch 3 (Figure 44). Fluorescent intensity within Cal33 2D cell cultures was consistent throughout the images, whereas, a clear gradient of fluorescent intensity was detected inside the 3D tumor spheroids. These images indicate that a significant drug penetration gradient of idarubicin was shown in Cal33 HNSCC 3D tumor spheroids other than 2D cell cultures (Figure 44).

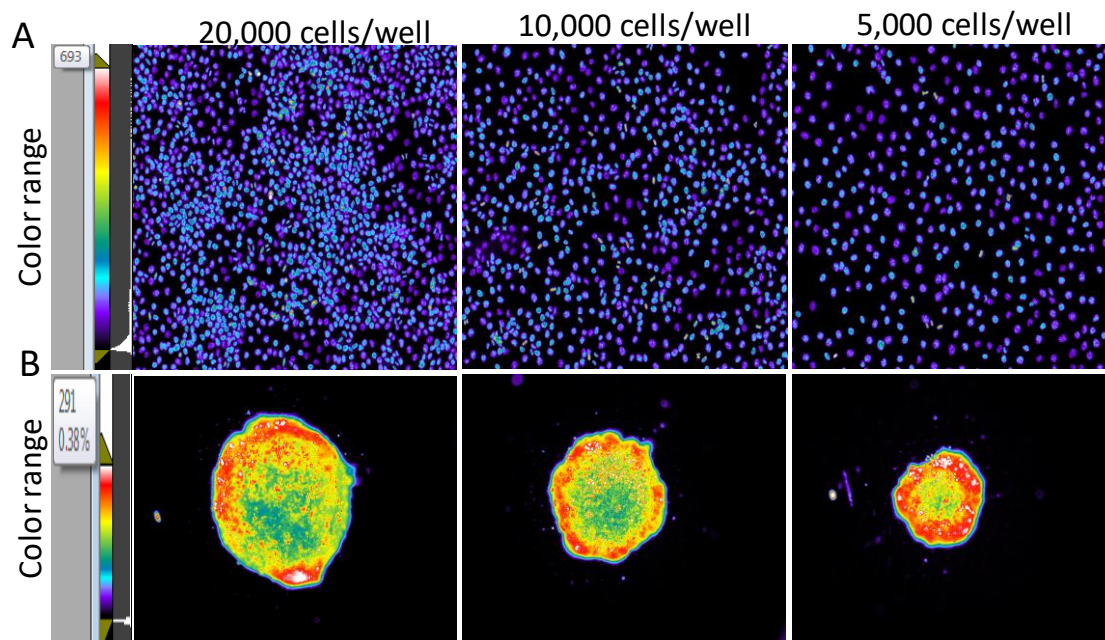
As we observed from images of Cal33 cells treated with ellipticine or idarubicin, both daunorubicin and doxorubicin showed a uniform distribution in 2D cell cultures and a significant drug penetration gradient in 3D tumor spheroids as well (Figure 45 & Figure 46).

Figure 45 Pseudo-color images of Cal33 HNSCC cells in 2D cultures and 3D tumor spheroids exposed to $10\mu\text{M}$ daunorubicin at 5,000, 10,000 and 20,000 cells/well. (A) Pseudocolor images from ch-2 FITC in 2D cell cultures; (B) Pseudocolor images from ch-2 FITC in 3D tumor spheroids.



Normal tissue culture microplates and 384-well ULA microplates were seeded by 5000, 10000 and 20,000 Cal33 HNSCC cells per well. $5\mu\text{L}$ of daunorubicin was added into wells and incubated for 15 min. The final concentration of ellipticine in wells was $10\mu\text{M}$

Figure 46 Pseudo-color images of Cal33 HNSCC cells in 2D cultures and 3D tumor spheroids exposed to 10 μ M doxorubicin at 5,000, 10,000 and 20,000 cells/well. (A) Pseudocolor images from ch-2 FITC in 2D cell cultures; (B) Pseudocolor images from ch-2 FITC in 3D tumor spheroids.

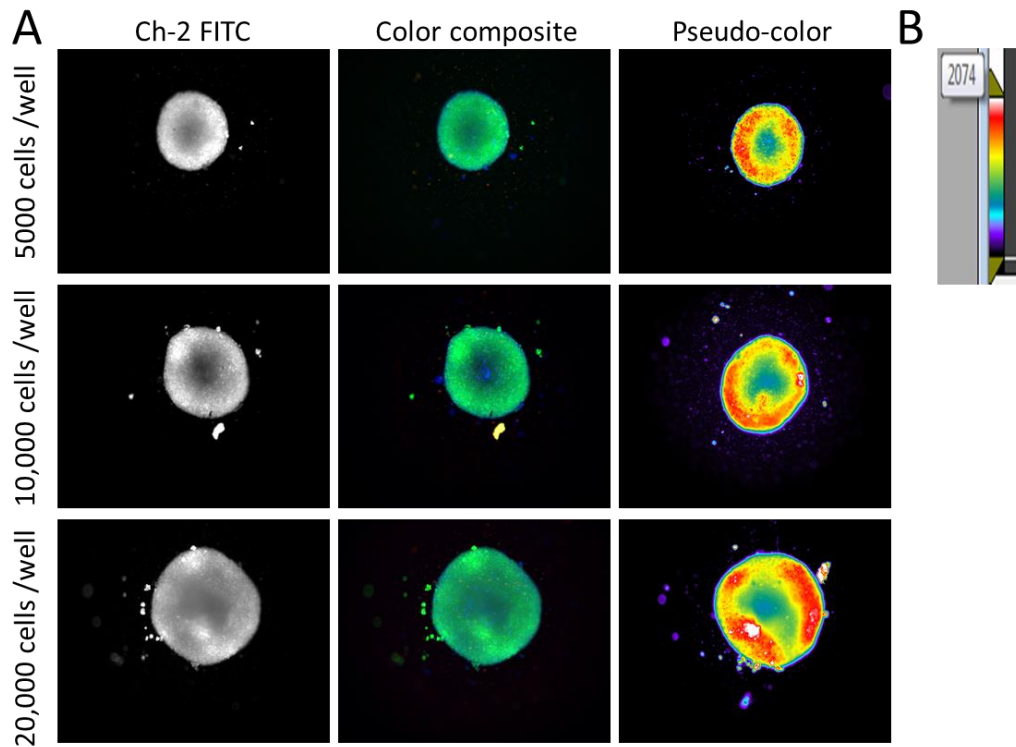


Normal tissue culture microplates and 384-well ULA microplates were seeded by 5000, 10000 and 20,000 Cal33 HNSCC cells per well. 5 μ L of doxorubicin was added into wells and incubated for 15 min. The final concentration of ellipticine in wells was 10 μ M.

3.3.4 FADU HNSCC 3D CONCENTRATION DEPENDENT ASSAY

Furthermore, we conducted experiments to determine the concentration dependent penetration of ellipticine, idarubicin, daunorubicin and doxorubicin on FADU HNSCC cell line in 384-well ULA microplate. Also, the fluorescence images of 3D FADU tumor spheroids exposed to ellipticine are shown in Figure 47. These images exhibited strong fluorescent signals in the green channel (Ch2, FITC), and the color composite images showed a combination of blue (Hoechst staining) together with a strong green signal (Figure 47). furthermore, the pseudo-color images of 3D FADU spheroids exposed to 12.5 μ M ellipticine indicate a clear gradient of fluorescent intensity was detected inside the 3D tumor spheroids at 5,000, 10,000 and 20,000 cells/well (Figure 47). These images indicate that a significant drug penetration gradient of ellipticine was shown in 3D FADU HNSCC tumor spheroids, same as Cal33 cells in 3D tumor spheroids (Figure 43, Figure 44, Figure 45 & Figure 46).

Figure 47 Grayscale and color composite images of 3D FADU HNSCC tumor spheroids + ellipticine treatment. (A) Greyscale and color composite images of ellipticine-treated (Ch 2) and pseudo-color images of 3D FADU HNSCC spheroids; (B) Color range of pseudo-color images.

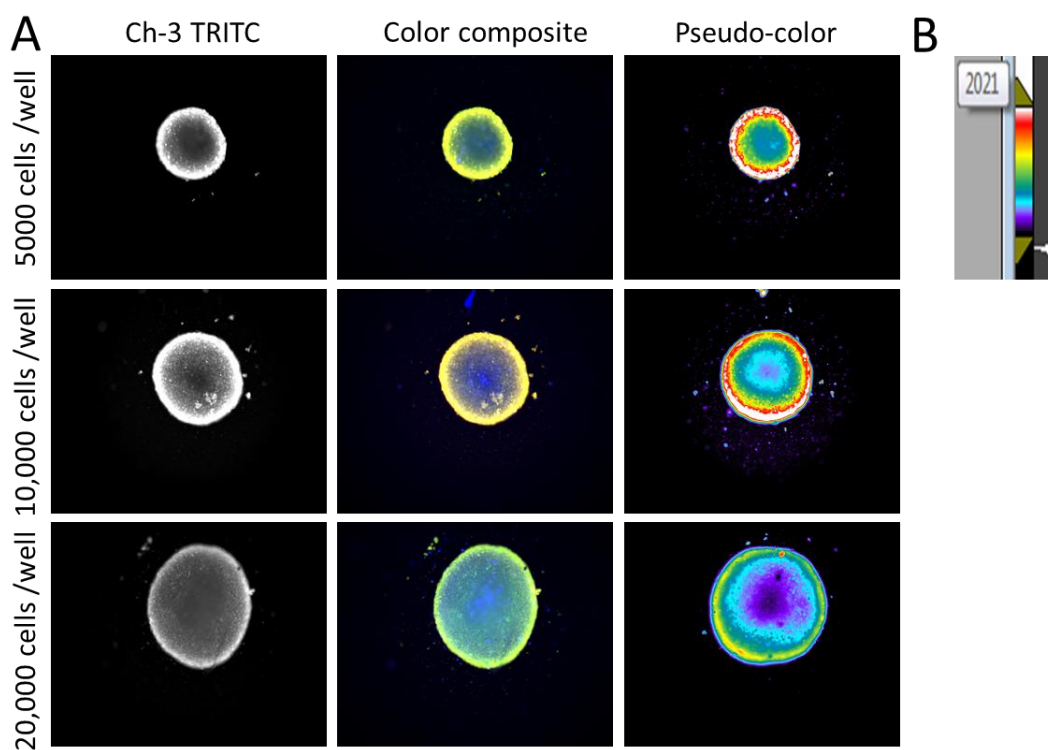


384-well ULA microplates were seeded by 5000 cells per well of FADU HNSCC cells. 5 μ L of ellipticine were added into wells with indicated concentration. After 15 min incubation at 37 $^{\circ}$ C, 5% CO₂ The 2D microplate was fixed and stained in 3.7% formaldehyde containing Hoechst-33342. The ULA microplates were washed by PBS for three times after the 45-min fixation. Images were then acquired on the IXM High-Content Analysis System and analyzed using MWCS image analysis module. The images are presented are representative of similar images obtained in at least 3 independent experiments.

As we observed from images of Cal33 cells exposed to idarubicin in 3D tumor spheroids (Fig. 44), fluorescent images of 3D tumor spheroid exposed to idarubicin from Ch 2 and Ch 3 produced strong fluorescent signals, and the color composite images showed a combination of blue, green and red signals in differently sized spheroids formed from the indicated seeding densities (Figure

48). the pseudo-color images of FADU cells in 3D tumor spheroids also indicate a gradient a clear gradient of fluorescent intensity at 5,000, 10,000 and 20,000 cells/well (Figure 48), which has been shown in the images of Cal33 cells exposed to idarubicin and seeded in 384-well ULA microplates (Figure 44).

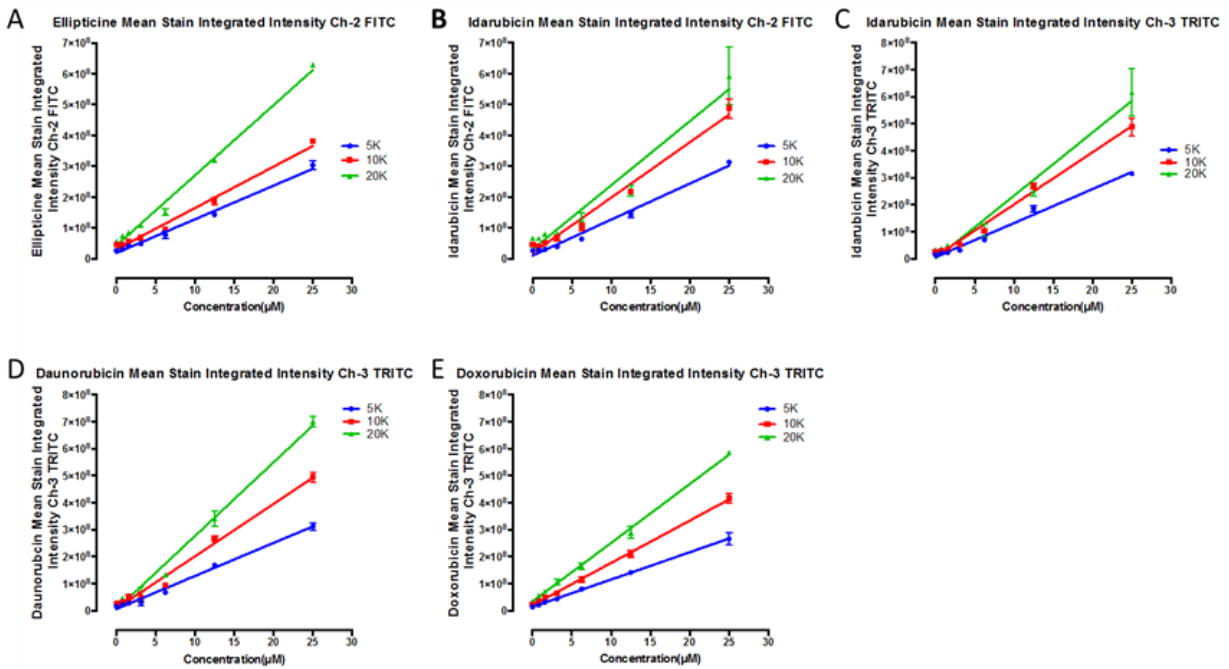
Figure 48 *Grayscale and color composite images of 3D FADU HNSCC tumor spheroids + idarubicin treatment. (A) Greyscale and color composite images of ellipticine-treated (Ch 3) and pseudo-color images of 3D FADU HNSCC spheroids; (B) Color range of pseudo-color images.*



384-well ULA microplates were seeded by 5000 cells per well of FADU HNSCC cells. 5 μ L of idarubicin were added into wells with indicated concentration. After 15 min incubation at 37°C, 5% CO₂ The 2D microplate was fixed and stained in 3.7% formaldehyde containing Hoechst-33342. The ULA microplates were washed by PBS for three times after the 45-min fixation. Images were then acquired on the IXM High-Content Analysis System and analyzed using MWCS image analysis module. The images are presented are representative of similar images obtained in at least 3 independent experiments.

Fluorescent intensity values were quantified from images of 3D FADU tumor spheroids exposed to the indicated concentrations of ellipticine, idarubicin, daunorubicin and doxorubicin. Same 3D concentration dependent penetration assay protocol and quantification analysis method was conducted on FADU HNSCC cells. Figure 49 portrays the integrated fluorescent intensity measurements obtained in the images of 3D tumor spheroids exposed to the indicated concentrations of ellipticine, idarubicin, daunorubicin, and doxorubicin for 15 min. These data show the integrated RFUs for ellipticine, idarubicin daunorubicin and doxorubicin increased linearly with respect to compound concentration (Figure 49). The linear correlation of the RFUs and the concentrations of idarubicin, daunorubicin and doxorubicin added to 3D tumor spheroids (Figure 49), is consistent with the linear relationship observed in 3D Cal33 tumor spheroids (Figure 20) and compounds in solution (Figure 8, Figure 9, Figure 10 & Figure 11). These data suggest that the 3D tumor spheroids formed in 384-well ULA microplates do not only amenable for Cal33 HNSCC cells, but also other HNSCC cell lines, like FaDu.

Figure 49 Fluorescent intensity of 3D FADU spheroids seeded at different densities and exposed to 10 μ M of the 4 compounds. Fluorescent intensity in 3D FADU spheroids from (A) Ch-1 Hoechst; (B) Ch-2 FITC; (C) Ch-3 TRITC.



384-well ULA microplates were seeded at the indicated seeding densities of FADU HNSCC cells. 3D FADU spheroids were exposed to the indicated concentration of ellipticine, idarubicin, daunorubicin and doxorubicin for 15 min. 3D FADU spheroids were fixed and stained in 3.7% Formaldehyde and Hoechst 33342. Fluorescent intensities of 4 compounds were acquired on IXM and analyzed using the MWCS image analysis module. Each concentration well was in triplicates and the assay was repeated at least three times.

4.0 CONCLUSIONS

We have successfully generated Cal33 and FaDu HNSCC tumor spheroids in 384-well ULA microplates to investigate and compare cytotoxicity and drug penetration in 2D and 3D Cal33 cell cultures. Cal33 tumor spheroids were significantly (>5-fold) more resistant to growth inhibition by ellipticine, idarubicin, daunorubicin and doxorubicin than the corresponding 2D cell cultures. We first measured the absorbance and fluorescence spectra of the four compounds in solution and demonstrated a linear relationship between fluorescent intensity (RFUs) and the concentration of idarubicin, daunorubicin and doxorubicin. To measure and quantify drug penetration, accumulation and distribution in 2D and 3D cell cultures we used the IXM high content platform to acquire digital images of cells and spheroids in Ch 1 (Hoechst), Ch 2 (FITC) and Ch 3 (TRITC), and used the MWCS image analysis module to extract and quantify the fluorescence intensities of the four compounds. Although we could not detect ellipticine fluorescence in PBS, cells exposed to ellipticine exhibited a strong fluorescence in images captured in the FITC channel that could be quantified using the MWCS image analysis module. We speculate that ellipticine becomes fluorescent after it intercalates with DNA or after ellipticine-DNA adducts have been formed. Consistent with our observations in solution, in 2D and 3D Cal33 cell cultures exposed to idarubicin, daunorubicin, doxorubicin, or ellipticine, the mean integrated fluorescent intensity (RFU's) detected in monolayer cells and spheroids increased linearly with respect to drug concentration. We conclude that the RFU's of idarubicin, daunorubicin, doxorubicin and ellipticine can be used to infer the relative concentration of these drugs within the cells of monolayers and tumor spheroids. In concentration and time dependent drug penetration experiments, the accumulation of ellipticine, idarubicin, daunorubicin and doxorubicin into 2D

and 3D Cal33 cultures exhibited very similar concentration and time dependent behaviors. In 2D Cal33 cell seeding density experiments, ellipticine, idarubicin, daunorubicin and doxorubicin accumulated uniformly in Cal33 cells independently of cell numbers. Even at the higher 2D cell seeding densities, the Cal33 cells do not appear to form many cell-cell contacts. In marked contrast, the RFU's detected in Cal33 spheroids exposed to the four drugs were higher as the number cells and corresponding spheroid sizes increased. The apparent differences in drug penetration and distribution within monolayer cells and spheroids were highlighted in the corresponding intensity gradient pseudo-color images. Cells in 3D spheroids exhibited a distinct fluorescent intensity gradient transitioning from high in the cells in the outside layers of the spheroid to low in cells in the inner core. The compacted three-dimensional multilayer architecture of spheroids promotes direct cell-cell contacts and cell-cell interactions that limit the diffusion and penetration of drugs throughout the spheroid. In order to reach the cells in the inner core of spheroids, drugs have to be taken up, pass through and then exit successive layers of cells. The larger the spheroid the more layers of cells the drugs need to penetrate and the longer this process is likely to take. In addition to representing a physical barrier to drug penetration and diffusion, it is possible that cell-cell contacts and cell-cell interactions might activate mechanisms that inhibit drug uptake and passage, or promote drug efflux. Our studies demonstrate that the cells in the interior of 3D tumor spheroids that are further from the spheroid surface experience lower drug concentrations than the cells in the exterior layers. In contrast the cells in 2D monolayer cultures are all exposed to same uniformed drug concentration. It has been observed that cells in the different regions or zones of spheroid cultures have different proliferative capacities; cells in the outer layers are actively proliferating, cells in the interior layer are quiescent, and in larger spheroids cells in the interior core may be necrotic. We speculate that the reduced penetration of

drugs into the interior cells of 3D tumor spheroids combined with the diminished proliferative capacity of these cells might contribute to the apparent resistance of 3D HNSCC spheroids to growth inhibition relative to 2D cultures exposed to these compounds. Based on the similarities between the microenvironments of cells in 3D tumor spheroid cultures and cell in solid tumors, and that cells in inner regions of spheroids are exposed to lower drug concentrations and have reduced proliferative capacities, we believe that incorporating 3D tumor models into the *in vitro* screening of cancer drugs will improve the correlation with *in vivo* efficacy in preclinical animal models and human clinical trials.

APPENDIX A

ABBREVIATION

1. National Cancer Institute ---NCI
2. Central nervous system ---CNS
3. Head and neck squamous cell carcinoma ---HNSCC
4. Multidrug resistance ---MDR
5. ATP-binding cassette transporter family ---ABC transporter family
6. Breast cancer resistance protein ---BCRP
7. Inhibitor of apoptosis proteins ---IAPs
8. Mitochondrial membrane permeabilization ---MMP
9. Extracellular matrix ---ECM
10. Two-dimensional ---2D
11. Three-dimensional ---3D
12. U.S. Food and Drug Administration ---FDA
13. Poly glycolic acid ---PGA
14. Poly lactic acid ---PLA
15. Ultra-low attachment ---ULA
16. CellTiter-Glo ---CTG
17. ImageXpress Micro ---IXM
18. Human papillomavirus ---HPV

19. Green fluorescent protein ---GFP
20. Red fluorescent protein ---RFP
21. Cytochrome P450 ---CYP
22. Phosphate-buffered saline ---PBS
23. Dimethyl sulfoxide ---DMSO
24. Fetal bovine serum ---FBS
25. Penicillin/streptomycin ---P/S
26. Dulbecco's Modified Eagle's Medium ---DMEM

BIBLIOGRAPHY

1. Shoemaker, R.H., *The NCI60 human tumour cell line anticancer drug screen*. Nat Rev Cancer, 2006. **6**(10): p. 813-823.
2. Kim, N., N. He, and S. Yoon, *Cell line modeling for systems medicine in cancers (review)*. Int J Oncol, 2014. **44**(2): p. 371-6.
3. Ma, Q. and A.Y. Lu, *Pharmacogenetics, pharmacogenomics, and individualized medicine*. Pharmacol Rev, 2011. **63**(2): p. 437-59.
4. Bussey, K.J., et al., *Integrating data on DNA copy number with gene expression levels and drug sensitivities in the NCI-60 cell line panel*. Mol Cancer Ther, 2006. **5**(4): p. 853-67.
5. Ocana, A., et al., *Preclinical development of molecular-targeted agents for cancer*. Nat Rev Clin Oncol, 2011. **8**(4): p. 200-9.
6. Freshney, R.I., *Culture of animal cells, a manual of basic technique*. John Wiley and Sons, inc.
7. Holohan, C., et al., *Cancer drug resistance: an evolving paradigm*. Nat Rev Cancer, 2013. **13**(10): p. 714-726.
8. Gottesman, M.M., *Mechanisms of cancer drug resistance*. Annu Rev Med, 2002. **53**: p. 615-27.
9. Gottesman, M.M., T. Fojo, and S.E. Bates, *Multidrug resistance in cancer: role of ATP-dependent transporters*. Nat Rev Cancer, 2002. **2**(1): p. 48-58.
10. Croop, J.M., et al., *The three mouse multidrug resistance (mdr) genes are expressed in a tissue-specific manner in normal mouse tissues*. Mol Cell Biol, 1989. **9**(3): p. 1346-50.
11. Fulda, S. and K.M. Debatin, *Extrinsic versus intrinsic apoptosis pathways in anticancer chemotherapy*. Oncogene, 2006. **25**(34): p. 4798-811.
12. Hanahan, D. and R.A. Weinberg, *The hallmarks of cancer*. Cell, 2000. **100**(1): p. 57-70.
13. Levine, B., S. Sinha, and G. Kroemer, *Bcl-2 family members: dual regulators of apoptosis and autophagy*. Autophagy, 2008. **4**(5): p. 600-6.
14. Deveraux, Q.L. and J.C. Reed, *IAP family proteins—suppressors of apoptosis*. Genes & development, 1999. **13**(3): p. 239-252.
15. Safa, A.R. and K.E. Pollok, *Targeting the Anti-Apoptotic Protein c-FLIP for Cancer Therapy*. Cancers (Basel), 2011. **3**(2): p. 1639-71.
16. Llambi, F., et al., *A unified model of mammalian BCL-2 protein family interactions at the mitochondria*. Molecular cell, 2011. **44**(4): p. 517-531.
17. Tannock, I.F., et al., *Limited penetration of anticancer drugs through tumor tissue a potential cause of resistance of solid tumors to chemotherapy*. Clinical cancer research, 2002. **8**(3): p. 878-884.
18. Lee, J., M.J. Cuddihy, and N.A. Kotov, *Three-dimensional cell culture matrices: state of the art*. Tissue Eng Part B Rev, 2008. **14**(1): p. 61-86.

19. Vaupel, P., F. Kallinowski, and P. Okunieff, *Blood flow, oxygen and nutrient supply, and metabolic microenvironment of human tumors: a review*. *Cancer Res*, 1989. **49**(23): p. 6449-65.
20. Wike-Hooley, J.L., J. Haveman, and H.S. Reinhold, *The relevance of tumour pH to the treatment of malignant disease*. *Radiother Oncol*, 1984. **2**(4): p. 343-66.
21. Tan, Q., et al., *Role of Autophagy as a Survival Mechanism for Hypoxic Cells in Tumors*. *Neoplasia*. **18**(6): p. 347-355.
22. Brown, J.M. and A.J. Giaccia, *The unique physiology of solid tumors: opportunities (and problems) for cancer therapy*. *Cancer research*, 1998. **58**(7): p. 1408-1416.
23. Tannock, I.F. and D. Rotin, *Acid pH in tumors and its potential for therapeutic exploitation*. *Cancer research*, 1989. **49**(16): p. 4373-4384.
24. Tredan, O., et al., *Drug resistance and the solid tumor microenvironment*. *J Natl Cancer Inst*, 2007. **99**(19): p. 1441-54.
25. Minchinton, A.I. and I.F. Tannock, *Drug penetration in solid tumours*. *Nat Rev Cancer*, 2006. **6**(8): p. 583-592.
26. Baker, B.M. and C.S. Chen, *Deconstructing the third dimension: how 3D culture microenvironments alter cellular cues*. *J Cell Sci*, 2012. **125**(Pt 13): p. 3015-24.
27. Jeffrey, S.S., P.E. Lønning, and B.E. Hillner, *Genomics-based prognosis and therapeutic prediction in breast cancer*. *Journal of the National Comprehensive Cancer Network*, 2005. **3**(3): p. 291-300.
28. Bleicher, K.H., et al., *Hit and lead generation: beyond high-throughput screening*. *Nat Rev Drug Discov*, 2003. **2**(5): p. 369-78.
29. Kyle, A.H., et al., *Direct assessment of drug penetration into tissue using a novel application of three-dimensional cell culture*. *Cancer Res*, 2004. **64**(17): p. 6304-9.
30. Kola, I. and J. Landis, *Can the pharmaceutical industry reduce attrition rates?* *Nat Rev Drug Discov*, 2004. **3**(8): p. 711-716.
31. Booth, B., R. Glassman, and P. Ma, *Oncology's trials*. *Nat Rev Drug Discov*, 2003. **2**(8): p. 609-610.
32. Breslin, S. and L. O'Driscoll, *Three-dimensional cell culture: the missing link in drug discovery*. *Drug Discov Today*, 2013. **18**(5-6): p. 240-9.
33. Ong, S.-M., et al., *Engineering a scaffold-free 3D tumor model for in vitro drug penetration studies*. *Biomaterials*, 2010. **31**(6): p. 1180-1190.
34. Lin, R.Z. and H.Y. Chang, *Recent advances in three-dimensional multicellular spheroid culture for biomedical research*. *Biotechnol J*, 2008. **3**(9-10): p. 1172-84.
35. Kunz-Schughart, L., *Multicellular tumor spheroids: intermediates between monolayer culture and in vivo tumor*. *Cell biology international*, 1999. **23**(3): p. 157-161.
36. Sutherland, R.M., *Cell and environment interactions in tumor microregions: the multicell spheroid model*. *Science*, 1988. **240**(4849): p. 177.
37. Hirschhaeuser, F., et al., *Multicellular tumor spheroids: an underestimated tool is catching up again*. *J Biotechnol*, 2010. **148**(1): p. 3-15.
38. Curcio, E., et al., *Mass transfer and metabolic reactions in hepatocyte spheroids cultured in rotating wall gas-permeable membrane system*. *Biomaterials*, 2007. **28**(36): p. 5487-5497.
39. Ward, J.P. and J.R. King, *Mathematical modelling of drug transport in tumour multicell spheroids and monolayer cultures*. *Mathematical biosciences*, 2003. **181**(2): p. 177-207.

40. Haycock, J.W., *3D cell culture: a review of current approaches and techniques*. 3D Cell Culture: Methods and Protocols, 2011: p. 1-15.
41. Toda, S., et al., *A new organotypic culture of thyroid tissue maintains three-dimensional follicles with C cells for a long term*. Biochemical and biophysical research communications, 2002. **294**(4): p. 906-911.
42. Vinci, M., et al., *Advances in establishment and analysis of three-dimensional tumor spheroid-based functional assays for target validation and drug evaluation*. BMC Biology, 2012. **10**(1): p. 1-21.
43. Kessel, S., et al., *High-Throughput 3D Tumor Spheroid Screening Method for Cancer Drug Discovery Using Celigo Image Cytometry*. Journal of laboratory automation, 2016: p. 2211068216652846.
44. Chandrasekaran, S., H. Deng, and Y. Fang, *PTEN deletion potentiates invasion of colorectal cancer spheroidal cells through 3D Matrigel*. Integrative Biology, 2015. **7**(3): p. 324-334.
45. Ravenscroft, S.M., et al., *A comparison of microtissue formation using either ultra-low adhesion plates or hanging drop*.
46. Koo, J.S., et al., *Impact of grade, hormone receptor, and HER-2 status in women with breast cancer on response to specific chemotherapeutic agents by in vitro adenosine triphosphate-based chemotherapy response assay*. Journal of Korean medical science, 2009. **24**(6): p. 1150-1157.
47. Eglen, R.M. and D.H. Randle, *Drug discovery goes three-dimensional: goodbye to flat high-throughput screening?* Assay and drug development technologies, 2015. **13**(5): p. 262-265.
48. Ivanov, D.P., et al., *In vitro co-culture model of medulloblastoma and human neural stem cells for drug delivery assessment*. J Biotechnol, 2015. **205**: p. 3-13.
49. TSUNODA, T., et al., *Establishment of a Three-dimensional Floating Cell Culture System for Screening Drugs Targeting KRAS-mediated Signaling Molecules*. Anticancer Research, 2015. **35**(8): p. 4453-4459.
50. Leung, B.M., et al., *Microscale 3D collagen cell culture assays in conventional flat-bottom 384-well plates*. J Lab Autom, 2015. **20**(2): p. 138-45.
51. Cadoni, G., et al., *A review of genetic epidemiology of head and neck cancer related to polymorphisms in metabolic genes, cell cycle control and alcohol metabolism*. Acta Otorhinolaryngologica Italica, 2012. **32**(1): p. 1-11.
52. Chaturvedi, A.K., et al., *Human papillomavirus and rising oropharyngeal cancer incidence in the United States*. J Clin Oncol, 2011. **29**(32): p. 4294-301.
53. Adelstein, D.J., et al., *Head and neck squamous cell cancer and the human papillomavirus: summary of a National Cancer Institute State of the Science Meeting, November 9-10, 2008, Washington, D.C*. Head Neck, 2009. **31**(11): p. 1393-422.
54. Johnston, P.A., et al., *High-Content pSTAT3/1 Imaging Assays to Screen for Selective Inhibitors of STAT3 Pathway Activation in Head and Neck Cancer Cell Lines*. Assay and Drug Development Technologies, 2014. **12**(1): p. 55-79.
55. Johnston, P.A., et al., *HCS campaign to identify selective inhibitors of IL-6-induced STAT3 pathway activation in head and neck cancer cell lines*. Assay Drug Dev Technol, 2015. **13**(7): p. 356-76.

56. Bauer, V.L., et al., *Establishment and Molecular Cytogenetic Characterization of a Cell Culture Model of Head and Neck Squamous Cell Carcinoma (HNSCC)*. Genes, 2010. **1**(3): p. 388-412.
57. Martin, D., et al., *The head and neck cancer cell oncogenome: a platform for the development of precision molecular therapies*. Oncotarget, 2014. **5**(19): p. 8906-23.
58. Erlichman, C. and D. Vidgen, *Cytotoxicity of adriamycin in MGH-U1 cells grown as monolayer cultures, spheroids, and xenografts in immune-deprived mice*. Cancer research, 1984. **44**(11): p. 5369-5375.
59. Durand, R.E., *Use of Hoechst 33342 for cell selection from multicell systems*. Journal of Histochemistry & Cytochemistry, 1982. **30**(2): p. 117-122.
60. Dudgeon, D.D., et al., *Characterization and optimization of a novel protein-protein interaction biosensor high-content screening assay to identify disruptors of the interactions between p53 and hDM2*. Assay Drug Dev Technol, 2010. **8**(4): p. 437-58.
61. Johnston, P.A., et al., *Development and validation of a high-content screening assay to identify inhibitors of cytoplasmic dynein-mediated transport of glucocorticoid receptor to the nucleus*. Assay Drug Dev Technol, 2012. **10**(5): p. 432-56.
62. Grantab, R.H. and I.F. Tannock, *Penetration of anticancer drugs through tumour tissue as a function of cellular packing density and interstitial fluid pressure and its modification by bortezomib*. BMC cancer, 2012. **12**(1): p. 1.
63. Minchinton, A.I. and I.F. Tannock, *Drug penetration in solid tumours*. Nat Rev Cancer, 2006. **6**(8): p. 583-92.
64. Fujiwara, A., T. Hoshino, and J.W. Westley, *Anthracycline antibiotics*. Critical Reviews in Biotechnology, 1985. **3**(2): p. 133-157.
65. Gewirtz, D., *A critical evaluation of the mechanisms of action proposed for the antitumor effects of the anthracycline antibiotics adriamycin and daunorubicin*. Biochemical pharmacology, 1999. **57**(7): p. 727-741.
66. Sartiano, G.P., W.E. Lynch, and W.D. Bullington, *Mechanism of action of the anthracycline anti-tumor antibiotics, doxorubicin, daunomycin and rubidazone: Preferential inhibition of DNA polymerase*. ALPHA. The Journal of antibiotics, 1979. **32**(10): p. 1038-1045.
67. Hortobagyi, G., *Anthracyclines in the treatment of cancer*. Drugs, 1997. **54**(4): p. 1-7.
68. Minotti, G., et al., *Anthracyclines: molecular advances and pharmacologic developments in antitumor activity and cardiotoxicity*. Pharmacol Rev, 2004. **56**(2): p. 185-229.
69. Attia, S.M., *Comparative aneugenicity of doxorubicin and its derivative idarubicin using fluorescence in situ hybridization techniques*. Mutat Res, 2011. **715**(1-2): p. 79-87.
70. Dalton, L., et al., *Synthesis of the tumour-inhibitory alkaloids, ellipticine, 9-methoxyellipticine, and related pyrido [4, 3-b] carbazoles*. Australian Journal of Chemistry, 1967. **20**(12): p. 2715-2727.
71. Auclair, C., *Multimodal action of antitumor agents on DNA: The ellipticine series*. Archives of Biochemistry and Biophysics, 1987. **259**(1): p. 1-14.
72. Stiborova, M., et al., *Molecular mechanisms of antineoplastic action of an anticancer drug ellipticine*. Biomed Pap Med Fac Univ Palacky Olomouc Czech Repub, 2006. **150**(1): p. 13-23.
73. Stiborova, M., et al., *The anticancer agent ellipticine on activation by cytochrome P450 forms covalent DNA adducts*. Biochem Pharmacol, 2001. **62**(12): p. 1675-84.

74. Arguello, F., et al., *Preclinical evaluation of 9-chloro-2-methylellypticinium acetate alone and in combination with conventional anticancer drugs for the treatment of human brain tumor xenografts*. Journal of cancer research and clinical oncology, 1998. **124**(1): p. 19-26.
75. Acton, E.M., et al., *Anticancer specificity of some ellipticinium salts against human brain tumors in vitro*. Journal of medicinal chemistry, 1994. **37**(14): p. 2185-2189.
76. Paoletti, C., et al., *Antitumor activity, pharmacology, and toxicity of ellipticines, ellipticinium, and 9-hydroxy derivatives: preliminary clinical trials of 2-methyl-9-hydroxy ellipticinium (NSC 264-137)*. Recent Results Cancer Res, 1980. **74**: p. 107-23.
77. Hannah, R., et al., *CellTiter-Glo™ Luminescent cell viability assay: a sensitive and rapid method for determining cell viability*. Promega Cell Notes, 2001. **2**: p. 11-13.